UNIVERSIDADE DE SÃO PAULO
FACULDADE DE ZOOTECNIA E ENGENHARIA DE ALIMENTOS

VERÔNICA MADEIRA PACHECO

Estudo de diferentes configurações de gaiolas de parto no desempenho de leitões e o desenvolvimento de um modelo computacional para detecção de posturas de matrizes

Pirassununga

2023

VERÔNICA MADEIRA PACHECO

Estudo de diferentes configurações de gaiolas de parto no desempenho de leitões e o desenvolvimento de um modelo computacional para detecção de posturas de matrizes

Versão Corrigida

Tese apresentada à Faculdade de Zootecnia e Engenharia de Alimentos da Universidade de São Paulo, como parte dos requisitos para a obtenção do Título de Doutor em Ciências.

Área de Concentração: Qualidade e Produtividade Animal

Orientador: Prof. Dra. Luciane Silva Martello
Co-orientador: Prof. Dr. Tami Marie Brown-Brandl

Pirassununga

2023

Ficha catalográfica elaborada pelo
Serviço de Biblioteca e Informação, FZEA/USP,
com os dados fornecidos pelo(a) autor(a)

M181e Madeira Pacheco, Verônica
Estudo de diferentes configurações de gaiolas de parto no desempenho de leitões e o desenvolvimento de um modelo computacional para detecção de postur / Verônica Madeira Pacheco ; orientador Luciane Silva Martello ; coorientador Tami Marie Brown-Brandl. -- Pirassununga, 2023.
103 f.

Tese (Doutorado - Programa de Pós-Graduação em Zootecnia) -- Faculdade de Zootecnia e Engenharia de Alimentos, Universidade de São Paulo.

1. gaiolas de parto. 2. comportamento animal. 3. zootecnia de precisão. 4. câmera de profundidade. 5. visão computacional. I. Silva Martello, Luciane, orient. II. Brown-Brandl, Tami Marie, coorient. III. Titulo.

USDA
United States Department of Agriculture

Research, Education, and Economics
Agricultural Research Service

Date: 06/03/2019
Project ID: 113.0
Project Title: Characterizing lactating sow posture in farrowing crates utilizing automated image capture and analysis system

Dear Dr. Rohrer,

The Institutional Animal Care and Use Committee has completed its review of your protocol. This letter constitutes official notification of the approval of your project. The IACUC approval is contingent upon following the project proposal as submitted and the submission of Annual Review reports. The approval for this protocol is effective to the expiration date of 01/31/2021.

You are responsible for informing the IACUC of any changes involving the care and/or use of animals prior to instituting these changes. The IACUC can be notified of proposed changes to animal use by submitting an Addendum Form. In addition, you are responsible for reporting any unanticipated problems involving research procedures or unexpected results of the procedures to the Attending Veterinarian and the IACUC Administrator.

Please note, it is the Principal Investigator's responsibility to ensure that Annual Reviews are submitted prior to the protocol anniversary date. The annual review form is attached to this communication and available on the USMARC intranet. It is also the Principal Investigator's responsibility to ensure that the 3-year protocol renewals are submitted for IACUC review prior to expiration. Reminders are sent out as a courtesy, but should not replace diligence on the part of the PI in submitting paperwork in a timely manner.

Brad Jones, Attending Veterinarian, will be in touch with you to set up a time that he can monitor the procedures outlined in your experiment. Please work with him on this important aspect of the IACUC process.

Thank you very much for your cooperation.

Sincerely, with best wishes for success,

Clay A. Lents
Chair, Institutional Animal Care and Use Committee

CC:
M.V. Boggess, CD
J.N. Krajewski, AO
B.T. Jones, AV
J.D. Ondrak, Veterinary Medical Officer

VERÔNICA MADEIRA PACHECO

Estudo de diferentes configurações de gaiolas de parto no desempenho de leitões e o desenvolvimento de um modelo computacional para detecção de posturas de matrizes

Tese apresentada à Faculdade de Zootecnia e Engenharia de Alimentos da Universidade de São Paulo, como parte dos requisitos para a obtenção do Título de Doutor em Ciências.

Área de Concentração: Qualidade e Produtividade Animal

Orientador: Prof. Dra. Luciane Silva Martello
Co-orientador: Prof. Dr. Tami Marie Brown-Brandl

Data de aprovação: ____/ ____/ ____

Presidente da Banca Examinadora

Prof. Dr. _____

Instituição _____

Banca Examinadora

Prof. Dr. _____

Instituição _____

Prof. Dr. _____

Instituição _____

Prof. Dr. _____

Instituição _____

Prof. Dr. _____

Instituição _____

AGRADECIMENTOS

À Deus que, apesar das minhas fraquezas, não se cansa de mostrar os seus propósitos na minha vida. Graças a Ele tenho muitos agradecimentos a fazer, por tantas pessoas maravilhosas cruzarem o meu caminho.

À minha família, minha inspiração constante!

Aos meus pais pela compreensão nos momentos difíceis, por me incentivarem desde pequena sobre a importância dos estudos e pela educação baseada em seus exemplos de caráter, respeito e amor ao próximo.

À minha avó Jacyra, pela fortaleza, e meu avô Nino, pela sabedoria, qualidades que somente os anos anos de vida podem proporcionar a corações bondosos como os seus. Agradeço todo amor, orações e todas as velinhas acesas.

Ao meu irmão Toninho e meu tio Lucas pelo amor e cumplicidade e por tornarem minha vida mais leve e alegre. À minha cunhada Eliana, à Giselle, aos meus sobrinhos, Francisco e Sofia e aos meus primos, João Lucas e Felipe, por encherem meu coração de amor.

Ao meu namorado Marcelo pelo amor, companheirismo e por me trazer tanta paz.

À minha orientadora, professora Luciane Martello que em 2013 me me deu uma chance em seu grupo (na época composto no total por nós duas) e desde então têm me incentivado e me ajudado a melhorar como pessoa e como profissional.

Ao professor Rafael, por acalmar os meus ânimos, por toda generosidade e paciência para me auxiliar no desenvolvimento deste e de outros trabalhos. Também por fazer parte do meu desenvolvimento pessoal e profissional.

Ao Edson, por toda dedicação a este e tantos projetos do laboratório.

À minha coorientadora, professora Tami Brown-Brandl por sempre fazer as perguntas certas e por estar sempre ao meu lado para encontrar as respostas. Obrigada por todas as oportunidades, pelos seus conselhos e por sua amizade.

À família Brown-Brandl e à Karen, por me receberem com tanto carinho durante o período que estive nos Estados Unidos. Em um período de pandemia, saber que estava entre pessoas tão especiais fez com que tudo ficasse mais leve.

Ao meu amigo-irmão Rafael, um anjo na minha vida. Por me receber em sua casa e no seu coração amigo.

À Isabella e Luciano, por me receberem com carinho e me auxiliarem durante a minha estadia em Nebraska.

Aos meus amigos e aos estagiários do Laboratório de Zootecnia de Precisão.

Aos trabalhadores do Setor de Suínos do US Meat Animal Research Center (USDA-USA), em especial ao John, sem o qual a coleta de dados não teria sido completa.

Ao laboratório de Inovação em Manejo Animal (Animal Management Inovation Lab) e à Universidade de Nebraska-Lincoln, pela oportunidade.

Ao Raj, por estar sempre disposto a ajudar e compartilhar seu conhecimento. Pela colaboração e em todos os projetos do grupo.

À Faculdade de Zootecnia e Engenharia de Alimentos da Universidade de São Paulo.

O presente trabalho foi realizado com apoio da Coordenação de Aperfeiçoamento de Pessoal de Nível Superior - Brasil (CAPES) - Código de Financiamento 001.

RESUMO

PACHECO, V. M. **Estudo de diferentes configurações de gaiolas de parto no desempenho de leitões e o desenvolvimento de um modelo computacional para detecção de posturas de matrizes.** 2023 103 F. Tese (Doutorado) – Faculdade de Zootecnia e Engenharia de Alimentos, Universidade de São Paulo, Pirassununga, 2023.

Na suinocultura, a maternidade é um período crucial para o desempenho dos animais já que o desenvolvimento de sistemas de parto e lactação que atendam as diferentes necessidades biológicas de matrizes e leitões ainda é um desafio. Estudar o padrão comportamental destes animais pode auxiliar na adoção sistemas cada vez mais eficientes e sustentáveis e o monitoramento contínuo e automático do comportamento pode ser uma ferramenta importante para a detecção do estado fisiológico dos animais e para a redução da mortalidade dos leitões. Dessa forma, este trabalho teve três objetivos principais. O primeiro visou avaliar o impacto de diferentes configurações de gaiolas de parto nos desempenho de leitões. Para isso, dados produtivos de 546 matrizes e 9123 leitões foram monitorados durante 36 ciclos lactação (32 dia/ciclo). Os tratamentos envolveram três tipos configuração de gaiolas de parto (tradicional, offset, diagonal), diferenciadas pelo posicionamento das matrizes nas baias. Os dados de desempenho de leitões (porcentagem de natimortos, porcentagem de mortalidade, porcentagem de esmagamento, ganho de peso médio diário (ADG)) foram monitorados de acordo com o Setor de Suínos do US Meat Animal Research Center (USDA-USA). Testaram-se os efeitos dos tratamentos nas características produtivas dos leitões e, como resultado, não foram encontradas diferenças significativas em relação aos tratamentos. O segundo objetivo deste trabalho, foi o desenvolvimento de um modelo classificador de posturas de matrizes, baseado em Redes Neurais Convolucionais (CNN). Neste caso, no mesmo Setor de Suídos do USDA-USA, imagens foram registradas com cameras Kinect V2® instaladas no topo de cada uma das gaiolas e classificadas por observadores treinados em cinco posturas (em pé, sentada, ajoelhada, decúbito ventral e decúbito lateral). Diferentes imagens (RGB, profundidade e mixed) foram utilizadas no desenvolvimento dos classificadores (MATLAB® R2022b - *Deep Learning Toolbox)* que foram avaliados a partir de métricas extraídas de uma matriz confusão comparando-se a respostas reais com as preditas pelo modelo. Os resultados deste estudo ilustram a melhora na classificação de posturas de matrizes usando imagens de profundidade nos modelos classificadores. No melhor modelo a acurácia foi de 94.7% e os valores de precisão e sensibilidade médios foram de 92.32% e 92.40%, respectivamente (F1-score = 92.36%). O modelo apresentou resultados promissores para as posturas de transição (sentada e ajoelhada).

Como último objetivo, três réplicas de quatro marcas de câmeras time-of-flight (Kinect v.2, Pico Zense, Pico Flexx e Azure Kinect) foram avaliadas em termos de repetibilidade de captura de dados, dimensões de painéis registrados pelas imagens e distorção radial. A repetibilidade foi comparada em termos de desvio padrão dos valores de distância registrados nas imagens. As dimensões dos painéis foram avaliadas nas imagens incluíram razão de área (px*cm-2) e volume estimado (cm^3). Já distorção radial foi avaliada comparando-se as medidas de distância e o coeficiente de variação em três segmentos das imagens. Os resultados indicam que a câmera Azure Kinect é a melhor câmera em termos de repetibilidade e estimativa de volume. A Pico Zense (câmeras 2 e 3) apresenta os menores valores de desvio padrão para medições de distância e a câmera Kinect v.2 os melhores resultados para medições de área.

Palavras-chave: bem-estar animal; câmeras de profundidade; gaiolas de parto alternativas; imagem de profundidade; mortalidade de leitões; modelagem computacional; visão computacional.

ABSTRACT

PACHECO, V. M. **Study of alternative farrowing crates on piglet performance and the development of a computational model for detecting sow postures.** 2023 103 F. PhD thesis – Faculdade de Zootecnia e Engenharia de Alimentos, Universidade de São Paulo, Pirassununga, 2023.

In pig farming, maternity is a crucial period for animal performance since the development of lactation systems that meet the different biological needs of sows and piglets is still challenging. Studying the behavioral pattern of these animals can help with the adoption of increasingly efficient and sustainable systems, and the continuous and automatic monitoring of behavior can be an important tool for detecting the physiological state of the animals, and for reducing piglet mortality. Thus, this work had three main objectives. The first aimed to evaluate the impact of different farrowing crate configurations on piglet performance. For this, productive traits of 546 sows, and 9123 piglets were monitored during 36 lactation cycles (32 days/cycle). The treatments involved three types of farrowing crate configurations (traditional, offset, diagonal), differentiated by the positioning of the sows in the pen. Piglet performance data (percent stillbirths, percent mortality, percent crush, average daily weight gain (ADG)) were monitored according to the Swine Sector of the US Meat Animal Research Center (USDA-USA). The effects of the treatments on the piglet performance data were tested, and as a result, there were no statistical in relation to the treatments. The second objective of this work was to develop a model to detect sow posture, based on Convolutional Neural Networks (CNN). In this case, in the same USDA-USA Swine Sector, images were recorded with Kinect V2® cameras installed on top of each crate and classified by trained observers in five postures (standing, sitting, kneeling, ventral decubitus and decubitus). Different types of images (RGB, depth, and mixed) were used in the development of the classifiers (MATLAB® R2022b - Deep Learning Toolbox). Metrics extracted from a confusion matrix comparing the actual and predicted responses were used to evaluate the performance of the classifiers. The results of this study illustrate an improvement in the classification of sow postures using depth images as input of classified models. The best model acchived an accuracy of 94.7%, and the mean precision and sensitivity values were 92.32% and 92.40%, respectively (F1-score = 92.36%). The model presented potential in the detection of transition postures (sitting and kneeling).

As a last objective, three replicas of four brands of time-of-flight depth cameras (Kinect v.2, Pico Zense, Pico Flexx and Azure Kinect) were evaluated in terms of repeatability of data, board dimensions, and radial distortion. Repeatability was evaluated in terms of standard deviation of the distance values recorded in the images. Board dimensions were evaluated in the images according to the area ratio ($px*cm^{-2}$) and estimated volume (cm3). Radial distortion was evaluated by comparing the distance measurements and the coefficient of variation in three segments of the images. The results indicate that the Azure Kinect camera presented the best results for repeatability and volume estimation. Pico Zense (cameras 2 and 3) displays the smallest standard deviation values for distance measurements. Kinect v.2 camera showed the best results for area measurements.

Key-words: alternative farrowing crates; animal welfare; computational modeling; computer vision; depth cameras; depth image; piglet mortality.

LISTA DE ILUSTRAÇÕES

LISTA DE TABELAS

SUMÁRIO

1 INTRODUÇÃO GERAL

A representação de um ambiente adequado de parto e lactação na produção de suínos ainda é um desafio. Conciliar as necessidades biológicas de matrizes e leitões dentro dos preceitos de bem-estar animal com um ambiente economicamente produtivo não é tarefa fácil. Estudar as respostas produtivas e comportamentais destes animais dentro desses sistemas pode auxiliar na adoção de técnicas mais eficientes e sustentáveis. Além disso, o monitoramento contínuo do comportamento, utilizando técnicas computacionais, pode ser uma ferramenta importante para a detecção de doenças, estresse térmico e na redução da mortalidade dos leitões.

Nesse sentido, a produção deste trabalho se deu em três capítulos. O primeiro visou avaliar o impacto de diferentes configurações de gaiolas de parto nos desempenho dos leitões. A hipótese é que as diferentes configurações de gaiolas de parto podem melhorar o desempenho dos leitões ao afastar a matriz da fonte de aquecimento e promover uma maior área livre de descanso para acomodar a leitegada. Assim, o objetivo foi investigar configurações alternativas às gaiolas de parto tradicionais, nas quais o posicionamento centralizado das matrizes na gaiola faz com que sejam afetadas pela fonte de aquecimento. Além disso, os leitões têm um espaço de descanso reduzido, o que aumenta o risco de morte por esmagamento.

O segundo capítulo trata do desenvolvimento de um modelo classificador de posturas de matrizes, baseado em Redes Neurais Convolucionais (CNN). A mortalidade dos leitões por esmagamento está diretamente relacionada às mudanças posturais das matrizes, sobretudo quando deitam ou quando rolam de um lado para o outro. Além disso, entender os padrões posturais das matrizes durante o período de lactação pode auxiliar o produtor a caracterizar o rebanho e detectar antecipadamente problemas que afetem o desempenho dos animais. A intenção do desenvolvimento desse classificador é substituir a investigação comportamental manual, que necessita de tempo e observadores treinados, por um método automático de avaliação de imagens, passível de gerar respostas rápidas para tomada de decisão nos sistemas produtivos. Neste capítulo há também a comparação de diferentes tipos de imagens que podem ser utilizadas no desenvolvimento de modelos computacionais, como é o caso das imagens coloridas (RGB: *red, green, blue* - vermelho, verde, azul), tradicionalmente utilizadas, e as imagens de profundidade. A hipótese é que pode ser desenvolvido um modelo baseado em CNN eficiente para a detecção de posturas de matrizes e com potencial de auxiliar os produtores na caracterização dos animais e na prevenção da morte dos leitões por esmagamento.

No último capítulo deste trabalho, três réplicas de quatro marcas de câmeras de profundidade do tipo tempo-de-vôo (*time-of-flight* -ToF) foram avaliadas. Este tipo de tecnologia têm crescido nos últimos anos por se tratar de um sensor que pode mapear o ambiente de forma tridimencional. Por outro lado os sensores ToF estão sujeitos a erros de distorção de forma, zonas não legíveis e ruídos de medição de distância que afetam a precisão e a estabilidade dos dados. Esses erros são consequência de diferentes fontes como o ambiente, o tipo de tecnologia e as propriedades intrínsecas de cada câmera. Entre as diferentes características dos sensores ToF, podemos encontrar aqueles que possuem maior distância de trabalho, maior o campo de visão, melhor resolução, e maior precisão no registro de dados de profundidade. Estas características podem definir a escolha do sensor mais dequado para cada tipo de problema e os processos de validação de sensores são importantes para garantir a coleta de informações precisas. A hipótese deste estudo é que as câmeras com tecnologias mais recentes apresentem melhor performance nos testes elaborados em relação às demais. Assim o objetivo foi avaliar a performance de quatro câmeras ToF (Kinect v.2, Pico Zense, Pico Flexx e Azure Kinect) em termos de repetibilidade na captura de imagens de cenas estáticas, do cálculo de dimensões de painéis a partir de imagens e da distorção radial entre o centro e as bordas das imagens.

2 CAPÍTULO I: REVISÃO BIBLIOGRÁFICA

2.1 Importância de um ambiente adequado no setor de parto e lactação da suinocultura

O aumento dos índices reprodutivos e o melhoramento genético são estratégias adotadas na produção animal para o aumento da produtividade. Tais estratégias influenciaram diretamente o tamanho da leitegada e as taxas de crescimento dos animais (E. M. Baxter et al., 2011). Apesar disso, o desenvolvimento dos animais a partir do melhoramento genético é fisiologicamente limitado e, dessa forma, estudar ambientes mais eficientes pode melhorar o desempenho, possibilitando que o animal expresse todo seu potencial genético, o bem-estar e aumentar as taxas de sobrevivência destes animais.

O desenvolvimento de um ambiente adequado no setor de parto e lactação da suinocultura ainda é um desafio pois conciliar as necessidades biológicas de matrizes e leitões, sobretudo em termos de conforto térmico, não é uma tarefa trivial. As tradicionais gaiolas de parto amplamente utilizadas foram criadas em 1960 com o objetivo principal de melhorar o bem-estar e reduzir a mortalidade dos leitões por esmagamento (King *et al.*, 2019; Loftus *et al.*, 2020). Além disso, o modelo de contenção dos animais traz outros benefícios como economia de espaço e melhorias no manejo sanitário e alimentar.

Apesar destas vantagens, gaiolas tradicionais apresentam problemas quanto ao bem-estar animal e têm recebido críticas por limitarem os movimentos e o comportamento natural das matrizes (Emma M. Baxter et al., 2015; A. K. Johnson et al., 2001). Assim, o estudo de gaiolas de parto alternativas que, apesar do confinamento, possam melhorar o bem-estar destes animais se torna indispensável (Lambertz et al., 2015). A tendência é que estas gaiolas sejam substituídas por sistemas de baias coletivas, no entanto, a escolha da melhor alternativa deve passar por estudos que considerem um equilíbrio entre a viabilidade econômica e aspectos do bem-estar animal. Além disso, estas gaiolas alternativas podem ser úteis para um período de transição entre os sistemas de baias individuais e coletivas e a individualização dos animais também contribui para estudos sobre o desempenho e o comportamento materno-filial.

Algumas gaiolas de parto alternativas que têm sido estudadas envolvem o aumento do tamanho da estrutura das gaiolas, ou a redução do tempo de permanência das matrizes no período de contenção, já que o esmagamento dos leitões pelas matrizes acontece principalmente nos primeiros dias após o parto. Além disso, também é interessante avaliar gaiolas de parto com o mesmo tamanho, mas com diferentes configurações e o seu impacto na performance dos leitões.

2.2 Gaiolas de parto tradicionais

As tradicionais gaiolas de parto desenvolvidas em 1960 contém uma área com dimensões de 1,52 m x 2,13 m, deixando a matriz centralizada e confinada em um espaço de 1,30 m^2 (Figura 1). Além do espaço limitar os seus movimentos, a posição centralizada da matriz faz com que a mesma seja afetada pela fonte de aquecimento dos leitões, prejudicando o seu conforto térmico e seu desempenho, uma vez que, como mencionado, as matrizes têm necessidades térmicas geralmente opostas às dos leitões.

Esta configuração também fornece uma pequena área livre de descanso para os leitões (duas áreas de 0,95 m^2). Segundo Q. Zhang e H. Xin (2005) no primeiro dia de nascimento, cada leitão ocupa uma área de 0.044 m^2 e, aos 14 dias de idade, 0.074 m^2. Assim, a recomendação dos autores para a dimensão de um tapete de descanso para 12 leitões é de 0.37 m^2. Considerando-se um tapete ideal de dimensões 1.14 x 0.32 m (0.37 m^2) em uma gaiola de parto tradicional, a área de aquecimento dos leitões acaba por ficar muito próxima à área de confinamento da matriz (Figura 1).

Sobre a fonte de aquecimento, uma lâmpada de calor de 175 W a uma altura de 76 cm do chão aquece uma área de raio de 60 cm, com a temperatura reduzindo gradativamente do centro para as extremidades da circunferência (Zhang e Xin, 2001). Assim, em uma gaiola de parto tradicional, com a lâmpada de aquecimento posicionada no centro do tapete, uma parte do calor emitido pela fonte de aquecimento também pode afetar a área da matriz (Figura 1).

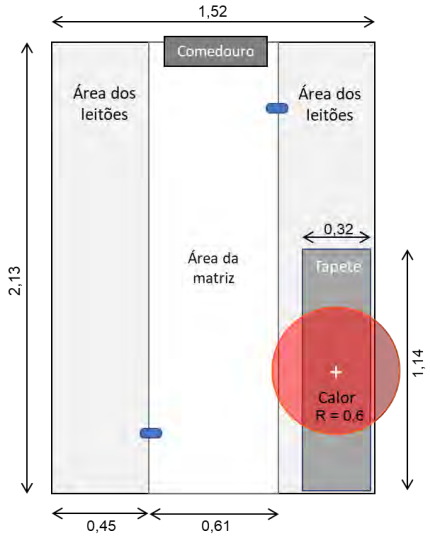

Figura 1. Configuração de uma baia de parto tradicional com o tapete de descanso e lâmpada de aquecimento (calor) para os leitões. Todas as dimensões estão em metros.

O espaço reduzido de descanso para os leitões não consegue acomodar de forma eficiente uma leitegada média de 12 leitões/matriz e a próximidade destes animais à área da matriz pode colocá-los em risco de morte por esmagamento. Adicionalmente, a fonte de aquecimento próxima a matriz e o espaço limitado para movimentação pode aumentar o seu desconforto e influenciar seu estado fisiológico e comportamental, o que afeta diretamente a taxa da mortalidade e o desempenho dos leitões.

Portanto, a busca por gaiolas de parto alternativas que melhorem as condições bem-estar e desempenho dos animais durante a fase de lactação e que sejam capazes de manter uma boa produtividade poderá contribuir com melhorias para o setor, sendo de grande interesse para técnicos e produtores.

2.3 Desempenho dos leitões na maternidade

A mortalidade dos leitões antes do desmame é um indicativo tanto econômico quanto um reflexo sobre o estado de bem-estar dos animais. A sobrevivência dos leitões na maternidade é um dos resultados mais importantes para a lucratividade do produtor e é influenciado, sobretudo, pela expressão coordenada entre os comportamentos da matriz e dos leitões e o ambiente (E. M. Baxter et al., 2011).

Existem algumas características de desempenho dos animais que são relacionadas com maiores taxas de mortalidade de leitões na fase de aleitamento. O aumento da leitegada, por exemplo, influencia a variação do peso dos leitões e a competição pelos tetos, o que pode aumentar o risco de morte por inanição. Além disso, o tamanho da leitegada pode potencializar as mortes por hipotermia já que os leitões tendem a nascer menores e ficam mais suscetíveis às baixas temperaturas (Schild et al., 2020).

Segundo Galiot et al. (2018) o crescimento e o peso dos leitões pré-desmame dependem, entre outros fatores, do peso ao nascimento, do tamanho e uniformidade da leitegada, da paridade da matriz e do ganho de peso durante as primeiras 24 horas após o nascimento. A alta paridade está relacionada com maiores taxas de mortalidade pois estas matrizes possuem menor controle muscular e dão luz a ninhadas maiores. Assim, estão mais propensas a ter partos longos e correm o risco de sofrerem exaustão (Schild et al., 2020).

A investigação de diferentes características de desempenho dos leitões pode trazer informações importantes sobre a eficiência do ambiente que os animais estão inseridos. Johnson,

Morrow-Tesch e McGlone (2001) estudaram o desempenho de leitões confinados em gaiolas de parto e ao ar livre. Foram avaliadas 20 matrizes e suas leitegadas e os autores não encontraram diferenças significativas nos dados de desempenho entre os tratamentos, com destaque para a taxa de mortalidade dos leitões.

Outros estudos demonstram diferenças significativas entre os dados de desempenho dos animais alojados em gaiolas de parto e ao ar livre, indicando que a conteção das matrizes melhora o desempenho dos leitões (Chidgey et al., 2015; Yun et al., 2019) e confirmam que a liberdade de movimentação das matrizes em baias livres podem aumentam o risco de morte por esmagamento, sendo que a taxa de mortalidade pode chegar a 25% (Marchant, Broom e Corning, 2001).

Hales et al. (2014) investigaram se o confinamento da matriz por um período limitado de dias após o parto afetaria a mortalidade dos leitões. Os autores indicaram um aumento na mortalidade dos leitões em sistemas que mantinham as matrizes livres e indicaram que as mortes acoteciam principalmente nos primeiros quatro dias após o parto. Além disso, os autores ressaltaram que o esmagamento foi responspavel por 65% das mortes do total de leitões estudados, e essa porcentagem foi maior em baias livres (83%). A porcentagem de mortalidade registrada após dez dias do parto em baias livres foi maior que 10% enquanto que nas baias que utilizaram alguns dias de confinamento para as matrizes, esta porcentagem foi menor que 6%.

Em uma revisão sistemática Glencorse et al. (2019) realizaram uma meta-análise dos resultados de publicações que compararam diretamente as gaiolas de parto tradicionais e as baias de parto livres do primeiro dia após o parto até o desmame. Os autores separaram 22 artigos para comparação e indicaram que há um aumento de 14% no risco relativo de mortalidade de leitões em baias de parto livres quando comparadas com as gaiolas de parto tradicionais.

Leonard et al. (2021a) estudaram o efeito do tamanho da baia de parição e o número de lâmpadas de calor no desempenho de leitões. Foram avaliadas gaiolas de parto tradicionais, gaiolas com área de descanso de leitões expandida e gaiolas com a área da matriz e dos leitões expandidas. Não foram observadas diferenças entre os tratamentos sobre as porcentagens de mortalidade e de esmagamento, nem sobre o número de leitões nascidos vivos e desmamados.

Nem sempre propostas alternativas de gaiolas de parto, mesmo com aumento de área disponível, resultam em melhorias produtivas ou de bem-estar. Por isso, é importante que todas as proposições de mudanças estruturais passem por estudos da eficência dos sistemas propostos por meio da avaliação da performance dos animais.

2.4 Comportamento das matrizes na maternidade

O monitoramento do comportamento das matrizes pode trazer informações importantes sobre o estado fisiológico das matrizes. Na maternidade suína, algumas das principais observações comportamentais estão relacionadas com o estresse térmico das matrizes pelo calor, principalmente nas gaiolas de parto tradicionais, onde há a limitação de seus movimentos e pela proximidade com fonte de aquecimento dos leitões.

A hipertermia nas matrizes, por exemplo, pode prolongar o trabalho de parto e influenciar na mortalidade dos leitões antes do nascimento. A qualidade e quantidade do leite materno também podem ser afetados pela hipertermia pois estão diretamente relacionadas com o estado nutricional das matrizes que, em desconforto térmico, tendem a reduzir a ingestão alimentar e de água.

A. K. Johnson et al. (2001) estudaram o comportamento de matrizes confinadas em gaiolas de parto e ao ar livre. Foram avaliadas 20 matrizes das 14 às 18 horas a cada 5 minutos. Os autores indicaram que houve diferença entre os tratamentos em relação a duração dos comportamentos ativa (em pé ou andando), deitada e bebendo. As matrizes alojadas ao ar livre gastavam mais tempo no comportamento ativa (27,7% do tempo avaliado), enquanto que as alojadas em gaiolas de parto gastavam mais tempo deitadas (90,9%), comendo(4.4%) ou bebendo (1.4%).

Liu et al. (2021) estudou o efeito do estresse térmico sobre as mudanças posturais das matrizes matrizes primíparas em torno do período de parto (72 h pré até 24 h pós-parto). Os autores indicaram que as mudanças posturais aumentaram significativamente, começando 24 h horas antes do parto tanto no tratamento controle quando no tratamento estrese térmico. ´No estudo, após o parto e em ambos os tratamentos, as matrizes se deitavam com o úbere virado para a área de descanso dos leitões. Apesar disso, as matrizes que estavam sob condições de estresse térmico reduziram o comportamento de amamentação em comparação as do tratamento controle.

Outro aspecto importante do monitoramento comportamental das matrizes está relacionado a frequência e a duração de mudanças posturais nas matrizes, parâmetros que são afetados em situações de desconforto térmico (Schild et al., 2020) e que estão diretamente relacionados com a disponibilidade das matrizes para amamentação e à porcentagem de esmagamento dos leitões.

Marchant, Broom e Corning (2001) estudaram a influência do comportamento das matrizes na mortalidade dos leitões em baias de parto livres. Os autores avaliaram 24 matrizes e suas leitegadas durante a primeira semana de lactação. A mortalidade de leitões registrada foi de 25%,

sendo que a mortalidade por esmagamento foi causa de 76% destas mortes e aconteceram principalmente quando as matrizes mudavam da posição em pé para deitada ou quando rolavam na posição deitada.

Wischner et al. (2009) compararam as mudanças posturais de matrizes em dois grupos: 20 matrizes que aprensentaram um ou mais leitões esmagados (C) e 20 matrizes que não tiveram nenhum episódio de esmagamento (NC). Os resultados do estudo indicaram que as matrizes NC estavam mais inquietas no período pré parto, especialmente as primíparas, que realizaram mais mudanças posturais. Além disso, as matrizes ficavam em pé e realizavam o comportamento de construção do ninho com maior frequência e duração que as matrizes C, particularmente 7 e 6 h antes do parto. No período pós-parto, não foram encontradas diferenças nos padrões de movimento das matrizes entre os dois tratamentos. Por outro lado, em comparação com as matrizes NC primíparas, as C primíparas mostraram mais movimentos de rolamento. Outros achados do estudo foram em relação as posturas sentada e decúbito lateral. As matrizes C ficaram mais tempo sentadas do que as NC, especialmente as multíparas e as matrizes NC realizaram o decúbito lateral por mais tempo e frequência como posição final ao se deitarem.

Embora a identificação de modificações comportamentais dos animais possa auxiliar no gerenciamento do rebanho de forma mais efetiva (Brown-Brandl et al., 2013) é uma tarefa trabalhosa e difícil de ser realizada continuamente no setor produtivo. O monitoramento geralmente é feito por pessoas especializadas que observam os animais no campo ou por meio de vídeo-imagens. As informações obtidas deste tipo de observação geralmente não são instantâneas, são subjetivas e são um desafio para a avaliação individual em grandes grupos de animais. Esses desafios têm impulsionado a busca por técnicas automáticas de detecção comportamental dos animais, as quais são baseadas em Inteligência Artificial, e visam substituir a observação humana para detectar padrões em imagens.

Conforme mencionado, mudanças posturais das matrizes podem refletir o seu estado fisiológico e estão relacionadas às mortes por esmagamento dos leitões. Assim, técnicas que auxiliem na identificação de posturas das matrizes podem contribuir para o desenvolvimento de sistemas que previnam o esmagamento de leitões, que caracterizem o padrão comportamental do rebanho e auxiliem a tomada de decisões pelos produtores.

2.5 Sistemas automáticos de visão computacional

Tecnologias recentes associadas a sistemas automatizados provocaram grandes avanços na pecuária de precisão ao permitir que o setor colete um grande volume de dados de forma contínua e com abordagens menos invasivas aos animais e menos intensivas em mão-de-obra. Por outro lado, esse grande volume de dados vem gerando novos desafios, já que a interpretação demanda tempo e pessoas especializadas para geração de conhecimento (Morota et al., 2018). Dessa forma, modelos computacionais baseados em Aprendizagem de Máquina têm sido incorporados a esses sistemas automatizados para gerar informações úteis a partir de bases de dados complexas e volumosas.

Aprendizagem de Máquina (*Machine Learning* - ML) é um ramo da Inteligência Artificial *(Artificial Intelligence* – AI) que busca o desenvolvimento de modelos computacionais que possam aprender a partir de um conjunto de dados. A ML é uma das ferramentas capazes de investigar analiticamente uma base de dados desorganizada e complexa e extrair padrões e tendências importantes para a geração de conhecimento (Silva, Peres e Boscaroioli, 2016). As tecnologias que são baseadas em ML tem como vantagens a eliminação da subjetividade humana e a possibilidade de desenvolver métodos não invasivos de monitoramento contínuo.

Entre as diferentes abordagens de ML estão as técnicas de visão computacional que simulam a capacidade da visão biológica de interpretar informações a partir de imagens. Um sistema de visão por computador tradicional inclui subtarefas relacionadas ao processamento de imagens, tais como detecção de bordas e cores, segmentação de imagens e reconhecimento de padrões.

Na pecuária de precisão, técnicas de visão computacional têm sido aplicadas em diferentes tipos de estudos, desde a identificação de comportamentos (Porto et al., 2015) e laminite (Viazzi et al., 2013) em vacas de leite, contagem de leitões (Tian et al., 2019) e identificação de doenças respiratórias (Jorquera-Chavez et al., 2021) em suínos, até a estimativa do volume de ovos de galinhas (Okinda et al., 2020).

No caso do presente estudo, este tipo de modelagem pode auxiliar na identificação de posturas em matrizes no período de lactação a partir de imagens. A identificação de posturas de forma automática pode auxiliar o produtor a caracterizar o seu rebanho de forma mais efetiva, identificando problemas fisiológicos nos animais. Além disso, a identificação de algumas posturas, como a ajoelhada, pode permitir o desenvolvimento de sistemas que evitem o esmagamento de leitões pelas matrizes. Neste contexto, as Redes Neurais Convolucionais, técnicas de visão

computacional amplamente utilizadas em processos de classificação de imagens, podem auxiliar no desenvolvimento de modelos computacionais de classificação de posturas em matrizes.

2.6 Redes Neurais Convolucionais

Redes Neurais Convolutionais (*Convolutional Neural Networks* – CNN) são um tipo especializado de rede neural para o processamento de dados que são apresentados em forma de matrizes, como é o caso das imagens. O nome convolucional demonstra que este tipo de rede utiliza operações de convolução que associam a matriz de entrada a filtros extratores de padrões.

A arquitetura básica de uma CNN é composta de dois estágios principais: o primeiro estágio é responsável pela extração de padrões e é composto por camadas convolucionais e de agrupamento; o segundo estágio consiste no processo de classificação, composto por uma camada completamente conectada aos neurônios de saída, como ocorre em uma rede neural convencional (Lecun et al., 2015).

As camadas convolucionais são responsáveis pela extração de padrões (*feature maps*) nas imagens. Esta extração é feita por meio de filtros (*kernel*) aplicados em subregiões da matriz (Figura 2). Cada tipo de filtro pode extrair um tipo diferente de informação que corresponde a um elemento visual capturado da imagem original. Todas as unidades da matriz recebem o mesmo filtro em cada etapa de convolução (Rodríguez Alvarez et al., 2018). Assim como na rede neural convencional, a aprendizagem da CNN ocorre com a atualização dos pesos sinápticos. Neste caso, os pesos sinápticos são os próprios filtros.

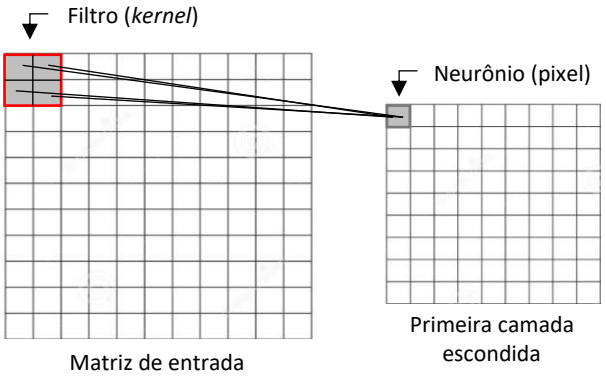

Figura 2. Exemplo de uma operação de convolução onde um filtro é aplicado a uma subregião da matriz de entrada. O filtro é deslocado por toda a matriz e, em cada subregião, o filtro extrai a informação para um neurônio da camada seguinte.

A convolução utiliza três ideias importantes que ajudam a melhorar o desempenho da máquina em um sistema de aprendizagem, que são: interações esparsas, compartilhamento de parâmetros e representações equivariantes. As interações esparças referem-se à utilização de filtros menores que a matriz de entrada que correm por todas as subregiões da matriz principal e detecta apenas padrões significativos, o que reduz os requisitos de memória do modelo e melhora sua eficiência estatística, já que a saída requer menos operações (Goodfellow, Bengio e Courville, 2016). O compartilhamento de parâmetros trata da utilização de um mesmo parâmetro para mais de uma função no modelo. Assim valor do peso aplicado a uma subregião da matriz de entrada está ligado ao valor de um peso aplicado em todas as outras subregiões. Já a representação equivariante é uma consequência do compartilhamento de parâmetros. Na prática isto significa que algumas mudanças de luminosidade ou posição aplicadas na imagem original, não interferem na representação de saída, assim o resultado de uma operação de convolução sobre uma imagem original e equivariada será o mesmo (Goodfellow, Bengio e Courville, 2016).

Em sequência às camadas de convolução, existem as camadas de agrupamento (*pooling*/*subsampling*). A função desta etapa é reduzir a dimensão das matrizes por meio da mesclagem de características semelhantes que foram extraídas na etapa anterior. Além disso, esta camada preserva informações importantes mantendo valores máximos de pixels em cada etapa de filtragem (Sharma et al., 2018). Este processo pode eliminar dados redundantes, o que facilita a aprendizagem e aumenta a rapidez do treinamento (Lecun et al., 2015; Rodríguez Alvarez et al., 2018).

Após as camadas de convolução e agrupamento, existe a penúltima camada, chamada de unidade linear retificada (ReLu) que transforma todos os números negativos provindos das camadas anteriores em zero. Isto auxilia a CNN a destacar os valores que foram aprendidos e eliminar dados irrelevantes, mantendo-a matematicamente estável (Sharma et al., 2018).

A última camada de uma CNN é a camada de classificação completamente conectada. Nesta camada, os resultados obtidos das camadas anteriores são organizados e conectados às categorias de classificação pré-definidas no início da construção do modelo. Adicionalmente uma camada final com uma função *Softmax* é frequentemente utilizada na saída do classificador como forma de distribuir os valores em probabilidades de estarem em cada uma das classes (Rodríguez Alvarez et al., 2018). Assim, a CNN oferece um nível de classificação como reposta a atribuição do dado de entrada.

A Figura 3 exemplifica o processo de aprendizagem de uma CNN que recebe como entrada uma imagem digital com três canais RGB. Como exemplo, uma etapa de convolução e uma etapa de agrupamento são responsáveis pela extração de padrões. As informações extraídas na primeira etapa são submetidas à camada completamente conectada na etapa de classificação. Dependendo do tipo de problema analisado, mais etapas de convolução e agrupamento podem ser aplicadas.

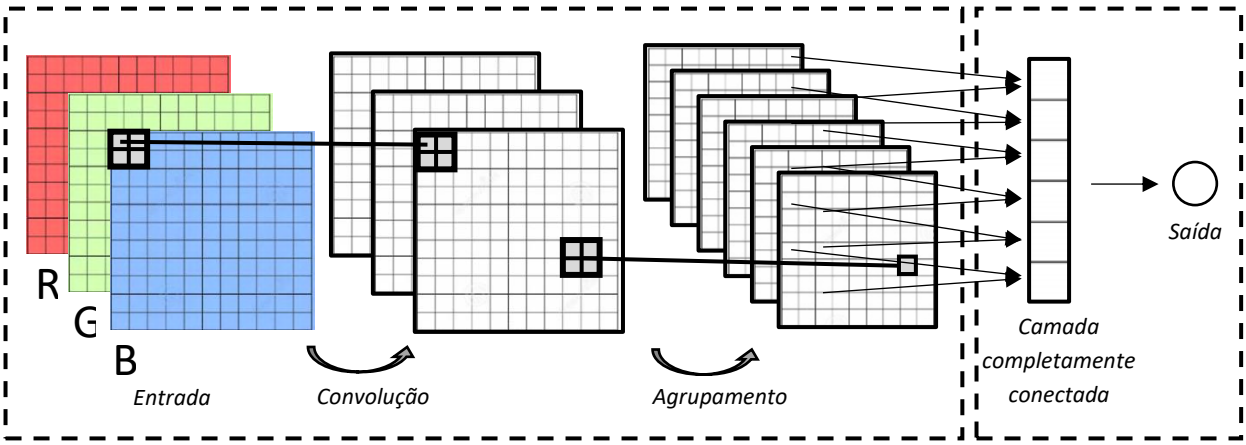

Figura 3. Exemplo de uma arquitetura básica de uma Rede Neural Convolucional.

Em função da estrutura apresentada e pela capacidade de detectar padrões em matrizes, as CNNs têm sido amplamente utilizadas na detecção e classificação de objetos em imagens. Nas pesquisas em suinocultura, as CNNs têm sido utilizadas para diferentes tarefas como

reconhecimento de face dos animais (Marsot et al., 2020), reconhecimento de comportamentos agressivos (Chen et al., 2020) e estimativa de peso corporal (Meckbach et al., 2021).

Silva et al. (2019) desenvolveram um algoritmo de visão computacional baseado em CNN para identificação do comportamento de nove suínos por vídeo- imagens RGB. Os comportamentos avaliados foram andando, bebendo, comendo, comendo junto, dormindo e dormindo junto e, na etapa de teste, o melhor modelo atingiu uma acurácia de 99%

Na maternidade, estes modelos também têm sido utilizados para a detecção de posturas de matrizes em lactação. Zheng *et al.*, 2018 estudaram um dectector de posturas de matrizes baseado em um tipo de CNN utilizado em tarefas de detectção de objetos (Faster-CNN). As posturas de classificação utilizadas foram em pé, sentado, decúbito esternal, decúbito ventral e decúbito lateral e foram identificadas em imagens de profundidade coletadas com sensores Kinect V2®. Antes de serem submetidas aos modelos, as imagens de profundidade passaram por pré-processamentos que tiveram a como objetivo eliminar ruídos, completar falhas, e melhorar o contraste. Os autores obtiveram 93.58% de acurácia na classificação de posturas, sendo que as categorias em pé, decúbito ventral e decúbito lateral apresentaram valores de precisão de 99.1%, 97.2% e 98.7%. As categorias com menores acertos foram as das posturas sentada e decúbito esternal, com valores de precisão de 77.6 e 76.3%.

Utilizando o mesmo banco de dados de Zheng *et al.* (2018), Zhu et al. (2020) propuseram um algoritmo de detecção (RGB-D Faster R-CNN) de dois fluxos, em que as imagens RGB e de profundidade foram fundidas e posteriormente classificadas em cinco posturas de matrizes (em pé, sentado, decúbito esternal, decúbito ventral e decúbito lateral.). O pre-processamento de imagens de profundidade foi o mesmo que o descrito no estudo anterior mas nenhum pré-processamento foi feito nas imagens RGB. No desenvolvimento do algoritmo, diversas técnicas de extração de padrões e fusão de imagens foram estudadas. Os resultados obtidos dos modelos com diferentes métodos de fusão de imagens foram comparados com os modelos que usaram apenas imagens RGB ou profundidade. Todos os métodos que utilizaram a fusão de imagens apresentaram resultados melhores que os que utilizaram apenas imagens individuais na entrada dos modelos.

As CNNs têm apresentado resultados promissores para identificação de posturas em matrizes lactantes e os estudos demonstram que a estratégia de fusão de imagens têm melhorado o desempenho dos modelos classificadores. Assim, estudar diferentes modelos computacionais para detecção posturas e avaliar o comportamento de diferentes imagens como entrada dos modelos

pode contribuir para o desenvolvimento de classificadores cada vez mais precisos e com o menor custo computacional possível.

2.7 Imagens RGB e de profundidade

No desenvolvimento de modelos para detecção de posturas de matrizes, geralmente são utilizados dois tipos de imagens: RGB e profundidade. As imagens RGB apresentam uma boa representação da cena em termos de cores e detalhes, mas perdem a informação de profundidade, importante para a detecção de algumas posturas de transição, principalmente nas imagens de vista superior. Por outro lado, apesar de apresentarem a informação tridimensional, as imagens de profundidade perdem em representação de cores e detalhes, o que pode ser importante para ajudar o modelo a distinguir os animais na cena.

O desenvolvimento das câmeras convencionais digitais tiveram início durante a Segunda Guerra Mundial mas se popularizaram a partir da década de 90. Durante todos estes anos, a qualidade dos sensores de captação e o processamento das imagens foram aperfeiçoados e permitem que a as imagens RGB tenham uma boa representação da cena com o mínimo de ruído. Imagens convencionais são definidas como funções de duas dimensões, onde cada pixel representa a intensidade daquele ponto em termos de níveis de cinza que variam do preto (menor intensidade) ao branco (maior intensidade).

Em termos computacionais, esses níveis de intensidade são representados utilizando-se um valor mínimo de oito bits por pixel, ou seja, isso possibilita a representação de 256 intensidades (2^8). No caso das imagens RGB, a aquisição pelos sensores é feita utilizando-se três filtros, sensíveis ao vermelho, ao verde e ao azul, respectivamente. Assim, a imagem RGB é formada pela combinação destas três imagens monocromáticas (Gonzalez e Woods, 2010). A formação destas imagens requer uma representação computacional mínima de 24 bits, pela soma dos três canais RGB de oito bits cada. Essa composição permite a representação de mais de 16 milhões de cores.

As imagens de profundidade são diferentes das imagens convencionais pois apresentam uma terceira informação que é a distância entre a câmera e a cena analisada, ou seja, com este tipo de imagem pode-se obter uma percepção de profundidade. Na Figura 4a observa-se um exemplo de imagem (matriz) de profundidade, onde cada ponto representa o valor de distância capturado de uma cena pela câmera. Dessa forma, se a imagem for plotada (Figura 4b), observa-se a projeção de um objeto.

0	0	0	0	0	0	0	0	0	0	0
0	0	0	0	0	0	0	0	0	0	0
0	0	80	80	80	80	80	80	80	0	0
0	0	80	140	140	140	140	140	80	0	0
0	0	80	140	160	200	160	140	80	0	0
0	0	80	140	160	200	160	140	80	0	0
0	0	80	140	140	140	140	140	80	0	0
0	0	80	80	80	80	80	80	80	0	0
0	0	0	0	0	0	0	0	0	0	0
0	0	0	0	0	0	0	0	0	0	0

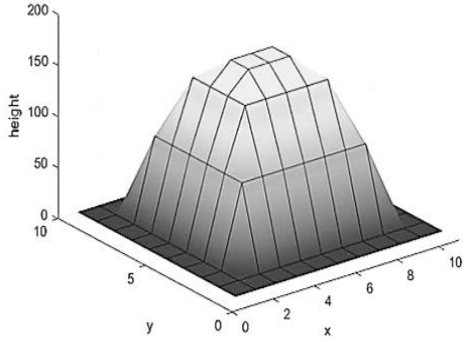

Figura 4. (a) Exemplo de uma matriz de profundidade representando a distância capturada pela câmera de profundidade da cena observada. (b) A matriz (imagem) de profundidade plotada em três dimensões.

As imagens de profundidade têm sido consideradas como um importante avanço para as técnicas de visão computacional nos últimos anos, uma vez que auxiliam nos processos de aprendizagem computacional ao permitir que as máquinas visualizem o mundo da mesma forma que os humanos enxergam, por uma perspectiva tridimensional.

Existem diversas câmeras comerciais de profundidade que estão sendo estudadas para o desenvolvimento sistemas automáticos de monitoramento na produção animal. Os tipos de tecnologias utilizadas por estes sensores podem ser divididos em três princípios diferentes: estereoscopia, luz estruturada e tempo de voo (ToF) (Condotta et al., 2020). Condotta et al. (2020) comparou estas diferentes technologias em ambientes abertos e fechados e indicou que a ToF é a melhor para ser utilizada em ambientes internos.

Apesar da tecnologia ser promissora, estes sensores estão sujeitos a erros de distorção de forma, zonas não legíveis e ruídos de medição de distância que afetam a precisão e a estabilidade dos dados coletados. Estes erros podem ser consequência de diferentes fontes como o ambiente, o tipo de tecnologia e de propriedades intrínsecas de cada câmera.

Os diferentes sensores ToF disponíveis no mercado e que apresentam variação nas suas especificações. Assim, os processos de teste e validação das diferentes tecnologias são importantes para garantir que os sensores coletem informações precisas e para a escolha do sensor que melhor se adapte a cada tipo de coleta de dados.

2.8 Câmeras de profundidade do tipo ToF

As câmeras de profundidade do tipo ToF são sensores capazes de medir a profundidade de cada ponto da cena, iluminando-a com uma luz infravermelha modulada (ou fonte de LED) e analisando o sinal que é refletido (Hourad et al., 2016). De acordo com o atraso da fase calculado entre as ondas de emissão e reflexão e a velocidade da luz, é possível calcular a distância da câmera para cada ponto da cena observada (eq. 1).

$$d = \frac{c*\varphi}{4*\pi*f_m} \quad (1)$$

d = Distância

c = Velocidade da luz

φ = Diferença de fase entre a onda emitida e refletida

f_m = Frequência modulada

A Figura 5 mostra um gráfico com a quantidade de documentos publicados por ano com a palavra chave "*depth sensor*". Após o ano de 2010 houve um grande salto no número de artigos publicados sobre tecnologias relacionadas a sensores de profundidade. Os avanços em microeletrônica, micro-óptica e micro-tecnologia permitiram o avanço das câmeras ToF a partir de 1990 (Foix, Alenyà e Torras, 2011).

O ano de 2010 está relacinado ao lançamento da câmera Kinect da Microsoft para video games. Antes deste período outros sensores de detectção de profundidade eram utilizados, como os scanner lasers, por exemplo, mas a grande diferença que este tipo de tecnologia trouxe foi combinar um grande campo de visão, capaz de cobrir toda a cena, com sensores de movimento. Na zootecnia de precisão, este tipo de tecnologia pode trazer muitas contribuições, uma vez que a forma do animal, seu movimento e localização no ambiente são dados que podem fornecer informações importantes sobre a produtividade e estado de saúde dos animais.

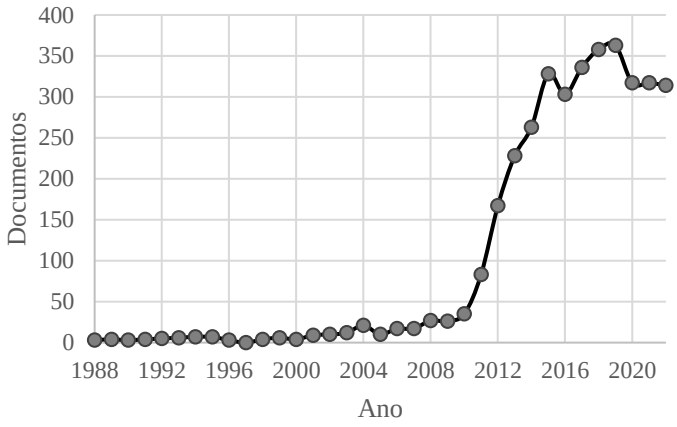

Figura 5. Número de artigos publicados até 2022 com a palavra-chave "depth sensor". Fonte: Scopus, 2023.

Os sensores com a tecnologia ToF permitem a captura de imagens de objetos com diferentes texturas e até o mapeamento em ambientes escuros. Além disso, em comparação com outros tipos de tecnologias, as cameras ToF são de baixo custo, permitem maior distância de trabalho e requerem baixa capacidade de processamento por softwares, o que viabiliza a aplicabilidade em tempo real.

Entre as desvantagens, estas câmeras apresentam erros que podem ser observados nas imagens por meio de distorções da forma dos objetos, regiões não legíveis e também pela falta de repetição dos valores de profundidade registrados ao longo do tempo. Em um sistema automático de monitoramento animal por meio de imagens, estes erros podem influenciar a detecção de objetos em pontos da cena, a recriação tridimensional do animal, importante na detecção de posturas e e estimativa de peso, e na comparação de cenas subsequentes, importante para monitorar o deslocamento dos animais no ambiente, pela falta de estabilidade dos dados.

A própria tecnologia ToF possui grande influência nos erros observados nos dados de profundidade. Como o valor de profundidade registrado depende da luz refletida pelos objetos na cena, fatores como a refletividade dos objetos, a distância da câmera, a luz ambiente e as propriedades intrínsecas das câmeras (e.g. resolução, frequência de modulação e poder de iluminação) podem afetar o sinal que é captado pelos sensores (Fang et al., 2020).

Entre os erros não controlados, chamados não sistemáticos, os que são comumente encontrados nas imagens de profundidade coletadas com as cameras ToF são erros de dispersão de luz, erros de caminhos múltiplos da luz e ambiguidade nas bordas dos objetos. O erro de dispersão

da luz está relacionado à baixa sensibilidade do sensor que, devido à reflexão de objetos próximos à imagem, introduzem distorções nos valores de profundidade em outras regiões. O erro de caminhos múltiplos da luz ocorre quando há a sobreposição de sinais infravermelhos refletidos e afetam o valor de profundidade calculado em um pixel do sensor. Este erro afeta principalmente regiões côncavas de objetos, causando distorções. A ambigüidade na borda de objetos ocorre quando os pixels próximos ao limite entre dois planos dão origem a distorções na estrutura tridimensional do objeto.

Apesar da aleatoriedade destes erros, algumas técnicas de calibração, processamento dos sinais de luz e repetição de medições podem ser utilizadas para melhorar e acurácia dos dados coletados e podem variar de acordo com a câmera utilizada. Assim, endender as dificuldades e vantagens da tecnologia e comparar diferentes câmeras ToF, pode auxiliar na escolha da melhor opção de uso, de acordo com cada tipo de problema e configuração experimental.

3 REFERÊNCIAS

Avila, A. S. de, Jácome, I. M. T. D., Faccenda, A., Panazzolo, D. M., & Müller, É. R. (2013). Avaliação e correlação de parâmetros fisiológicos e índices bioclimáticos de vacas holandês em diferentes estações. *Revista Eletrônica Em Gestão, Educação e Tecnologia Ambiental*, *14*(14), 2878–2884. https://doi.org/10.5902/2236117010747

Baxter, E. M., Lawrence, A. B., & Edwards, S. A. (2011). Alternative farrowing systems: Design criteria for farrowing systems based on the biological needs of sows and piglets. *Animal*, *5*(4), 580–600. https://doi.org/10.1017/S1751731110002272

Baxter, Emma M., Adeleye, O. O., Jack, M. C., Farish, M., Ison, S. H., & Edwards, S. A. (2015). Achieving optimum performance in a loose-housed farrowing system for sows: The effects of space and temperature. *Applied Animal Behaviour Science*, *169*, 9–16. https://doi.org/10.1016/j.applanim.2015.05.004

Brown-Brandl, T. M., Rohrer, G. A., & Eigenberg, R. A. (2013). Analysis of feeding behavior of group housed growing-finishing pigs. *Computers and Electronics in Agriculture*, *96*, 246–252. https://doi.org/10.1016/j.compag.2013.06.002

Chen, C., Zhu, W., Steibel, J., Siegford, J., Wurtz, K., Han, J., & Norton, T. (2020). Recognition of aggressive episodes of pigs based on convolutional neural network and long short-term memory. *Computers and Electronics in Agriculture*, *169*(October 2019), 105166. https://doi.org/10.1016/j.compag.2019.105166

Chidgey, K. L., Morel, P. C. H., Stafford, K. J., & Barugh, I. W. (2015). Sow and piglet productivity and sow reproductive performance in farrowing pens with temporary crating or farrowing crates on a commercial New Zealand pig farm. *Livestock Science*, *173*, 87–94. https://doi.org/10.1016/j.livsci.2015.01.003

Condotta, I. C. F. S., Brown-Brandl, T. M., Pitla, S. K., Stinn, J. P., & Silva-Miranda, K. O. (2020). Evaluation of low-cost depth cameras for agricultural applications. *Computers and Electronics in Agriculture*, *173*(April), 105394.

https://doi.org/10.1016/j.compag.2020.105394
Galiot, L., Lachance, I., Laforest, J. P., & Guay, F. (2018). Modelling piglet growth and mortality on commercial hog farms using variables describing individual animals, litters, sows and management factors. *Animal Reproduction Science*, *188*(July 2017), 57–65. https://doi.org/10.1016/j.anireprosci.2017.11.009
Glencorse, D., Plush, K., Hazel, S., D'souza, D., & Hebart, M. (2019). Impact of non-confinement accommodation on farrowing performance: a systematic review and meta-analysis of farrowing crates versus pens. *Animals*, *9*(11). https://doi.org/10.3390/ani9110957
Hales, J., Moustsen, V. A., Nielsen, M. B. F., & Hansen, C. F. (2014). Higher preweaning mortality in free farrowing pens compared with farrowing crates in three commercial pig farms. *Animal*, *8*(1), 113–120. https://doi.org/10.1017/S1751731113001869
Johnson, A. K., Morrow-Tesch, J. L., & McGlone, J. J. (2001). Behavior and performance of lactating sows and piglets reared indoors or outdoors. *Journal of Animal Science*, *79*(10), 2571–2579. https://doi.org/10.2527/2001.79102571x
Jorquera-Chavez, M., Fuentes, S., Dunshea, F. R., Warner, R. D., Poblete, T., Unnithan, R. R., Morrison, R. S., & Jongman, E. C. (2021). Using imagery and computer vision as remote monitoring methods for early detection of respiratory disease in pigs. In *Computers and Electronics in Agriculture* (Vol. 187, p. 106283). https://doi.org/10.1016/j.compag.2021.106283
King, R. L., Baxter, E. M., Matheson, S. M., & Edwards, S. A. (2019). Temporary crate opening procedure affects immediate post-opening piglet mortality and sow behaviour. *Animal*, *13*(1), 189–197. https://doi.org/10.1017/S1751731118000915
Lambertz, C., Petig, M., Elkmann, A., & Gauly, M. (2015). Confinement of sows for different periods during lactation: Effects on behaviour and lesions of sows and performance of piglets. *Animal*, *9*(8), 1373–1378. https://doi.org/10.1017/S1751731115000889
Lecun, Y., Bengio, Y., & Hinton, G. (2015). Deep learning. *Nature*, *521*(7553), 436–444. https://doi.org/10.1038/nature14539
Leonard, S. M., Xin, H., Brown-Brandl, T. M., Ramirez, B. C., Johnson, A. K., Dutta, S., & Rohrer, G. A. (2021). Effects of farrowing stall layout and number of heat lamps on sow and piglet behavior. *Applied Animal Behaviour Science*, *239*. https://doi.org/10.1016/j.applanim.2021.105334
Liu, L., Tai, M., Yao, W., Zhao, R., & Shen, M. (2021). Effects of heat stress on posture transitions and reproductive performance of primiparous sows during late gestation. *Journal of Thermal Biology*, *96*(November 2020), 102828. https://doi.org/10.1016/j.jtherbio.2020.102828
Loftus, L., Bell, G., Padmore, E., Atkinson, S., Henworth, A., & Hoyle, M. (2020). The effect of two different farrowing systems on sow behaviour, and piglet behaviour, mortality and growth. *Applied Animal Behaviour Science*, *232*(September), 105102. https://doi.org/10.1016/j.applanim.2020.105102
Marchant, J. N., Broom, D. M., & Corning, S. (2001). The influence of sow behaviour on piglet mortality due to crushing in an open farrowing system. *Animal Science*, *72*(1), 19–28. https://doi.org/10.1017/S135772980005551X
Marsot, M., Mei, J., Shan, X., Ye, L., Feng, P., Yan, X., Li, C., & Zhao, Y. (2020). An adaptive pig face recognition approach using Convolutional Neural Networks. *Computers and Electronics in Agriculture*, *173*(April), 105386. https://doi.org/10.1016/j.compag.2020.105386
Meckbach, C., Tiesmeyer, V., & Traulsen, I. (2021). A promising approach towards precise

animal weight monitoring using convolutional neural networks. *Computers and Electronics in Agriculture*, *183*(February), 106056. https://doi.org/10.1016/j.compag.2021.106056

Morota, G., Ventura, R. V., Silva, F. F., Koyama, M., & Fernando, S. C. (2018). Big data analytics and precision animal agriculture symposium: Machine learning and data mining advance predictive big data analysis in precision animal agriculture. *Journal of Animal Science*, *96*(4), 1540–1550. https://doi.org/10.1093/jas/sky014

Okinda, C., Sun, Y., Nyalala, I., Korohou, T., Opiyo, S., Wang, J., & Shen, M. (2020). Egg volume estimation based on image processing and computer vision. *Journal of Food Engineering*, *283*(March), 110041. https://doi.org/10.1016/j.jfoodeng.2020.110041

Porto, S. M. C., Arcidiacono, C., Anguzza, U., & Cascone, G. (2015). The automatic detection of dairy cow feeding and standing behaviours in free-stall barns by a computer vision-based system. *Biosystems Engineering*, *133*, 46–55. https://doi.org/10.1016/j.biosystemseng.2015.02.012

Q. Zhang, & H. Xin. (2005). Resting Behavior of Piglets in Farrowing Crates Equipped With Heat Mats. *Applied Engineering in Agriculture*, *21*(6), 1067–1071. https://doi.org/10.13031/2013.20032

Rodríguez Alvarez, J., Arroqui, M., Mangudo, P., Toloza, J., Jatip, D., Rodríguez, J. M., Teyseyre, A., Sanz, C., Zunino, A., Machado, C., & Mateos, C. (2018). Body condition estimation on cows from depth images using Convolutional Neural Networks. *Computers and Electronics in Agriculture*, *155*(December 2017), 12–22. https://doi.org/10.1016/j.compag.2018.09.039

Schild, S. L. A., Baxter, E. M., & Pedersen, L. J. (2020). A review of neonatal mortality in outdoor organic production and possibilities to increase piglet survival. *Applied Animal Behaviour Science*, *231*(November 2019), 105088. https://doi.org/10.1016/j.applanim.2020.105088

Sharma, N., Jain, V., & Mishra, A. (2018). An Analysis of Convolutional Neural Networks for Image Classification. *Procedia Computer Science*, *132*(Iccids), 377–384. https://doi.org/10.1016/j.procs.2018.05.198

Silva, C. C. B. ; Santos, J. V. ; Oliveira, D. C. G. ; Sardinha, E. J. S. ; Savastano Junior, H. ; Martello, L. S. ; Sousa, Rafael Vieira de . Construção de um algoritmo de classificação de comportamento de suínos utilizando vídeo-imagens. In: V Workshop Internacional de Ambiência de Precisão, 2019, Campinas. V Workshop Internacional de Ambiência de Precisão. Campinas, 2019. v. 2019. p. 94-96.

Tian, M., Guo, H., Chen, H., Wang, Q., Long, C., & Ma, Y. (2019). Automated pig counting using deep learning. *Computers and Electronics in Agriculture*, *163*(September 2018), 104840. https://doi.org/10.1016/j.compag.2019.05.049

Viazzi, S., Bahr, C., Schlageter-Tello, A., Van Hertem, T., Romanini, C. E. B., Pluk, A., Halachmi, I., Lokhorst, C., & Berckmans, D. (2013). Analysis of individual classification of lameness using automatic measurement of back posture in dairy cattle. *Journal of Dairy Science*, *96*(1), 257–266. https://doi.org/10.3168/jds.2012-5806

Wischner, D., Kemper, N., Stamer, E., Hellbruegge, B., Presuhn, U., & Krieter, J. (2009). Characterisation of sows' postures and posture changes with regard to crushing piglets. *Applied Animal Behaviour Science*, *119*(1–2), 49–55. https://doi.org/10.1016/j.applanim.2009.03.002

Yun, J., Han, T., Björkman, S., Nystén, M., Hasan, S., Valros, A., Oliviero, C., Kim, Y., & Peltoniemi, O. (2019). Factors affecting piglet mortality during the first 24 h after the onset of parturition in large litters: Effects of farrowing housing on behaviour of postpartum sows.

Animal, *13*(5), 1045–1053. https://doi.org/10.1017/S1751731118002549

Zhang, Q., & Xin, H. (2001). Responses of piglets to creep heat type and location in farrowing crate. *Applied Engineering in Agriculture*, *17*(4), 515–519.

Zheng, C., Zhu, X., Yang, X., Wang, L., Tu, S., & Xue, Y. (2018). Automatic recognition of lactating sow postures from depth images by deep learning detector. *Computers and Electronics in Agriculture*, *147*(August 2017), 51–63. https://doi.org/10.1016/j.compag.2018.01.023

Zhu, X., Chen, C., Zheng, B., Yang, X., Gan, H., Zheng, C., Yang, A., Mao, L., & Xue, Y. (2020). Automatic recognition of lactating sow postures by refined two-stream RGB-D faster R-CNN. *Biosystems Engineering*, *189*, 116–132. https://doi.org/10.1016/j.biosystemseng.2019.11.013

4. CAPÍTULO II: Avaliação de gaiolas de parto alternativas no desempenho de leitões antes do desmame

Este capítulo faz parto do artigo “Evaluation of the litter's performance until weaning in alternative farrowing stalls” que será submetido para a revista Livestock Science.

Abstract

Piglet mortality during the lactation period is a concern for swine production and is a consequence of a set of complex interactions between sow, piglet, environmental, and management factors. While crushing by the sow may be the ultimate cause of piglet mortality, there are many factors influencing the outcome, including parity, thermal stress, and animal housing systems. New farrowing systems are continuously being developed; however, it is difficult for producers to make decisions without any basis. Thus, the main objective of this study was to evaluate the impact of different farrowing stall layouts on the performance trait of piglets. A total of 546 sows and 9123 piglets were monitored during 36 lactation cycles. The sows were a randomly assigned to three types of farrowing stalls layouts (standard, diagonal, and offset) in three rooms (20 sows by room). All farrowing stalls had the same space allocations (2.7 m by 1.8 m– and 2.1 m by 0.6 m for the sow area). The three types of farrowing stalls were blocked by the positioning within the room. Piglet performance traits (percent of stillborns, percent of mortality, percent of overlays, and average daily weight gain (ADG) and sows (health and parity) were monitored according to the standard operating procedures of the US Meat Animal Research Center (USMARC). The results indicated treatment, parity, and season effects on some piglet performance traits. The offset farrowing stall presented a lower percentage of stillborns than the standard. No differences were found in the performance traits between the diagonal crate and the other treatments. P1 sows presented lower ADG than P2, P3, and P4 sows. Autumn and Summer presented higher PO values than Spring and Winter, and Summer presented lower ADG values than the other seasons. The study concluded that the adoption of farrowing stall systems with the confinement of sows further away from the heating source can be an alternative to conventional farrowing stalls for the reduction of the percent of overlays in sows with mortalities above 2 piglets. In addition, the influence of the season on the piglet production traits demonstrated the importance of proper management of the environment, even in systems with a certain level of temperature control. Further studies associating heat stress, behavior and performance traits of the animals can

contribute to better investigate the proposed systems and to explain the effects found for parity and season on piglet production performance.

4.1 Introduction

One of the biggest problems in swine production is the mortality of piglets, especially due to the crushing by sows during the lactation period. Mortality before weaning is both an economic indicator and a reflection of the welfare state of the animals. There are several factors associated with piglet performance, and among these factors are the sow parity, climatic variables, and housing systems.

Traditional farrowing stalls with the sow crated were created in the 60's with the main objective of improving the animal well-being and reducing piglet mortality by crushing (King et al., 2019; Loftus et al., 2020). In addition, these farrowing stalls bring other benefits, such as space saving and improved management of feed and sanitary conditions. Despite these benefits, these types of systems are not fully effective in preventing mortality by crushing since the reduced resting space, and the proximity of the sow area for the piglets cannot accommodate them efficiently and put them at risk of mortality by crushing.

Previous studies have demonstrated significant differences in the performance of piglets between farrowing stalls with or without crates, indicating that sow confinement reduces piglet mortality (Chidgey et al., 2015; Yun et al., 2019). Marchant et al. (2001) studied the influence of sow behavior on piglet mortality due to crushing in farrowing systems without the confinement of the sow and reported a high piglet mortality (25%) during the first week of lactation. In another study, Heidinger et al. (2022) investigated the mortality of piglets in different types of farrowing stalls and found that the live born piglet mortality was lower in confined sows (up to 13.7%), than in sows without confinement (17.4%). The authors also mentioned that more research is needed on different design criteria in the same type of farrowing stalls, since the types studied varied not only in design, but also in the construction materials and equipment used, which can interfere with the performance of the animals.

Leonard et al. (2021a) studied the impact of traditional farrowing stalls, stalls with expanded piglet resting areas, and stalls with expanded sow and piglet areas on piglet performance. No differences were found between treatments regarding the number of piglets born, the number of overlays, and the number live at birth. The authors mentioned that additional studies on the

quality and usability of the space should also be considered, in addition to the amount of space available in the farrowing pens.

Some studies have mentioned that high sow parity is related to high mortality rates and piglet weight gain, as these sows are more likely to be older, have less muscle control, are more likely to farrow over a longer period of time and risk suffering from exhaustion (Galiot et al., 2018; Schild et al., 2020). High parity sows also tend to have larger and less uniform litters which causes weaker piglets to remain closer to the sows, increasing the risk of death by crushing (Liu et al., 2022). Rangstrup-Christensen et al. (2018) studied parity as a risk factor for mortality and crushing of piglets in outdoor organic systems and found a higher mortality risk for piglets raised by older sows.

Climatic factors are also associated with piglet mortality due to crushing. Overall, studies show that there is a positive association between environmental factors and piglet performance (Wegner et al., 2014; Liu et al., 2021). Despite this, this influence may not be direct, especially in controlled environments, where system management plays an important role in the microenvironment of the animals. An indoor environment presents a certain control of the climatic conditions and the social components that are associated to the animals throughout the production period, but the environment cannot be prescribed by a set of standards, because there is a combination of management factors, nutrition, animal health, stress at birth that influence the performance of these animals and are in constant change from birth to 8 weeks of life (Ramirez et al., 2022). A simple example of the challenge in managing the environment can be observed in the control of the piglet heating systems. During the colder seasons, piglets tend to suffer from lower temperatures and seek to warm up close to the sow, increasing the risk of death by crushing. On the other hand, the hottest seasons tend to be uncomfortable for sows. Hyperthermia can, for example, prolong labor and influence piglet mortality before birth. The quality and quantity of breast milk can also be affected, as they are directly related to the nutritional status of the sows, which, due to thermal discomfort, tend to reduce food and water intake. In addition, thermal discomfort affects the frequency and duration of postural changes in sows (Schild et al., 2020), which is directly related to their availability for suckling and the crush rate of piglets. Normally, in controlled environments, the temperature in the lactation room is kept within favorable limits for the sows and a heating source is offered to the piglets. However, other factors can affect these

microenvironments created for each one. Ventilation and humidity, for example, can change according to the season and the handling of windows and doors.

L. Rangstrup-Christensen et al. (2018) studied season as a risk factor for early piglet mortality and crushing and found a lower risk of mortality during spring and a higher risk during summer. Leonard et al. (2021) studied the use of one or two lamps to provide additional heat to piglets in farrowing stalls. The authors found a 20% increase in the use of the heating area by piglets when two heating lamps were provided in the environment. Regarding sows, the use of two heat lamps provided a small increase in lying behavior.

These studies demonstrate that there are several factors that can influence the performance of sows and piglets in the farrowing system. Furthermore, it is important to continue evaluating the performance of piglets in farrowing systems, whether with or without crates, because such information can help to find better solutions for this phase, to obtain balanced responses between welfare and economic viability of the production systems. In this context, studying the litter performance traits in new designs can help identify systems that are increasingly sustainable and in line with consumer demand.

In addition to the aforementioned works, which studied different systems and sizes of farrowing pens and different confinement periods for sows, it would be interesting to investigate different configurations of farrowing stalls, with the same size and construction materials, and their impact on litter performance traits. Changing the position of the sow's confinement area in the pen can promote different free resting areas for the piglets and modify the microclimate of the sow, which may be further away from the piglets' heat source. Thus, the objectives of the present study were to evaluate the effect of different farrowing stall layouts on piglet performance after accounting for the impacts of season and parity. The hypothesis is that the new arrangements can improve their performance by promoting a larger resting area for piglets and placing sows further away from the piglet heating source.

4.2 Material and Methods

This study was conducted between January 2020 to May 2021at the USDA-ARS U.S. Meat Animal Research Center (USMARC) in accordance with federal and institutional regulations regarding proper animal care practices and were approved by the Institutional Animal Care and Use Committee of the US Center for Animal Research (2015-21) (IACUC approval: 1837).

A total of 546 sows and 9123 piglets were housed in three types of farrowing pens that differed in sow crate location (treatments). The animals were randomly distributed and monitored during 36 lactation cycles and the following piglet production parameters were collected: percent of stillborns, percent of overlays, percent of mortality and average daily weight gain.

4.2.1 Location and facilities

The experiment was conducted at the US Department of Agriculture - Agricultural Research Service - US Meat Animal Research Center in Clay Center, Nebraska, USA, located at 40°31'27.39"N,98°7'56, 69 " W. The collections were carried out in a farrowing facility where the sows were stalled individually in three rooms with a capacity of 20 animals each, totaling 60 farrowing stalls.

Inside the rooms, the animals were distributed in two rows of ten pens, so that the animals in one row faced the animals in the other row at 1.2 m distance. The building was climate controlled with a hallway to precondition the air. The air temperature inside the rooms starts around 25 °C and was gradually reduced to 20 °C at the end of the lactation cycle. When the room temperature was high, the system incorporated evaporative cooling. Then deflectors allowed fresh air into the rooms whenever the exhaust fans were turned on the opposite wall. During the winter, the hallway shutters were manually closed, and fresh air was then supplied through an air duct suspended from the ceiling the entire length of each room with openings at each sow space. However, in periods of low air temperatures, the supplemental forced air heaters preheat the air in the hallway. Additionally, 10 cm radiate tube heaters were placed directly above the farrowing stalls.

The installation consisted of individual feeding troughs (Sow Max AdLib Sow Feeder – Hog Slat) that were arranged in the direction of the central corridor of each room. Two nipple drinks supplied water ad libitum to both sows and piglets.

The flooring was a 1 cm wide – T-slat through the space. The waste management was handled using a shallow pit and a manual flush system using a 1,900 L manual water dump for each 10 crates that operated twice a day.

4.2.2 Farrowing stall layouts

The farrowing stalls had the same size regardless of the treatments with 1.83 m (L) × 2.5 m (C) × 1.2 m (A), and the sow confinement area was 0.61 m (L) x 2.14 m (C) x 1,50 m (A). The entire floor area was found to be metal slats, with a slat width of 8.5 mm and a gap of 9.5 mm between the slats (TriDEK, Hog Slat, Inc.; Newton Grove, NC, USA). The slats had non-slip grip cutouts and were the same throughout the entire pen. A rubber mat was placed under the heat lamp area. The treatments involved three types of farrowing stalls (standard, diagonal, and offset) differentiated by the positioning of the sow crate in the area. For the standard configuration, the sow crate was placed in the middle of the stall; in diagonal configuration, the sow crate was placed diagonally in the stall, and in the offset configuration the crate was rearranged to the side of the stall. The farrowing stall configurations are shown in Figure 1.

Supplemental heating for the piglets had a 175 W ceramic infrared lamp placed over a rubber mat (1.14 x 0.32 m) positioned at the rear of each pen. Each lamp was covered by metal lamp protectors and suspended so that the average temperature on the mat was around 36 °C. The heat lamps started operating approximately two days before the expected farrowing date and remained on until the piglets were approximately 21 days old. All lamps operated connected to a thermostat which automatically turned off if the ambient air temperature exceeded 5.5 °C above the nominal ambient temperature (approximately 25 °C).

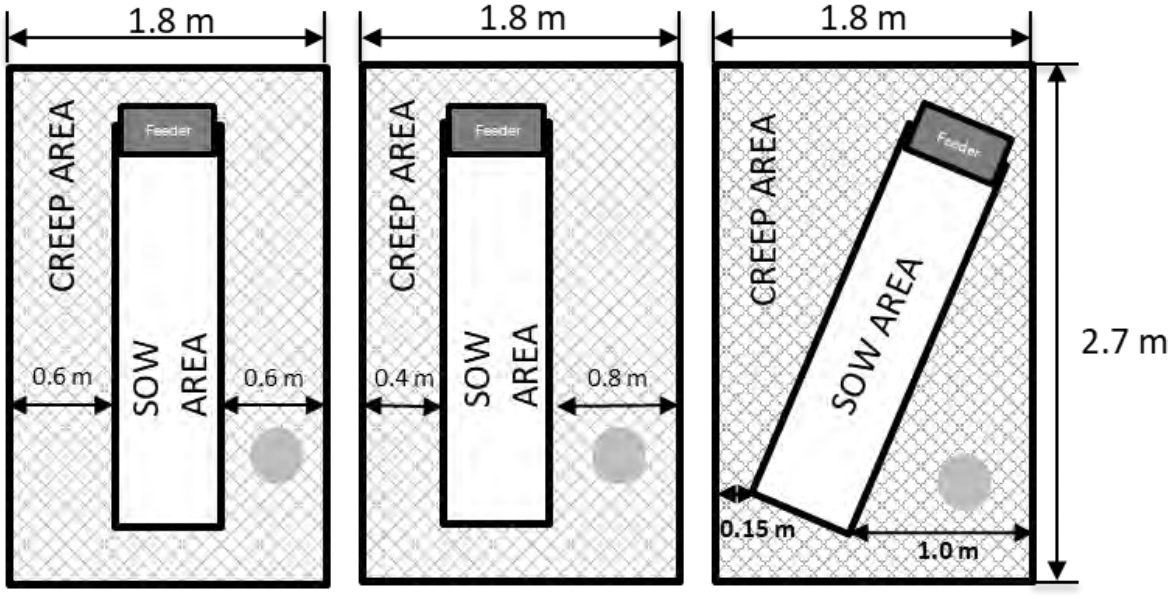

Figure 6. Three experimental farrowing stall layouts used in the experiment: (A) standard stall layout, (B) offset, and (C) diagonal. Piglets could circulate throughout the all the stall (creep area)

and the sows movements were limited to an area of 2.1 m by 0.6 m (sow area). All dimensions are in meters.

The treatments were present in the same number and were randomly distributed within the rooms. Positions were maintained throughout the experiment and all available stalls were used for data collection (Figure 2).

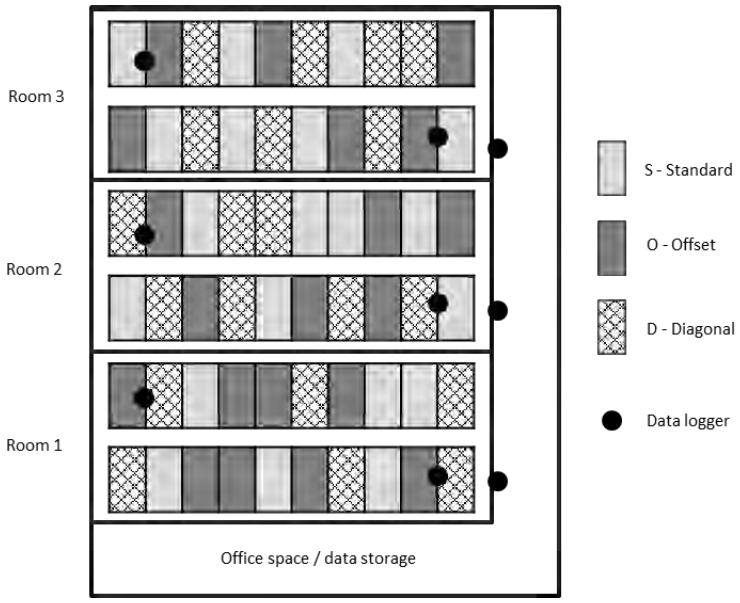

Figure 7. Experimental layout for all cycles. Layout treatments were assigned to a stall so that each position had the same number of treatments tested. Heat lamps were placed in the back part of the stalls for all treatments.

4.2.3 Animals and management

The experiment had 36 data collection cycles. In each cycle, a group of up to 20 pregnant sows (Landrace x Yorkshire) of different parities (parity 1 (P1), parity 2 (P2), parity 3 (P3), and parity 4 (P4)) were monitored for 32 days. After this period, the group left the room, which was cleaned and disinfected for another group of 20 sows to enter the study. Each group of sows in the room represented a cycle. The mean weight of the sows was 191.84 ± 29.79 kg, and the mean number of piglets born was approximately 13.96 ± 3.91 animals/sow. Some sows entered the experiment more than once.

The sows were fed with a corn-soy ration once a day for up to three days after farrowing and then ad libitum feed was provided. Feed was also provided to piglets from approximately 21

days of age until weaning at 28 days. Drinking water was provided as ad libitum to piglets and sows using two nipple drinkers.

Trained animal caretakers followed standard operating procedures: drying mineral powder was distributed onto the mats under supplemental heat lamps; piglets were weighed and ear-tagged on the first day; tails docked, needle teeth clipped, castration and iron injections were administered to the piglets three days after birth. As necessary for achieving consistent litter sizes, cross-fostering of piglets was carried out.

More details of materials and handling practices commonly used in the facilities where the experiment was conducted can be found in (Leonard et al., 2020)..

4.2.4 Data collection

4.2.4.1 Characterization of the climate environment

To monitor the microclimate of the installation, two data loggers (XR440, Pace Scientific, Boone, NC, USA) were installed in each of the rooms suspended 1.2 m from the floor. One data logger was installed over the first stalls at the hallway end of the room and the other at the opposite end of the room where ventilation fans resided. These devices automatically collect relative air humidity and dry bulb temperature data throughout the experiment, 24 hours a day, recording data every 5 minutes. From these data, the software also provided the dew point temperature.

4.2.4.2 Production data

Trained caretakers recorded all important information related to the production and health of the sows and piglets. Thus, litter performance traits were collected on each litter and included: number born, number live at birth, number of mummies, number of stillborns, number overlays, other causes of death (euthanasia), total mortality, and total weaned by sow. Piglets were weighed individually 24 hours after birth and one day before weaning. In addition, the lactation period was accounted for. With this information, the percent of stillborns (PS), percent of overlays (PO), pre weaning mortality (PWM), and average daily weight gain (ADG), were calculated according to the eq. 1, 2, 3, and 4, respectively.

$$PS = \frac{Number\ of\ stillborns}{Total\ number\ of\ piglets\ born} * 100 \quad (1)$$

$$PO = \frac{Number\ of\ overlays}{Total\ number\ of\ piglets\ born \pm fostered} * 100 \quad (2)$$

$$PWM = \frac{Number\ dead}{Total\ number\ born \pm fostered} * 100 \quad (3)$$

$$ADG = \frac{Weight\ at\ weaning - Weight\ at\ birth}{\frac{Days\ of\ lactation}{Number\ of\ \ piglets\ at\ weaning}} \quad (4)$$

4.2.4.3 Statistical analysis

Preliminary data was collected to determine the number of samples required. Based on the analysis, to achieve 85% statistical power in detecting differences in the percentage of overlays between treatments, it was determined that at least 48 sows for each treatment group needed to be monitored. All collected data were organized in an electronic spreadsheet and statistically analyzed using the SAS® 9.3 software (SAS Institute Inc., Cary, NC, USA). Percentage of stillborns (PS), percentage of overlays (PO), and average daily weight gain (ADG) were the piglet performance traits investigated according to the fixed effects: farrowing stalls, parity, season, and their interactions. Sow health was used as a random effect. Total number of pigs born was included as a covariable to the PS model and total number of pigs raised by sow (litter size) to the PO, and ADG models. Since PS and PO were not normally distributed, a logarithm function was used in the transformation of the data prior to the analysis. Comparisons of means were performed by ANOVA and student t test, using the Mixed procedure at a significance level of $p < 0.10$.

An additional analysis was performed to evaluate the impact of farrowing stall layout on high-mortality litters. This analysis used only sows with PWM greater than two piglets from the data. PS, PO and ADG were compared according to treatments.

4.3 Results

4.3.1 Description of the thermal environment

During the collection period, the values of the environmental variables were close in the three where the average dry bulb temperature and the mean relative humidity were below 25 ºC

and 80%. Despite the dry bulb temperature having presented little variation, the dew point temperature varied greatly (Table 1, Figure 2).

Table 1. Mean and standard deviation (stdev) of the environmental variables and Temperature Humidity Index obtained during the experiment.Parameters obtained from the average daily values monitored during the experiment.

Parameter	Mean + stdev	Min	Max
Dry Bulb Temperature (ºC)	23.61 ± 1.28	14.72	30.42
Wet Bulb Temperature (ºC)	16.88 ± 3.03	13.90	25.20
Relative Humidity (%)	52.76 ± 4.98	26.30	97.07
Dew Point (ºC)	12.49 ± 1.53	3.30	26.78
Enthalpy (kJ/kg)	51.08 ± 10.54	41.34	82.12
Temperature Humidity Index*	69.75 ± 2.68	67.11	78.04

Temperature and Humidity Index (THI) calculated with the equation THI = 0.72(DBT+WBT)+40.6 (Thom, 1959) where the DBT is the dry bulb temperature and WBT the web bult temperature.

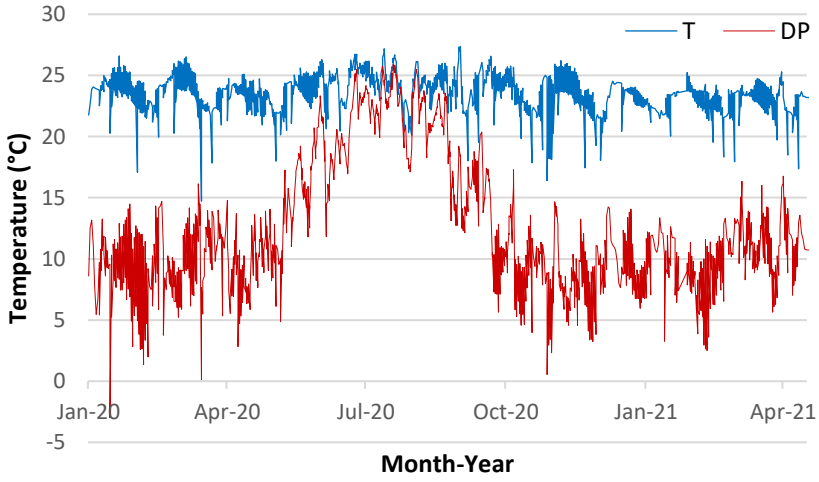

Figure 8. Air temperature (T) and dew point (DP) distribution from the data were collected on 36 cycles of sows entering the farrowing facility. Three farrowing rooms were used, and collection occurred from January 2020 to May 2021. Data represent the average daily values recorded by data loggers inside the rooms.

4.3.2 Thermal distribution in the farrowing stall layouts

To evaluate the thermal distribution in the farrowing stalls, an image was obtained with a thermal camera (FLIR) and superimposed on the three types of evaluated layouts (standard, offset, and diagonal) (Figure 4). In the images, the colors red, yellow, and green represent the highest

temperature values. These areas were warmer because of the heat lamp that provides supplemental heat to the piglets in the resting area and was closer to the sow area in the offset and diagonal treatments compared to the standard treatment.

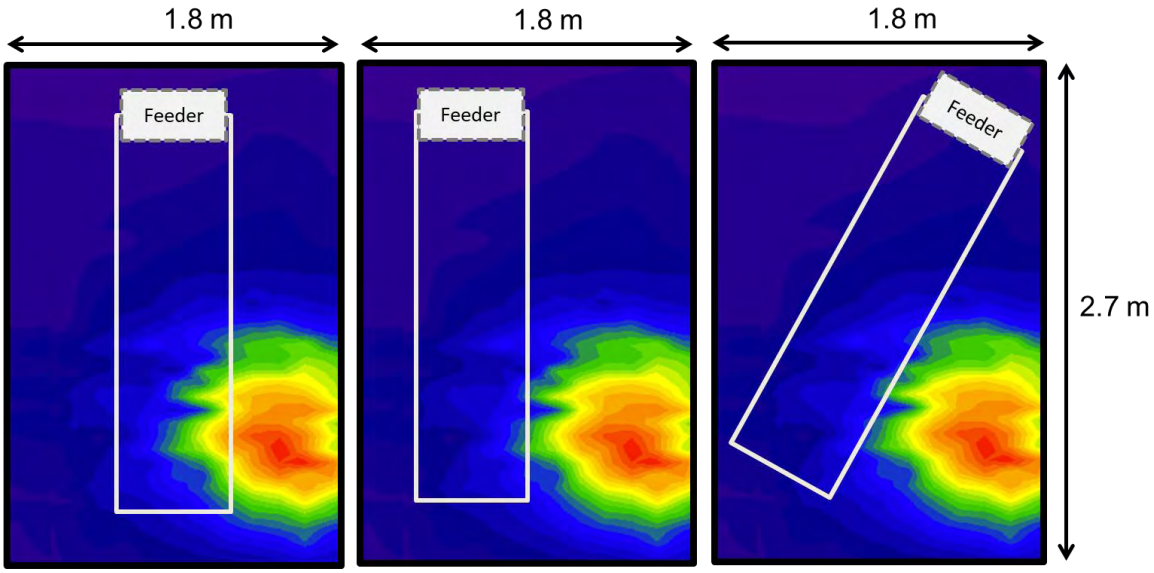

Figure 9. Thermal distribution in the farrowing stall layouts obtained with a thermal camera (FLIR).

4.3.3 Treatments and productive parameters

Litters were eliminated from the dataset due causes not associated with experimental treatments were excluded from the study (e.g., sow injuries and deaths, and change of sows between the treatments). In addition, sows with 100% stillborns and treatments with above 80% euthanized piglets were excluded from the dataset. No significant differences were found in the distribution of sow parity between treatments. Of the 651 evaluations in the study, 35.48% of the sows were P1, 30.26% P2, 19.51% P3, and 14.65% P4. A total of 9123 piglets were born and the average by treatment was 14.18 ± 3.88 (standard), 13.97 ± 3.74 (diagonal), and 13.74 ± 4.12 (offset). A summary of all production data by treatment can be seen in Table 2. A total of 9123 piglets were born and the average by treatment was 14.18 ± 3.88 (standard), 13.97 ± 3.74 (diagonal), and 13.74 ± 4.12 (offset). The PWM was above 16% for all treatments and the PO for S, D, and O was 6.02%, 5.49%, and 8.04%. respectively. In relation to the coefficient of variation, S treatment presented greater value than D and O, both for PWM (81.47%) data and for the PO (162.66%). The ADG of piglets were close for all treatments (mean = 238.23 g) but the coefficient of variation for D was lower (12.83%) than for O (13.11%) and S (14.07%).

Table 2. Summary of production data by treatment: mean, standard error (SE) and coefficient of variation (CV). Values obtained in relation to the general data collected in the experiment.

Parameter	Standard (n = 210)			Diagonal (n = 216)			Offset (n = 225)		
	Mean	**SE**	**CV**	**Mean**	**SE**	**CV**	**Mean**	**SE**	**CV**
Parity	2.18	0.07	47.62	2.08	0.07	52.05	2.15	0.07	49.39
Lactation length	26.29	0.14	7.94	26.37	0.12	6.78	26.38	0.14	8.17
Number born	14.18	0.27	27.40	13.97	0.25	26.78	13.74	0.27	29.96
Number live at birth	12.93	0.25	27.95	12.94	0.23	26.49	12.72	0.24	28.92
Litter size	11.62	0.13	15.94	11.74	0.11	13.63	11.88	0.12	14.71
Total weaned by sow	10.90	0.12	16.37	11.06	0.10	13.95	11.11	0.09	12.78
Pre weaning mortality[a]	18.83	1.06	81.47	17.77	0.95	78.96	16.99	0.84	74.03
Percent mummies[b]	2.95	0.47	231.16	1.46	0.25	255.20	1.90	0.34	265.83
Percent stillborns[c]	5.32	0.61	166.64	5.48	0.54	144.23	4.89	0.46	139.88
Percent overlays[d]	6.02	0.68	162.66	5.49	0.53	143.00	6.17	0.54	130.45
Percent other causes[e]	5.69	0.60	152.71	6.34	0.61	140.62	4.89	0.46	141.28
ADG[f]	237.79	2.31	14.07	239.62	2.09	12.83	237.27	2.07	13.11

[a] Calculated using the number of mortalities (number of mummies, number of stillborns, number of overlays, and other causes of dead) divided by number of piglets live a birth ± cross-fostered piglets;
[b] Calculated using the number of mummies divided by number of piglets born;
[c] Calculated using the number of stillborns divided by number of piglets born;
[d] Calculated using the number of overlays divided by number of piglets live a birth ± cross-fostered piglets;
[e] Calculated using the number of mortalities by other causes (diarrea, euthanasia) divided by number of piglets live at birth ± cross-fostered piglets;
[f] Calculated subtracting the piglets weight (g) at birth from weaning divided by the number of piglets at weaning, and by the days of lactation.

No interaction effects were observed between the variables farrowing stall treatments, parity, and season on productive traits (PS, PO, and ADG).

Farrowing stall treatments only presented statistical differences for PS ($p = 0.06$) with higher value for standard (5.77 ± 0.87%) in comparison with the offset treatment (5.35 ± 0.86%). Season influenced PO ($p = 0.01$), and ADG ($p = 0.0017$). PO was higher in the autumn (8.55 ± 0.84%) and summer (8.21 ± 0.95%) than spring (5.64 ± 0.77%) and winter (4.56 ± 0.71%). ADG was lower in the summer (231.6 ± 3.03 g) compared to the other seasons (mean = 243.7 ± 2.30 g). Parity affected ADG ($p < 0.0001$). Piglets from P1 showed lower ADG (218.6 ± 20.06 g) than parities parity 2 (243.9 ± 2.16 g), 3 (251.7 ± 2.65 g), and 4 (248.5 ± 3.06 g).

Table 3. Person values of the piglet performance traits (percent stillborns (PS), percent overlays (PO) and average daily gain (ADG)) by farrowing stall treatment, season, and parity. Values obtained in relation to the general data collected in the experiment.

Parameter	Treatment			Effects (p)
	Standard	Diagonal	Offset	
PS[a]	5.77 ± 0.87 a	5.60 ± 0.88 a,b	5.35 ± 0.86 b	0.06
PO[b]	7.22 ± 0.72	6.17 ± 0.75	6.63 ± 0.71	0.17
ADG[c]	237.9 ± 2.18	242.2 ± 2.19	242.0 ± 2.14	0.29
Parameter	**Season**			**Effects (p)**
	Spring	**Summer**	**Autumn**	**Winter**
PS[a]	5.34 ± 0.90	6.02 ± 1.05	4.96 ± 0.94	5.98 ± 0.85	0.11
PO[b]	5.42 ± 0.76 a	8.19 ± 0.92 b	8.55 ± 0.83 b	4.52 ± 0.70 a	0.0074
ADG[c]	243.3 ± 2.32 a	231.6 ± 3.03 b	242.0 ± 2.48 a	245.8 ± 2.10 a	0.0017
Parameter	**Parity**				**Effects (p)**
	1	**2**	**3**	**4**	
PS[a]	5.71 ± 0.83	5.31 ± 0.87	4.37 ± 0.97	6.90 ± 1.09	0.11
PO[b]	5.33 ± 0.66	6.65 ± 0.72	7.26 ± 0.85	7.45 ± 0.99	0.36
ADG[c]	218.6 ± 2.06 a	243.9 ± 2.16 b	251.7 ± 2.65 c	248.5 ± 3.06 b,c	<0.0001

[a] Calculated using the number of stillborns divided by number of piglets born;
[b] Calculated using the number of overlays divided by number of piglets live a birth ± cross-fostered piglets;
[c] Calculated subtracting the piglets weight (g) at birth from weaning divided by the number of piglets at weaning, and the days of lactation.
Data with different letter within a row differ significantly (a,b,c $P < 0.10$);

When data from sows with mortality greater than two piglets were observed (Tables 4, and 5), treatment influenced PO ($p = 0.09$) (Table 4). In this case, standard treatment presented higher PO (11.31 ± 1.07%) than the offset treatment (10.68 ± 1.14%).

Table 4. Summary of production data by treatment: mean, standard deviation (Std) and coefficient of variation (CV). Values obtained in relation to the selected data (excluding the sows with mortality less or equal to 2 piglets).

Parameter	Standard (n = 97)			Diagonal (n = 92)			Offset (n = 87)		
	Mean	SE	CV	Mean	SE	CV	Mean	SE	CV
Parity	2.29	0.11	48.01	2.26	0.12	50.31	2.43	0.11	43.85
Lactation length	26.37	0.20	7.45	26.25	0.20	7.29	26.72	0.29	7.96
Number born	16.09	0.33	20.08	16.03	0.31	18.87	16.55	0.34	19.01
Number live at birth	13.87	0.34	24.29	14.10	0.31	21.06	14.59	0.33	21.16
Litter size	11.62	0.21	17.59	11.73	0.19	15.54	12.45	0.20	15.36
Total weaned by sow	10.49	0.19	17.99	10.62	0.16	14.70	10.99	0.14	12.22
Pre weaning mortality[a]	31.40	1.29	40.464	31.29	0.98	30.08	29.95	0.87	27.23
Percent mummies[b]	4.75	0.88	181.98	2.21	0.42	184.80	3.93	0.77	183.80
Percent stillborns[c]	9.05	1.09	119.16	9.91	0.96	92.49	7.87	0.79	94.09
Percent overlays[d]	10.04	1.26	123.40	9.33	0.98	101.31	11.31	1.00	82.90
Percent other causes[e]	9.90	1.08	107.52	11.71	1.10	89.80	8.46	0.90	99.47
ADG[f]	236.37	3.28	13.67	235.54	3.09	12.59	237.17	2.99	11.75

Parameter	Treatment			Effects (p)
	Standard	Diagonal	Offset	
PS[a]	9.30 ± 1.03	9.93 ± 1.18	7.76 ± 1.09	0.13
PO[b]	11.31 ± 1.07 a	10.69 ± 1.22 a,b	10.68 ± 1.14 b	0.09
ADG[c]	235.0 ± 3.94	235.9 ± 4.43	239.5 ± 4.18	0.58

Parameter	Season				Effects (p)
	Spring	Summer	Autumn	Winter	
PS[a]	8.56 ± 1.09	9.08 ± 1.44	8.45 ± 1.37	9.89 ± 1.17	0.44
PO[b]	8.57 ± 1.11 a	14.20 ± 1.50 b	12.73 ± 1.42 b	8.07 ± 1.20 a,b	0.0006
ADG[c]	237.1 ± 4.06 a	228.1 ± 4.99 b	237.7 ± 4.99 a,b,c	244.2 ± 4.22 a,c	0.04

Parameter	Parity				Effects (p)
	1	2	3	4	
PS[a]	9.67 ± 1.23 a,c	7.99 ± 1.09 b	8.16 ± 1.48 a,b	10.20 ± 1.36 c	0.03
PO[b]	10.42 ± 1.26	11.01 ± 1.12	12.21 ± 1.53	9.93 ± 1.40	0.93
ADG[c]	215.0 ± 4.25 a	241.3 ± 4.15 b	251.7 ± 2.65 c	248.5 ± 3.06 b,c	<0.0001

[a] Calculated using the number of stillborns divided by number of piglets born;
[b] Calculated using the number of overlays divided by number of piglets live a birth ± cross-fostered piglets;
[c] Calculated subtracting the piglets weight (g) at birth from weaning divided by the number of piglets at weaning, and the days of lactation;
Data with different letter within a row differ significantly (a,b,c $P < 0.10$);

4.4 Discussion

4.4.1 Treatments and litter performance traits

Piglet performance traits are related to the performance and physiology of the animals during the lactation period. Thus, PS, PO and ADG are piglet performance traits commonly evaluated to describe the efficiency of the production system. In the present study, for the total data, the average PWM was 17.84%. The value found for PWM is lower than the 25% reported by Marchant et al. (2001) when evaluating PWM due to crushing in sows housed in free stalls during the first week of lactation and higher than the average PWM reported by Heidinger et al. (2022) (13.7%) when investigating different periods of sow confinement in farrowing pens.

It was expected with this study that the modification of the farrowing stall layouts by shifting the sows away from the heating source and promoting a greater rest-free area for piglets could improve the performance of piglets. In this study, when using the general data, no significant differences were found in PO, and ADG. The only piglet performance trait that showed a statistical difference between treatments was PS, with the offset treatment having a lower percentage of stillborns than the standard. This difference may have occurred due to the layout promoting better thermal comfort for the sows, which may have impacted the final gestation period. Despite this, physiological or behavioral parameters of the sows that could confirm this theory were not investigated in this study. Future studies evaluating such characteristics among the different proposed alternative stalls may explain this effect found. Despite differing in layouts, the treatments studied maintained an equal but expanded size in relation to a traditional farrowing stall. It would also be interesting if these same treatments were also studied in a traditional farrowing stall, which has a smaller size, to assess whether moving the sow away from the heating source would have a bigger impact on production traits.

When evaluating sows with mortality greater than 2 piglets, the evaluations show that PO was affected by treatments. A possible explanation for this could be that the selected sows had larger litters (16.2 piglets per sow), different from the general data that presented an average of 14 piglets per sow. Larger litter tends to compete for nursing space and occupy more resting areas, which can put animals at risk of crushing.

Other studies, as Leonard et al. (2021a), investigated the effect of the size of the farrowing stalls and the number of heat lamps on the performance of piglets. The authors compared traditional farrowing stalls, stalls with expanded piglet rest area, and stalls with expanded area for sows and

piglets. The authors found no differences between treatments in percentage of mortality, percentage of overlays, number of piglets born alive or in the total number of piglets weaned per sow. As in the present study, the authors found statistical differences in percent of stillborn between stall layouts. The authors mentioned that in addition to the amount of space available, the usability of the space should also be considered. As mentioned, in the present study, when this usability was considered, no significant differences were found in the litter performance traits studied between the treatments when using the general data. On the other hand, when evaluating the sows with the highest number of mortalities, the offset treatment had a lower PO than the standard one. This may indicate that, for sows with larger litters, simply modifying the farrowing stall layout, providing a larger resting area for piglets, can contribute to the reduction of mortalities due to overlays.

Moustsen et al. (2013) evaluated four different periods of sow confinement: sows released throughout the lactation period, sows crated from day 0 to 4 postpartum, sows crated from day 0 to 7 postpartum, and crated from introduction to the pen until day 7. The authors reported fewer piglet mortality when sows were confined compared with sows without any movement restraint. There was no significant difference in piglet mortality between the other confinement periods evaluated.

In addition to the mentioned studies, other studies reported that the confinement of the sow reduces piglet mortality (Chidgey et al., 2015; Yun et al., 2019). Despite the growing outcry for the adoption of systems without the confinement of sows, such studies facilitate the evaluation of different physiological and environmental aspects in the productive parameters, since these types of individual systems have a standardized system that favors the individual monitoring of animals. A consensus on the best type or management has not yet been observed, but studies with sows in crates are important to obtain information to improve the management of this system. The greatest effects on piglet performance have been observed between animals with and without confinement, with productive gains for confinement. Additionally, studies report that most mortalities occur in the first week after farrowing. This information, combined with the findings of this study, may indicate that the adoption of slightly larger farrowing systems, with confinement of sows for a shorter period and further away from the heating source, may be an alternative to the conventional farrowing stalls and a step forward for the adoption of increasingly sustainable systems. As mentioned, further studies associating the behavior and productive parameters of the animals can also contribute to a better investigation of the proposed systems. In addition, studies from the

perspective of the environment and the season of the year can provide relevant information about systems and animals.

4.4.2 Season and parity affecting litter performance traits

Sow parity and season of the year were also investigated factors on piglet performance characteristics, as studies indicate that high parity and high temperatures are directly related to reduced piglet performance. In this study, parity did not influence PS, or PO, but it did influence ADG since P1 sows had piglets with lower ADG than sows P2, P3, and P4 (Table 3). Leonard et al., (2021a) studied piglet performance between different farrowing stall treatments and found that parity influenced besides the ADG, percent of mortality, and percent of overlays. The authors mentioned that P4 sows presented higher PO than P1 and higher PM than P1 and P2. In relation to ADG, piglets from P1 sows had lower ADG than those from P2, P3 and P4.

Li et al. (2023) studied the effect of maternal behaviors (postural, nursing, defense, and sow-piglet communication) of primiparous and multiparous sows on litter weight and number of piglets crushed. The authors found that the multiparous sows showed good maternal behavior in relation to the time spent in a certain posture, feeding arrangement, care for lying down and response to the “piglets' request for help”. However, these differences did not influence litter weight and the number of crushed piglets since no differences were observed in these traits between primiparous and multiparous sows. Therefore, the better maternal ability of the multiparous sows can be an explanation for the difference in weight gain found in this study between P1 sows in relation to P2, P3, and P4. Primiparous sows tend to be more responsive to piglets and, as young, are dealing with their own development. Thus, it may be that the sows were less available for breastfeeding and, moreover, part of the energy that could be used for milk production was being used for their own development.

In this study, even in a controlled environment, the influence of the season on the PO, and ADG was verified. Autumn and Summer presented higher PO values than Spring and Winter and, summer presented higher ADG than the other seasons. One explanation for these differences could be the increase in RH in summer and autumn when evaporative cooling pads are activated to mitigate the high air temperature. The increase in RH may cause thermal discomfort in the sows and change their behavior, which, consequently, affects the performance of piglets. The quality and quantity of breast milk can be affected by hyperthermia as they are directly related to the

nutritional status of the sows, which, in thermal discomfort, tend to reduce food and water intake. In addition, it can affect the frequency and duration of postural changes in sows (Schild, Baxter, and Pedersen, 2020), which is directly related to their availability for suckling and the crushing rate of piglets.

Another explanation for the increase in PO in autumn and summer may be due to piglets being less likely to seek the heating area during warmer ambient temperatures. This makes them more vulnerable to being crushed when they rest in areas closer to the sow. Additionally, the management of windows also directly influences the heat flow in the environment. In this study, the temperature amplitude of the environment was greater in autumn than in other periods. Thus, if the windows are not closed and opened correctly, low temperatures may flow over the piglets, which seek to warm up closer to the sows.

Studying the behavior of sows, piglet location, and assessing stress are important and complementary information that should be studied in future studies.

4.5 Conclusion

The aim of this study was to evaluate the effect of different farrowing stall layouts, parity, and season on the piglet performance traits before weaning. The offset farrowing stall presented a lower percentage of stillborns than the standard and lower percent of overlays when evaluating sows with higher number of mortalities. P1 sows presented lower ADG than P2, P3, and P4 sows. Autumn and Summer presented higher percent of overlays than Spring and Winter, and Summer presented lower ADG values than the other seasons. Further studies associating heat stress, behavior and performance traits of the animals can contribute to better investigate the proposed systems and to explain the effects found for parity and season on piglet production performance.

Acknowledgement

Mention of trade names or commercial products in this publication is solely for the purpose of providing specific information and does not imply recommendation or endorsement by the USDA. The USDA prohibits discrimination in all its programs and activities on the basis of race, color, national origin, age, disability, and where applicable, sex, marital status, familial status, parental status, religion, sexual orientation, genetic information, political beliefs, reprisal, or because all or

part of an individual's income is derived from any public assistance program (Not all prohibited bases apply to all programs). USDA is an equal opportunity employer.

This study was financed in part by the Coordenação de Aperfeiçoamento de Pessoal de Nível Superior – Brasil (CAPES) – Finance Code 001

4.6 References

Chidgey, K. L., Morel, P. C. H., Stafford, K. J., & Barugh, I. W. (2015). Sow and piglet productivity and sow reproductive performance in farrowing pens with temporary crating or farrowing crates on a commercial New Zealand pig farm. *Livestock Science*, *173*, 87–94. https://doi.org/10.1016/j.livsci.2015.01.003

Galiot, L., Lachance, I., Laforest, J. P., & Guay, F. (2018). Modelling piglet growth and mortality on commercial hog farms using variables describing individual animals, litters, sows and management factors. *Animal Reproduction Science*, *188*(July 2017), 57–65. https://doi.org/10.1016/j.anireprosci.2017.11.009

Heidinger, B., Maschat, K., Kuchling, S., Hochfellner, L., Winckler, C., Baumgartner, J., & Leeb, C. (2022). Short confinement of sows after farrowing, but not pen type affects live-born piglet mortality. *Animal*, *16*(2), 100446. https://doi.org/10.1016/j.animal.2021.100446

King, R. L., Baxter, E. M., Matheson, S. M., & Edwards, S. A. (2019). Temporary crate opening procedure affects immediate post-opening piglet mortality and sow behaviour. *Animal*, *13*(1), 189–197. https://doi.org/10.1017/S1751731118000915

Leonard, S. M., Xin, H., Brown-Brandl, T. M., Ramirez, B. C., Johnson, A. K., Dutta, S., & Rohrer, G. A. (2021a). Effects of farrowing stall layout and number of heat lamps on sow and piglet behavior. *Applied Animal Behaviour Science*, *239*(April), 105334. https://doi.org/10.1016/j.applanim.2021.105334

Leonard, S. M., Xin, H., Brown-Brandl, T. M., Ramirez, B. C., Johnson, A. K., Dutta, S., & Rohrer, G. A. (2021b). Effects of farrowing stall layout and number of heat lamps on sow and piglet behavior. *Applied Animal Behaviour Science*, *239*. https://doi.org/10.1016/j.applanim.2021.105334

Li, Shang *et al*. Comparison between maternal behaviors of primiparous and multiparous sows. **Livestock Science**, [S.L.], v. 267, p. 105127, jan. 2023. Elsevier BV. http://dx.doi.org/10.1016/j.livsci.2022.105127.

Liu, L., Tai, M., Yao, W., Zhao, R., & Shen, M. (2021). Effects of heat stress on posture transitions and reproductive performance of primiparous sows during late gestation. *Journal of Thermal Biology*, *96*(November 2020), 102828. https://doi.org/10.1016/j.jtherbio.2020.102828

Loftus, L., Bell, G., Padmore, E., Atkinson, S., Henworth, A., & Hoyle, M. (2020). The effect of two different farrowing systems on sow behaviour, and piglet behaviour, mortality and

growth. *Applied Animal Behaviour Science*, *232*(September), 105102. https://doi.org/10.1016/j.applanim.2020.105102

Marchant, J. N., Broom, D. M., & Corning, S. (2001). The influence of sow behaviour on piglet mortality due to crushing in an open farrowing system. *Animal Science*, *72*(1), 19–28. https://doi.org/10.1017/S135772980005551X

Moustsen, V. A., Hales, J., Lahrmann, H. P., Weber, P. M., & Hansen, C. F. (2013). Confinement of lactating sows in crates for 4 days after farrowing reduces piglet mortality. *Animal*, *7*(4), 648–654. https://doi.org/10.1017/S1751731112002170

Ramirez, B. C., Hayes, M. D., Condotta, I. C. F. S., & Leonard, S. M. (2022). Impact of housing environment and management on pre-/post-weaning piglet productivity. *Journal of Animal Science*, *100*(6), 1–12. https://doi.org/10.1093/jas/skac142

Rangstrup-Christensen, L., Krogh, M. A., Pedersen, L. J., & Sorensen, J. T. (2018). Sow level risk factors for early piglet mortality and crushing in organic outdoor production. *Animal*, *12*(4), 810–818. https://doi.org/10.1017/S1751731117002178

Schild, S. L. A., Baxter, E. M., & Pedersen, L. J. (2020). A review of neonatal mortality in outdoor organic production and possibilities to increase piglet survival. *Applied Animal Behaviour Science*, *231*(November 2019), 105088. https://doi.org/10.1016/j.applanim.2020.105088

Wegner, K., Lambertz, C., Daş, G., Reiner, G., & Gauly, M. (2014). Climatic effects on sow fertility and piglet survival under influence of a moderate climate. *Animal*, *8*(9), 1526–1533. https://doi.org/10.1017/S1751731114001219

Yun, J., Han, T., Björkman, S., Nystén, M., Hasan, S., Valros, A., Oliviero, C., Kim, Y., & Peltoniemi, O. (2019). Factors affecting piglet mortality during the first 24 h after the onset of parturition in large litters: Effects of farrowing housing on behaviour of postpartum sows. *Animal*, *13*(5), 1045–1053. https://doi.org/10.1017/S1751731118002549

5. CAPÍTULO III: Classificador de postura de matrizes baseado em aprendizagem profunda utilizando imagens RGB e de profundidade

Este capítulo faz parto do artigo “Deep Learning sow posture classifier based on depth and RGB images” que será submetido para a revista Biosystems Engineering

Abstract

Determining changes in sow posture can provide information on the production and health of animals. However, manually evaluating images is extremely time-consuming and standard image processing approaches can require seconds per image to process. The use of deep learning techniques has the advantage of being a more efficient method when compared to traditional image processing. However, transition sow postures such as sitting, and kneeling are difficult to discern using RGB images alone. The aim of this study is to compare the use of different images as input to models based on deep learning for the detection of sow postures. Using Kinect v.2 cameras, images were collected from 7 sows housed in farrowing crates. A total of 26362 images were labeled manually according to the postures (“standing”, “kneeling”, “sitting”, “ventral recumbency”, and “lateral recumbency”). Deep learning algorithms (AlexNet) were adapted to detect sow postures from five types of images: color, depth (depth image transformed into grayscale), and mixed (images composed with the color and depth images). The results showed that the models that used depth and mixed images presented the best results in all situations when compared with the models that used only RGB images as input. The best model used only depth images as input and presented an accuracy of 94.7%. The average precision value was 92.32% and the recall value was 92.40% (F1-score = 92.36%). The results of this study illustrate an improvement in the classification of postures using depth images as input of the classifier. Other studies may contribute to the development of increasingly rapid and accurate models by using a larger database, evaluating different fused methods, computational models, systems, and breeds of sows, and incorporating additional postures.

5.1 Introduction

Currently in the US swine industry, lactating sows are housed in farrowing crates to protect the piglets from overlays. However, even with the use of farrowing crates, the pre-weaning mortality for piglets is 17.3% (Stalder, 2018).. The risk factors contributing to pre-weaning mortality are generally classified into three main categories: piglet factors, sow factors, and environmental factors. Muns et al. (2016) highlights the need to understand sow comfort, as sow comfort impacts piglet development and the risk of crushing.

Accessing the behavior of pigs is important to identify their state of health and well-being and can provide important information about the performance of the production system (Brown-Brandl et al., 2013). Sow posture changes can result in piglet crushing, mostly by sows lying down (Damm et al., 2005). More importantly, it appears that the sow's control over the final stages of laying is critical (Anna K. Johnson & Marchant-Forde, 2008). Slower postural changes may be a sign of more protective mothers and be related to lower piglet mortality rates from crushing.

However, the investigation of behaviors is still performed manually, depending on trained observers and time to evaluate the data, which makes it impossible to generate quick answers for decision making. Therefore, to evaluate the interaction between the crates and the sow, there is a need to develop automatic detection methods. Thus, Deep Learning techniques have been used as an automatic way to assess the behavior of lactating sows. Such computational models, based on artificial intelligence, allow a quick interpretation of data, and have great potential for use in production systems. On the other hand, the type of data used to train these models plays an important role in getting the most accurate results.

Several works use RGB and depth images to detect sow postures (Bonneau et al., 2021; Kasani et al., 2021; Lao et al., 2016). Despite providing a good representation of the scene, the RGB image is a two-dimensional function representing a three-dimensional scene. By losing depth information, detecting transitional postures such as sitting, and kneeling is more challenging. On the other hand, depth images, even adding depth information, lose in terms of color representation and scene details, important information to differentiate the animal from the other objects in the image.

Zheng et al. (2018) studied a Convolutional Neural Network (CNN)-based posture detector and used only depth images from sows in its development. The authors obtained an average accuracy of 93.58% (five posture classes). The highest precision values were for the standing

(99.1%), ventral (97.2%), and lateral recumbency (98.7%) classes and the lowest for the sitting (76.6%) and sternal recumbency (76.3%) postures. Zhu et al. (2020) used the same database for the detection of postures but used different methods of merging RGB and depth images in the development of the computational models. The fusion methods used in the different models showed superior results in relation to the ones that used only depth or RGB images, with the most precise model achieving precisions above 90% for all posture classes. The optimal model demonstrated an accuracy of 95.47%, along with precision values of 99.7% for standing, 96.5% for sitting, 90.7% for sternal decubitus, 90.9% for ventral decubitus, and 99.4% for lateral decubitus.

In another study, Bonneau et al. (2021) compared the effectiveness of CNNs and segmentation methods in detecting sow postures from videos captured by a top-down oblique imaging camera. The models were trained on RGB images and classified into four postures: sitting, standing, lying sternally, and lying laterally. The authors found that CNN-based models were more efficient than segmentation-based methods with F1 scores of 97.7% and 93.3%, respectively. The study also evaluated the impact of environmental and animal variations by testing the models on different databases. The authors observed an average decrease of approximately 17% in the F1 score due to environmental and individual variations between the training and test data.

These studies demonstrate that CNNs are promising in identifying sow postures. Furthermore, combined image fusion methods can contribute to the development of more accurate models. New studies for the detection of different postural categories in different systems, with different species of sows, may contribute to the development of increasingly accurate models.

Thus, this study aims to develop a computational model for the classification of sow postures using different types of images as the input of the classifiers. The hypothesis is that by merging the RGB and depth images, some features in the images can be highlighted which can help the models to classify the sow postures.

5.2 Materials and Methods

The experiment was conducted at the United States Department of Agriculture - Agricultural Research Service of the US Meat Animal Research Center in Clay Center, Nebraska, the United States. Data collection was performed in accordance with federal and institutional regulations regarding proper animal care practices and was approved by the U.S. Center for Animal Research Institutional Animal Care and Use Committee (2015-21) (IACUC approval: 1837).

The collections were carried out from July to September 2020 in a farrowing facility where the six sows (Landrace x Yorkshire) were individually installed in metallic pens. The building has an automatically controlled microclimate so that the air temperature inside the rooms was maintained at around 25°C and was gradually reduced to 20°C during the lactation cycle. The installation consisted of individual feeders and two nipple drinkers. Animal waste fell from the stalls through fully slatted metal floors into a shallow, sloping pit in each room.

At the top of each crate, at a height of 2.55 m, a single depth camera (Kinect V2®) was installed in waterproof plastic boxes that were fixed to a metal structure to collect images (top view) of the pens and animals. Such cameras were responsible for collecting either the color (RGB) and depth (distance matrix) images 24 hours a day at an average rate of one image every 2.5 seconds. The cameras were connected to minicomputers (Windows 10 Home, Microsoft, Redmond, WA, USA) located in front of each of the bays that ran the image collection program developed in MATLAB® R2019b software (The MathWorks Inc.). The minicomputers were connected via Ethernet cables to data storage stations (DS1621+, Synology Inc, Bellevue, WA) with five hard drives (ST10000VN0004, Seagate Technology LLC, Cupertino, CA, USA).

5.2.1 Sow posture classification

A total of 23362 images of the six sows were analyzed over a period of 12 hours a day for 9 days. Images were labeled by trained observers into five categories of sow postures (Table 5): "standing", "sitting", "kneeling", "ventral recumbency" and "lateral recumbency".

Table 5. Ethogram of the postures used for the classification of images and for the development of the computational model.

Posture	**Description**	**Number of images**
Standing	Animal supporting the body on all four legs	8622
Sitting	Animal supporting the body on both front legs (bent hind legs)	4420
Kneeling	Animal supporting the body on its hind legs (folded front legs)	1333
Ventral recumbency	Animal lying vertically with front legs hidden/hind legs and udder could be visible (right side, left side) or not;	2225
Lateral recumbency	Animal lying on its side with all four legs turned to the side	6762
Total		26362

5.2.2 Image pre-processing

Three types of images were tested as inputs to the developed computational models (Figure 11): color (RGB image), depth (depth image transformed into grayscale) and a mixed image composed with the depth and color image. For the construction of grayscale images, instead of using fixed values to transform the distance values, a normalization method was adopted. In this method, the maximum limit adopted was equal to the maximum distance value verified in each depth image. For the minimum limit, the value of 2200 mm was subtracted from the maximum value captured and the result was recorded for each image. This 2200 mm value was thought to be according to that of the matrix in the scene. The normalization method was adopted to overcome the difference in the distance recorded by the cameras (different fields of view and calibrations). This was adopted to overcome the difference in distance recording by the cameras (different fields of view and calibrations). The mixed image was created using the RGB image combined with the colorized depth image. Specific limits between the middle and top part of the farrowing crate were associated with a range of colors. This range was chosen so that there was a division between the bottom and top of the animal. Thus, in the kneeling and sitting posture, only one part of the animal was colored (front or rump). In the standing posture the whole animal was colored and in the lying postures no coloring was added (Figure 11).

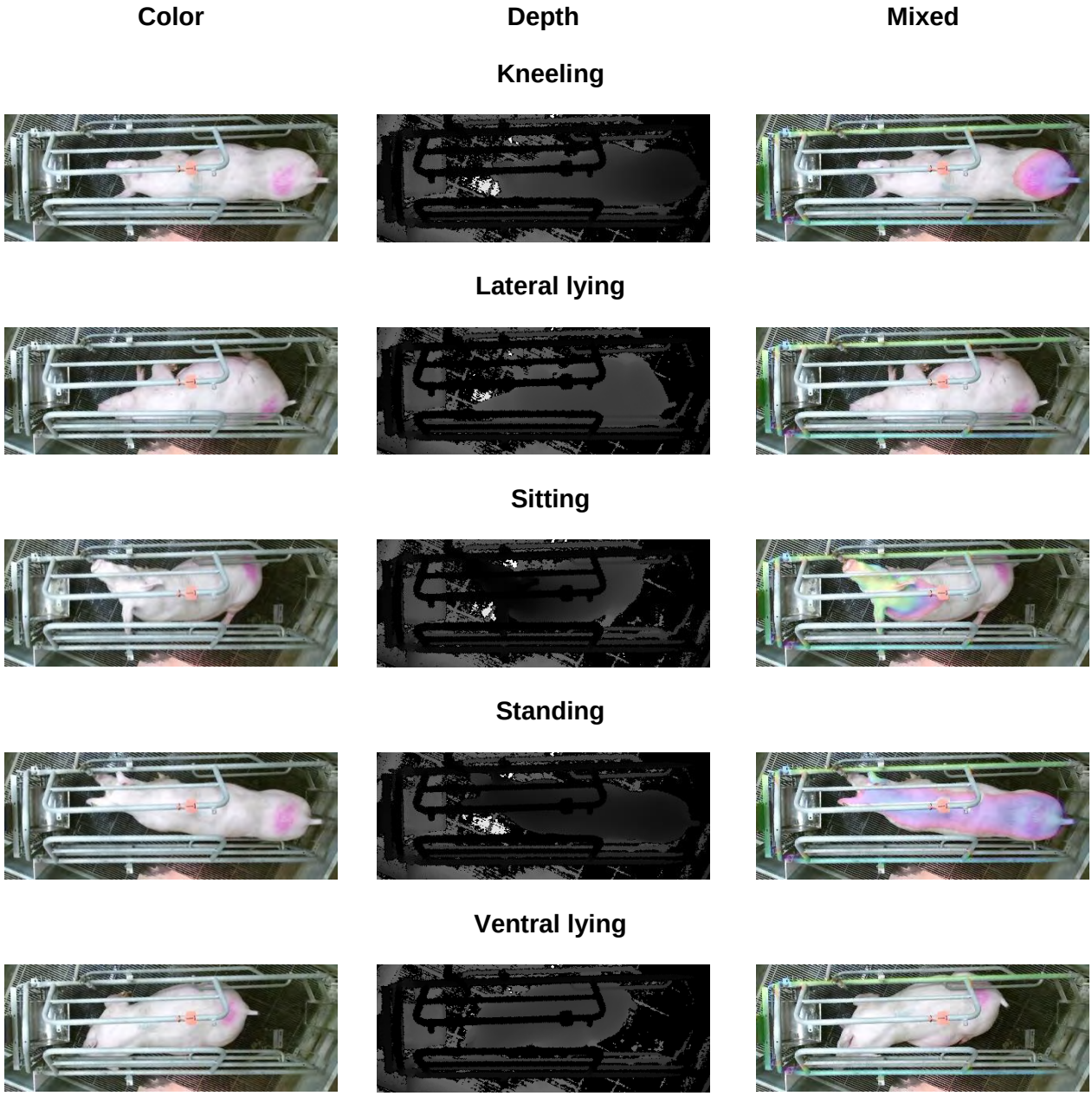

Figure 10. Examples of the three types of images tested in the development of computational models for the classification of five postures (kneeling, lateral lying, sitting, standing, and ventral lying). For the composition of the database, 9 sows were monitored with depth cameras (Kinect v.2) for 9 days (12 hr/day). A total of 26362 images were randomly selected from the database.

5.2.3 Development of computational models

An AlexNet-based Convolutional Neural Network architecture was developed with the MATLAB® R2022b software (Deep Learning Toolbox Model for AlexNet Network, and Deep

Learning Toolbox). The first step in model development was to divide each dataset (RGB, depth, and mixed images) into training (80%), validation (10%) and test (10%) sets. Such dataset was provided to the classifiers through the input layer. Data augmentation techniques (reflection and translation) were used to augment the training database. The pre-trained neural network AlexNet (Krizhevsky et al., 2012) was used, replacing the last layer of classification by the new learning categories: the sow postures (standing, sitting, kneeling, lateral and prone positions). Number of epochs, learning rate, batch size, and solver were defined empirically and through literature. The classifier's performance was evaluated using metrics extracted from a confusion matrix, comparing real responses (classified by an observer) and the responses predicted by the model. Through the confusion matrix, it is possible to evaluate the efficiency of the classifiers in terms of average accuracy, precision, recall, and F1-Score. These metrics were thoroughly described and summarized by Sokolova & Lapalme (2009) and can be computed using the formulas described in the Table 6. All metrics were calculated based on the values identified in the confusion matrix as true positives (t_p), true negatives (t_n), false positives (f_p), and false negatives (f_n). Values identified as t_p are those correctly identified as belonging to the class and t_n are the values correctly identified as not belonging to the class. The f_p values are those misidentified as belonging to the class and the f_n misidentified as not belonging to the analyzed class (Sokolova & Lapalme, 2009).

Table 6. Metrics extracted from a confusion matrix for multiclass classification.

Measure	Formula	Measure	Formula
$Average\ Accuracy$	$\frac{\sum_{i=1}^{l} \frac{tp_i + tn_i}{tp_i + fn_i + fp_i + tn_i}}{l}$	$Precision_{\mu}$	$\frac{\sum_{i=1}^{l} tp_i}{\sum_{i=1}^{l} (tp_i + fp_i)}$
$F1 - Score_M$	$\frac{2 \times Precision_i \times Recall_i}{Precision + Recall}$	$Recall_{\mu}$	$\frac{\sum_{i=1}^{l} tp_i}{\sum_{i=1}^{l} tp_i + fn_i}$

Values identified in the confusion matrix (t_p) true positives, (t_n) true negativas, (f_p) false positives, and (f_n) false negatives. Recall and precision values were calculated by class: (μ) micro-average. F1-Score was calculated for all classes: (**M**) macro-average.

5.3 Results

In the first round of tests, 12 models were developed (4 for each type of image: RGB, grayscale and mixed) and the results of the best classifiers are presented in Table 7. The accuracies achieved were, 94.7%, 91.0%, and 95.4%, respectively for the grayscale, RGB and mixed model. The best result was obtained by the classifier that used grayscale images with an F1-score of 92.36%.

Table 7. Results obtained from the classifiers trained with the different images (RGB, grayscale and mixed) in a first test stage.

Image	**Metrics (%)**			
	Precision	**Recall**	**Acc**	**F1-score**
Grayscale	92.40	92.32	94.7	92.36
RGB	80.98	89.76	91.0	85.14
Mixed	89.18	93.82	95.4	91.44

The confusion matrix of the grayscale image model is presented in Table 8. The correct classifications represented an average accuracy of 94.7%, distributed in the class “kneeling” (5.4%), “lateral recumbency” (24.9%), “sitting” (18.9%), “standing” (36.6%) and “ventral recumbency” (7.3%). The average precision value was 92.32% and the recall was 92.40% (F1-score = 92.36%), with the “ventral decubitus” class showing the lowest precision (75.0%) and recall (77.5%). All other classes showed values above 93.0% for precision and above 92.0% for recall. The “sitting” and “standing” classes showed the best performances with accuracy and recall values above 98.0%.

The precision results indicate that the models made some mistakes when bringing data from other classes and classifying them as if they were the desired output (Table 8). In the first model, the average accuracy error was 7.68% and the class in which the model made the most errors was "ventral recumbency". Of the 594 images classified for this class, the classifier was correct in 524 (88.2%) and the errors occurred randomly, with most of them occurring in the lateral recumbency classes (23 images = 3.9%) and sitting (25 images = 4.2%).

Regarding the recall results (Table 8), the only class that presented a value lower than 92% was “ventral recumbency” (77.0%). This means that the model classified 77.0% of the “ventral recumbency” samples correctly and classified the remaining 23% of “ventral recumbency” images as other classes. The biggest error occurred in the "lateral decubitus" class (45 imagens = 1.9%).

Table 8. Confusion matrix of the first test between the predicted class by the grayscale image classifier and the true label, obtained from the postural categories labeled manually.

True label	Predicted label					Recall
	Kneeling	**Lateral rec.**	**Sitting**	**Standing**	**Ventral rec.**	
Kneeling	**126 (5.4%)**	2 (0.1%)	0 (0.0%)	4 (0.2%)	1 (0.0%)	94.7%
Lateral rec.	0 (0.0%)	**622 (24.9%)**	0 (0.0%)	0 (0.0%)	54 (2.3%)	92.0%
Sitting	1 (0.0%)	0 (0.0%)	**438 (18.9%)**	1 (0.0%)	2 (0.1%)	99.1%
Standing	3 (0.1%)	0 (0.0%)	4 (0.2%)	**855 (36.6%)**	0 (0.0%)	99.2%
Ventral rec.	1 (0.0%)	45 (1.9%)	5 (0.2%)	0 (0.0%)	**171 (7.3%)**	77.0%
Precision	96.2%	93.0%	98.0%	99.4%	75.0%	**94.7%**

A second test step was performed with the best computational model that used grayscale images. The intention of this second stage was to balance the images between the classes, since the "sitting" and "ventral recumbency" and "lateral recumbency" classes presented a much larger number of images than the others, which can make it difficult for the classifier to learn. Thus, the classes with the greatest number of images were reduced to 3000 images each. Results are presented in table 9. Reducing the number of images of some classes to balance the database did not favor model learning. There was a small reduction in accuracy compared to the model developed in the first stage, from 94.7% to 92.9%. In this case, average precision result was 92.46% and the average recall value was 90.36% (F1-score = 91.40%)

As in the previous model, the precision results indicate that the model with balanced classes also made some mistakes when bringing data from other classes and classifying them as the desired output. In this case, the average precision error was 7.54%, and the classes in which the model made the most mistakes were "lateral recumbency" and "ventral recumbency". Of the 1012 images classified for the "lateral recumbency" posture, the classifier was correct in 871 (86.1%) and the errors occurred in the ventral "recumbency" (124 images = 12.2%) and "kneeling" (17 images < 0.1%) classes.

Regarding recall results, the most significant errors occurred in the "kneeling" and "ventral recumbency" classes, which presented recall values of 81.8% and 78.4%, respectively. The "kneeling" class had 400 test images to be found by the classifier, which found 327 images (81.7%). The errors happened randomly in the lateral recumbency (17 images = < 0.1%), sitting (12 images = < 0.1%), standing (29 images = 0.1%)), and ventral recumbency (15 images = < 0.1%) classes).

Table 9. Confusion matrix of the second test between the predicted class by the grayscale image classifier and the true label, obtained from the postural categories labeled manually.

True label	Predicted label					Recall
	Kneeling	**Lateral rec.**	**Sitting**	**Standing**	**Ventral rec.**	
Kneeling	**327 (8.7%)**	17 (0.1%)	12 (0.3%)	29 (0.8%)	15 (0.4%)	81.8%
Lateral rec.	5 (0.1%)	**871 (24.9%)**	1 (0.0%)	0 (0.0%)	23 (0.6%)	96.8%
Sitting	2 (0.1%)	0 (0.0%)	**869 (23.1%)**	4 (0.1%)	25 (0.7%)	96.6%
Standing	3 (0.1%)	0 (0.0%)	6 (0.2%)	**884 (23.5%)**	7 (0.2%)	98.2%
Ventral rec.	7 (0.2%)	124 (1.9%)	12 (0.3%)	1 (0.0%)	**524 (13.9%)**	78.4%
Precision	95.1%	86.1%	96.6%	96.3%	88.2%	**92.9%**

5.4 Discussion

Metrics extracted from the confusion matrices were used to evaluate the efficiency of CNN-based classifier models that used different image types. The findings demonstrated that the inclusion of depth information improved the performance of the models, with both grayscale and mixed models achieving greater accuracy and F1-score values than models that solely utilized RGB images. The classifiers that used grayscale images exhibited superior performance in all the tests.

In the first test stage, the classifier presented the lowest precision value for the “ventral recumbency” class, and the errors occurred randomly. Images classified by observers as “ventral recumbency were those in which the sow was lying on her belly with her legs hidden, or when she was lying on her belly but with her hind legs turned to the side. In addition, other variations occur, the sow could have the head position higher, or lying down. These variations in this class may have added a greater challenge for the classifier who found some similarities in these images with the other classes. For example, if the sow was sitting but with its head down, this position could be similar to "ventral recumbency". The “side-lying” position can also look like “ventral recumbency” as all four legs are turned to the side. For this reason, the model classified as "ventral decubitus" some images that were from other categories and this was the class that the classifier ended up getting more confused.

The opposite also occurred, and the images that originally belonged to the "ventral recumbency" class were also classified among the other classes. This can be observed by the recall value, which was lower for this class. As explained earlier, the "lateral recumbency" position can look like "ventral recumbency" with the hind legs stretched out.

Except for the "ventral recumbency" posture, the classifier presented great recall results, with emphasis on the "kneeling" and "sitting" postures, which are a challenge, as the key to detecting these postures is the difference in height between the front and the back part of the animal. In top view RGB images, these classes are challenging as this difference is not evident. This is an advantage of using depth images, as the distance information can favor the learning of the classifier. This may be the explanation for the grayscale images that showed good results in the classifiers, as they carry the depth information due to the difference in pixel intensity.

In the second test, when the data were balanced across classes, this did not seem to help the classifier learn. The total amount of images may have played a more important role than the balance between classes. Perhaps, balanced classes added to a larger number of images could have contributed to the improvement of the results. In the case of the results of this second test, there was a decrease in the recall value for the “kneeling” class and a small improvement in the recall and accuracy of the “ventral recumbency” class compared to the previous classifier. These differences in results may have been random and not the result of any important change in the classifier's learning process, since the number of images was reduced and slightly modified from one dataset to another.

Kasani et al. (2021) investigated eight deep learning-based feature extraction frameworks to classify four sow postures (sitting, lying right, lying left, and standing) from RGB image dataset collected from animals (Yorkshire x Landrace) housed in gestation crates. Different from this study, all models that used RGB images presented high average accuracy (> 99%). An explanation for the inferior performance of the model trained with RGB images in the present study may be the number of postures (five) used for classification in the current study. Furthermore, postures such as kneeling, and the division of the lying posture into two categories added greater challenges to the training of the models. Bonneau et al. (2021) also obtained better results for classifying sow postures using only RGB images. The matrix posture classes adopted were sitting, standing, sternal decubitus and lateral decubitus, and the images captured by an oblique top-down camera. In the study by Bonneau et al. (2021) the angle of view provided by the top-down oblique camera may have facilitated the model's ability to detect these postures, as the shape of the animals differs when viewed from a top view versus an oblique top-down view. The kneeling posture was also not evaluated in that study.

Zheng et al. (2018) studied a CNN-based posture classifier using depth imaging and found an average accuracy of 93.58% and an F1-Score of 90%, values slightly lower than those found for this study when only depth image was used (94.70%, and 92.36%, respectively). Although the results were close, some differences in the studies may have influenced the results of the studies and show room for improvement in the results of the classifier developed in this study. One of them may be related to the type of facility in which the animals were housed. While the sows in this study were confined in farrowing crates, the sows in the aforementioned study were in free farrowing pens, which may have added variations in the images analyzed, as the sow can move freely through the pens.

Other differences between this study and the one developed by Zheng et al. (2018) indicate that the performance of the model developed in this study can still be improved. Despite having used the same number of postures as in the current study (five), the authors did not use the "kneeling" posture, which is challenging posture to detect, since it is similar to other postures when using a top view image. The authors also used strategies to improve the images, including random noise compensation, hole filling, and image depth enhancement. Furthermore, they used a pre-trained network (ZFNet) as a model to detect sow postures. In the current study, the distance values of the depth image were only transformed into a grayscale range, and the AlexNet network was used to detect postures. These data indicate that the models developed in the current study showed good average accuracies and that they can still be improved with the use of a larger database, and different image pre-processing strategies to further improve the quality of these images.

In this work, the models composed with the mixed images improved in the classifications in comparison with the ones that used the RGB images, but they were not better than the ones that used the depth images only. CNNs detect patterns in images by detecting shapes and cores. Although an observer can visually detect the different colors integrated into the mixed images, the way computer models mathematically analyze an image is different. For some reason, the models were more efficient in detecting the intensity difference in different classes of depth images.

Zhu et al. (2020) studied different computer models and different image fusion methods to detect sow postures (“standing”, “sitting”, “sternal recumbency”, “ventral recumbency” and “lateral recumbency”). Different from the results of this study, all image fusion methods presented better results than the models trained with RGB, and the depth images separately. The authors found the best model using an image concatenation method, the precision values for the postures:

"standard", "sitting", "sternal recumbency", "ventral recumbency" and "lateral recumbency" were, respectively, 99.74%, 96.49%, 90.77%, 90.91%, and 95.47%. The sows in the aforementioned study were of a different breed (MeiHua) and were individually housed in open farrowing pens. Furthermore, the best model developed by the authors contained two CNNs that evaluated the RGB and depth images separately, before concatenating the results. These may have been some differences that explain the different results found in this study. Similar to the current study, there were classification errors between sitting, sternal and ventral recumbency postures that may have similarities due to the variation in height between head, shoulder, and rump, which may have made learning the model difficult. Despite not having presented the best result of this work, the mixed images presented promising results that can be explored in other studies. Future work can be explored with variations in the chosen distance thresholds for image colorization, and different color palettes.

Despite having demonstrated difficulty in detecting the "ventral recumbency" category, this developed model would already be useful in several applied situations. For example, if a producer has the need to develop a model to alert when the sow is kneeling to avoid crushing the piglets, this model showed the potential to detect this posture. Additionally, suppose the producer wants to characterize the daily behavior of a sow's postural changes. In this case, the model can characterize how much time the sow spends lying, sitting, or standing, although differentiating the lying classes was challenging for the classifier. These results are presented in table 10 and indicate that the condensation of the categories "ventral decubitus" and "lateral decubitus" ("lying down" class) maintained all accuracy, precision, and recall results above 95%.

Table 10. Results extracted from the confusion matrix of the classifier developed in the first stage with condensed ventral recumbency and lateral recumbency classes (laying class).

True label	**Predicted label**				**Recall**
	Kneeling	**Lateral rec.**	**Sitting**	**Standing**	
Kneeling	**126 (5.6%)**	3 (0.1%)	0 (0.0%)	4 (0.2%)	94.73%
Lying	1 (0.0%)	**892 (36.6%)**	5 (0.2%)	0 (0.0%)	99.33%
Sitting	1 (0.0%)	2 (0.0%)	**438 (17.9%)**	1 (0.0%)	99.00%
Standing	3 (0.1%)	0 (0.0%)	4 (0.2%)	**855 (35.0%)**	99.09%
Precision	96.18%	99.44%	97.98%	96.06%	**95.10%**

5.5 Conclusion

This study aimed to explore the use of diverse image types as input to computer models to detect the postures of lactating sows. The intention was to evaluate whether different images could aid to the learning of the models and enhance the classification results. The models that used only the depth image or the depth image combined with RGB achieved superior accuracies compared to the model that used only RGB images as input. The "ventral recumbency" category had the most difficulty being classified correctly. Despite this challenge, the model with depth images presented 94.7% and 92.36% accuracy and F1-score values, respectively. In addition, the classifier performed well in the classification results in transition postures (sitting and kneeling). The results of this study illustrate the improvement in posture classification using depth images. Other studies can contribute to the development of increasingly faster and more accurate models, using a larger database, evaluating different combined methods for the images, computational models, systems, breeds of sows, and incorporating additional postures.

Acknowledgement

This work was supported by the Coordenação de Aperfeiçoamento Pessoal (CAPES) [001, 2019], Pirassununga, Brazil.

5.6 References

Bonneau, M., Benet, B., Labrune, Y., Bailly, J., Ricard, E., & Canario, L. (2021). Predicting sow postures from video images: Comparison of convolutional neural networks and segmentation combined with support vector machines under various training and testing setups. *Biosystems Engineering*, *212*, 19–29. https://doi.org/10.1016/j.biosystemseng.2021.09.014

Brown-Brandl, T. M., Rohrer, G. A., & Eigenberg, R. A. (2013). Analysis of feeding behavior of group housed growing-finishing pigs. *Computers and Electronics in Agriculture*, *96*, 246–252. https://doi.org/10.1016/j.compag.2013.06.002

Damm, B. I., Forkman, B., & Pedersen, L. J. (2005). Lying down and rolling behaviour in sows in relation to piglet crushing. *Applied Animal Behaviour Science*, *90*(1), 3–20. https://doi.org/10.1016/j.applanim.2004.08.008

Johnson, A. K., & Marchant-Forde, J. N. (2008). Welfare of Pigs in the Farrowing Environment. In *The Welfare of Pigs*. https://doi.org/10.1007/978-1-4020-8909-1_5

Kasani, P. H., Oh, S. M., Choi, Y. H., Ha, S. H., Jun, H., Park, K. hyun, Ko, H. S., Kim, J. E., Choi, J. W., Cho, E. S., & Kim, J. S. (2021). A computer vision-based approach for behavior recognition of gestating sows fed different fiber levels during high ambient temperature. *Journal of Animal Science and Technology*, *63*(2), 367–379.

https://doi.org/10.5187/JAST.2021.E35

Lao, F., Brown-Brandl, T., Stinn, J. P., Liu, K., Teng, G., & Xin, H. (2016). Automatic recognition of lactating sow behaviors through depth image processing. *Computers and Electronics in Agriculture*, *125*, 56–62. https://doi.org/10.1016/j.compag.2016.04.026

Muns, R., Nuntapaitoon, M., & Tummaruk, P. (2016). Non-infectious causes of pre-weaning mortality in piglets. *Livestock Science*, *184*, 46–57. https://doi.org/10.1016/j.livsci.2015.11.025

Stalder, K. J. (2018). *2017 Pork Industry Productivity Analysis*. 1–12.

Zheng, C., Zhu, X., Yang, X., Wang, L., Tu, S., & Xue, Y. (2018). Automatic recognition of lactating sow postures from depth images by deep learning detector. *Computers and Electronics in Agriculture*, *147*(August 2017), 51–63. https://doi.org/10.1016/j.compag.2018.01.023

Zhu, X., Chen, C., Zheng, B., Yang, X., Gan, H., Zheng, C., Yang, A., Mao, L., & Xue, Y. (2020). Automatic recognition of lactating sow postures by refined two-stream RGB-D faster R-CNN. *Biosystems Engineering*, *189*, 116–132. https://doi.org/10.1016/j.biosystemseng.2019.11.013

6. CAPÍTULO IV: Comparação de quatro câmeras de profundidade baseadas em tecnologia de tempo de vôo

Este capítulo faz parto do artigo "Comparison of four depth cameras based on time-of-flight technology" que será submetido para a revista Computers and Electronics in Agriculture.

Abstract

The use of depth sensors for precision animal management has grown in recent years, with the ability to capture animals in many different lighting conditions. Time-of-flight (TOF) cameras are a technology that has demonstrated good performance for capturing images in indoor conditions. However, with the continuous turnover in commercially available cameras, there is a need for an objective comparison between cameras. Cameras with different sensors and optics can greatly vary in terms of accuracy and repeatability. The objective of this study is to test four time-of-flight depth cameras in terms of values of repeatability, dimensions and radial distortion in the images obtained with Pico Flexx, Kinect v.2, Pico Zense and Azure Kinect cameras. Images from each camera were collected while viewing structures of foam boards in different positions within the images, with distances ranging from 100 to 300 cm. Repeatability was compared in terms of standard deviation of the distance values registered in the images. The dimensions of the boards collected from the images include area ratio ($px*cm^{-2}$), and estimated volume with equations developed with the different parameters of the cameras. Radial distortion was evaluated by comparing distance measurements and coefficient of variation in three segments selected from the center to the board of the images (vertical, horizontal, and diagonal positions. The results indicate Azure Kinect camera presented the best results in terms of repeatability and volume estimation. Pico Zense (cameras 2 and 3) presented the smaller standard deviation values for distance measurements. All cameras showed similar curves between experimental and theoretical measurements for the calculation of the area ratio of the boards.

6.1 Introduction

In recent decades, there has been a remarkable increase in the exploration of range-sensing technologies due to their ability to map three-dimensional surfaces and their wide applicability in various areas of study. (Horaud et al., 2016). The images captured by these sensors have advantages over traditional color images, as depth images are robust to variations in illumination, color, rotation angle, and scale. (Cai et al., 2017). Additionally, this technology also has a lower cost than laser scanners and is highly portable, making it more flexible for use on mobile platforms. (Lachat et al., 2015).

Cameras with these features offer highly informative images and have emerged as a significant advance for computer vision-based systems in recent years, allowing machine learning models to perceive the world like a human perception, in a three-dimensional way. The use of computer vision techniques for animal monitoring has also been gaining ground, enabling non-invasive, continuous, real-time assessments. The use of depth imaging in systems like this can make many contributions to animal monitoring, as three-dimensional images make it easier to detect the shapes, movements, and movements of animals in their environment, thus providing valuable information about their productivity and health status. Some examples in Precision Livestock Farming are the use of the depth sensors to access body mass (Condotta et al., 2018), detect behaviors (Chen et al., 2020; Zhu et al., 2020), and monitor diseases (Van Hertem et al., 2018) in animals.

There are several commercial depth cameras and the types of technologies used by these sensors can be divided into three different principles: stereoscopy, structured light, and time of flight (ToF) (Condotta et al., 2020). Condotta et al. (2020) compared different technologies of depth cameras in relation to their accuracy and repeatability when being used to measure object dimensions while varying the objects' positions within the image, size, and distance from the camera. Among the studied technologies, the authors reported that time-of-flight (ToF) cameras had the smaller error when measuring different sizes of objects when compared to the others that rely on structured light and/or stereoscopy. The authors also reported that ToF technology is best technology for indoor applications.

Cameras based on ToF technology work by emitting a modulated infrared light and capturing the signal reflected from the scene. Using to the time required for the signal to complete this journey and the speed of the light, it is possible to calculate the distance from the sensor to

each point in the scene (Lachat et al., 2015). Because ToF cameras use modulated light, they can capture images of objects with different textures and even map dark environments. In addition, compared to other types of technologies, ToF cameras are low cost, allow longer working distances, and require little software processing power, which allows them to be applied in real-time.

Despite these advantages, ToF sensors are subject to errors that can affect the accuracy and stability of the data which can be observed in the images by distortions of the objects' shape, non-readable regions, and by the lack of repetition of the depth values recorded over time. In an automatic image-based animal monitoring system, these errors can influence the detection of animals at specific areas of the scene, the three-dimensional recreation, important for animal posture detection and weight estimation, and the comparison of subsequent scenes, important for monitoring the movement of animals in the environment.

The ToF technology itself has a large influence on the observed errors in the depth data. Since the depth value recorded by the sensors depends on the light reflected by objects in the scene, factors such as object reflectivity, distance from the scene, ambient light, and the intrinsic properties of each camera (e.g., resolution, modulation frequency, and illumination power) can affect the captured signal (He et al., 2016; Fang et al., 2020). These errors can affect the quality of results, and a comparison of available ToF cameras stands to benefit studies related to computer vision that intend to leverage the power of these new technologies. Validation processes are important to ensure that sensors are collecting accurate information and to detect the sensor that best serves certain types of purposes. Therefore, the objective of this study is to compare depth sensors based on ToF technology in relation to their accuracy and repeatability when monitoring objects in indoor scenes

6.2 Materials and Methods

Three replicates of four brands of time-of-flight cameras (Kinect v.2, Pico Zense, Pico Flexx, and Azure Kinect; Figure 11) were tested in the same internal environment. These cameras have differences in terms of specifications such as field of view (FoV), resolution, and range measurement (Table 11)

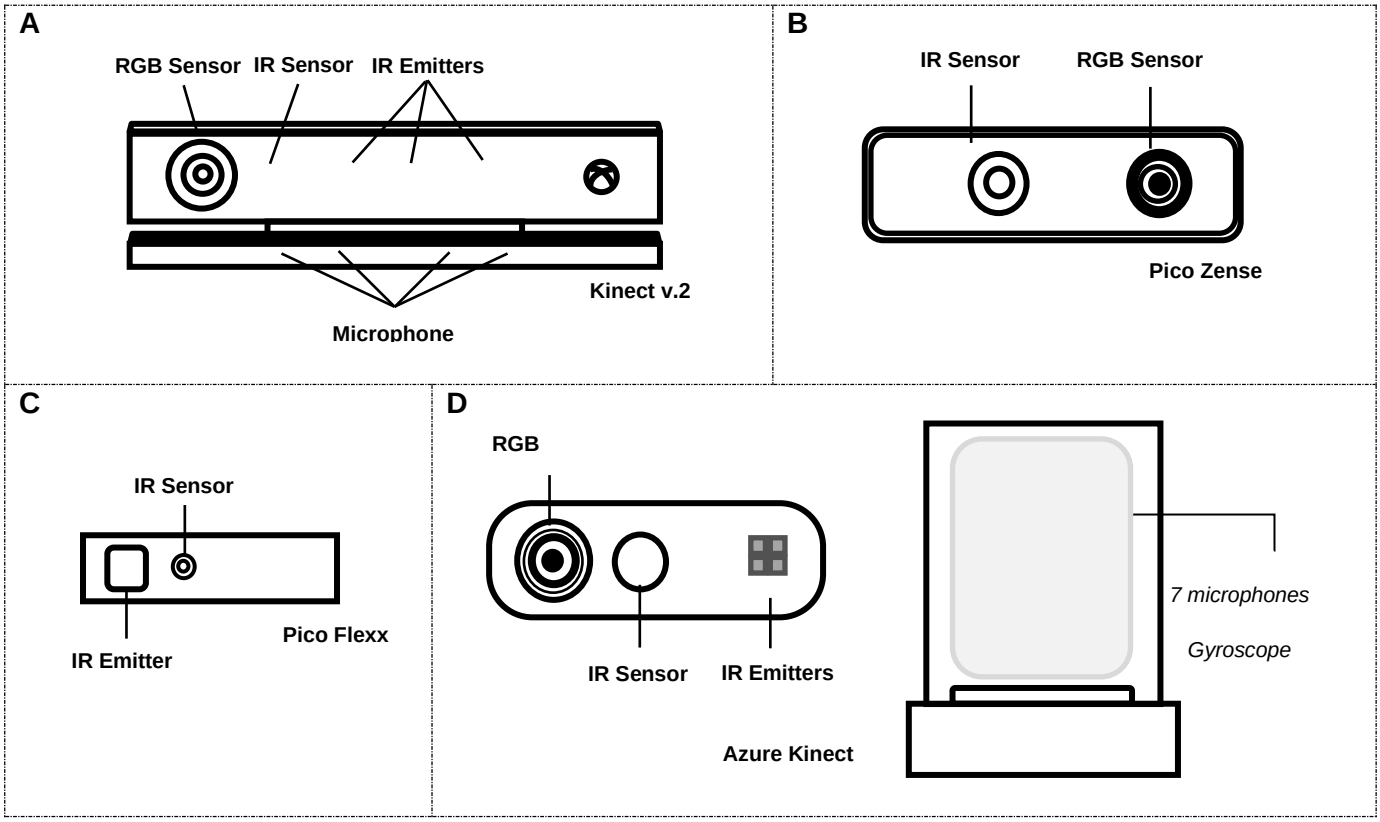

Figure 11. Components of the commercial depth cameras used in this study (out of scale). (A) Microsoft Kinect v.2, (B) Pico Zense, (Pico Technology) (C) CamBoard Pico Flexx (PMD Technologies), (D) Azure Kinect (Microsoft).

Table 11 Specifications of Pico Flexx, Kinect v.2, Pico Zense, and Azure Kinect depth cameras.

Camera	Measuring range (m)	Depth resolution	RGB max resolution	FoV depth	Frame rate (FPS)	Price (US$)
Pico Flexx	0.1 - 4.0	224 x 171	-	62º x 45º	45	390
Kinect v.2	0.5 - 4.5	512 x 424	1920 x 1080	70º x 60º	15/30	140
Pico Zense	Range 0 (0.35 - 1.45)	640 x 480	1920 x 1080	69° x 51°	30	299
	Range 1 (3.0)					
	Range2 (4.4)					
	Range3 (4.8)					
	Range4 (5.6)					
Azure Kinect	NFOV unbinned (0.5 - 3.86)	640 x 576	3840 x 2160	75° x 65°	0, 5, 15, 30	399
	NFOV 2x2 binned (SW) (0.5 -	320 x 288	2560 x 1440	75° x 65°	0, 5, 15, 30	
	WFOV 2x2 binned (0.25 - 2.88)	512 x 512	1920 x 1080	120°	0, 5, 15, 30	
	WFOV unbinned (0.25 - 2.21)	1024 x	1280 x 720	120° x	0, 5, 15	
	Passive IR (N/A)	1024 x	4096 x 3072	N/A	0, 5, 15, 30	

6.2.1 Experimental Design and Data Collection

In this study, four experiments were developed (Figure 12). The first one aimed to verify the repeatability of data collected by the cameras, where several frames of a scene were registered keeping the depth cameras fixed in the same position. The idea was to verify the variation of the distance values recorded between the different frames. In the second experiment, a comparison was made between the values of the actual dimensions and those obtained through images of panels of different sizes. In the third experiment, an analysis of the radial distortion of the images obtained by the depth cameras was performed. The idea was to compare the data from the central region of the images with the pixels from the edges. In the last experiment the phenomenon of absorption of infrared light by a black surface in the depth image was evaluated. Software linked to the cameras (PicoZenseUTool) or algorithms developed according to the Software Development Kit (SDK) of each camera were used to capture the images.

For the repeatability experiment, a 91 x 61 cm panel was kept in the central region of the field of view (Figure 12-a). In the experiment to obtain the dimensions of objects from the images, three panels of different dimensions (10 x 10, 20 x 20, and 30 x 30 cm) were kept in front of the cameras, in the central position of the field of view of the cameras (Figure 12-b). To access the radial distortion, a 30 cm wide bar was placed in front of the cameras in three different positions (horizontal, vertical, and diagonal) so that the length of the bar fit the entire field of view of the cameras (Figure 12-c). For all experiments, the images were obtained by three cameras of each brand 5 different distances from the panels (100, 150, 200, 250 and 300 cm).

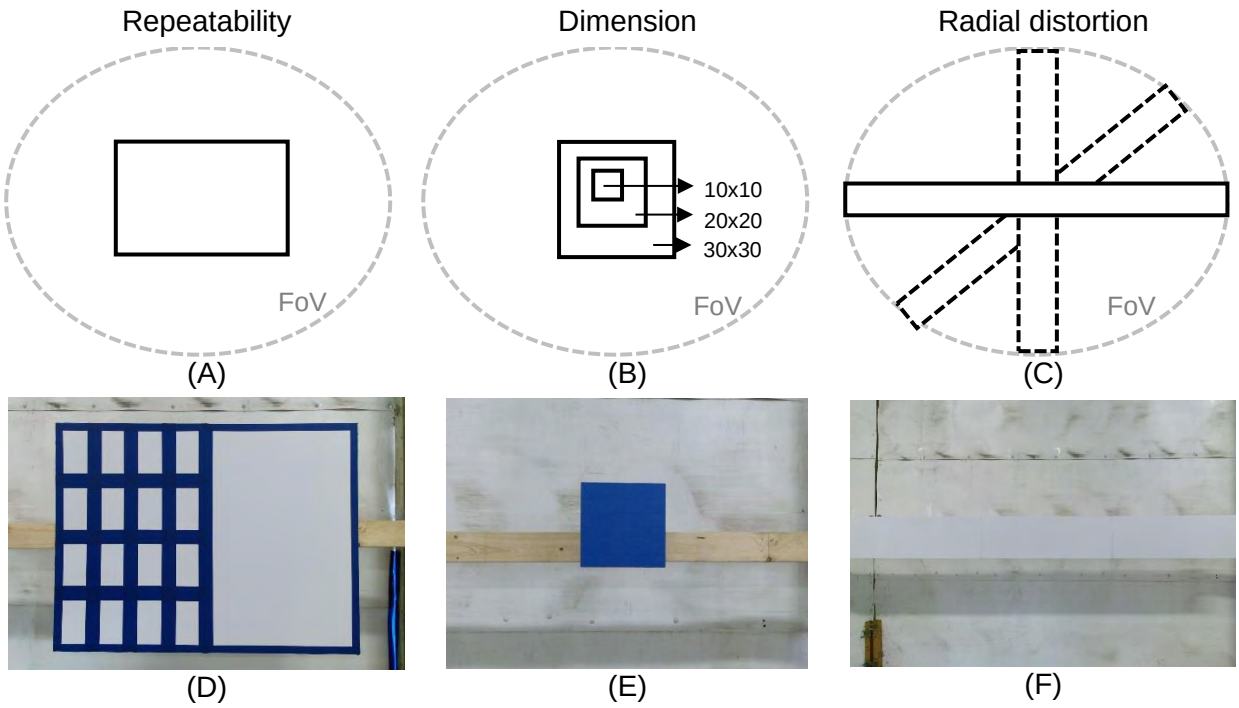

Figure 12. Representation of the three analyzes under the cameras' field of view (FoV) performed in the study: (A) and (D) repeatability, (B) and (E) dimensions, and (C) and (F) radial distortion.

6.2.2 Image Analysis

After data collection, algorithms (MATLAB) were developed to access the board data in the images, needed for the analysis of repeatability, dimensions, radial distortion, and black surface. To do this, morphological operations were applied to the images to separate the foam boards from the background. Once the boards were isolated from the background, different parameters were extracted from the images. The segmented pixels of interest in the images contained the values of the distance between the panels and the cameras (depth images). With these values, different parameters for comparing results (percent, mean, standard deviation, coefficient of variation) were calculated. In the case of the board dimension analysis, to find the theoretical volume (between the board and the wall) from the images, the maximum distance to the wall was subtracted from the distance values recorded by the cameras (Figure 13).

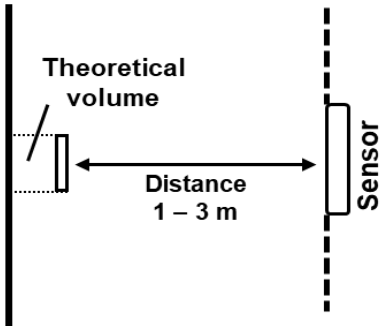

Figure 13. Representation of the data collection with the sensor and the board positioned at the scene.

6.2.3 Repeatability analyze

Repeatability values were compared in terms of standard deviation between distance values obtained from 15 images for each camera on each of the distances analyzed (100, 150, 200, 250, 300 cm).

6.2.4 Dimension analysis

To add to the utility of the depth images in the future, an equation to relate the distance to pixel size was required. To accomplish this, ratios for area were calculated by dividing the pixels by the actual dimensions of the foam board resulting in pixel*cm-2. Regression models were developed relating camera distance to area ratios and for comparing actual and calculated values within images. From the regression equations obtained for each camera, it was possible to calculate the area for each pixel, which allowed finding the theoretical volume of each board. For this, the area of each pixel was multiplied by the depth value (between the board and the wall) and all the values found for each pixel were summed up.

6.2.5 Radial distortion analysis

The effects of radial distortion on the images were investigated in three segments selected from the center to the edge of the images (Figure 14), and the distance values were compared between them as a function of the mean, standard deviation (Std) and coefficient of variation (CV).

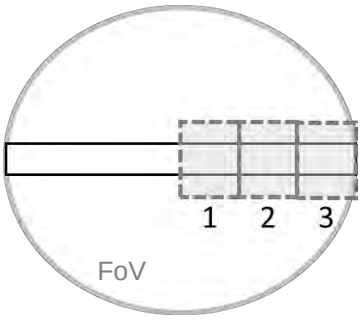

Figure 14. Demonstration of the three segments analyzed in the images to access the radial distortion.

6.3 Results

6.3.1 Repeatability

Repeatability values were compared in terms of standard deviation between depth values obtained from 15 images for each camera (Figure 15). The camera that proved to be more stable in this analysis was the Azure Kinect in NFoV mode, with a mean value of standard deviation of 6.83 followed by the same camera in WFoV mode (8.80). The other cameras showed higher mean values of standard deviation, in order: Pico Zense - cameras 1 and 4 (19.61) and cameras 2 and 3 (27.94), Kinect v.2 (29.50) and Pico Flexx (33.31).

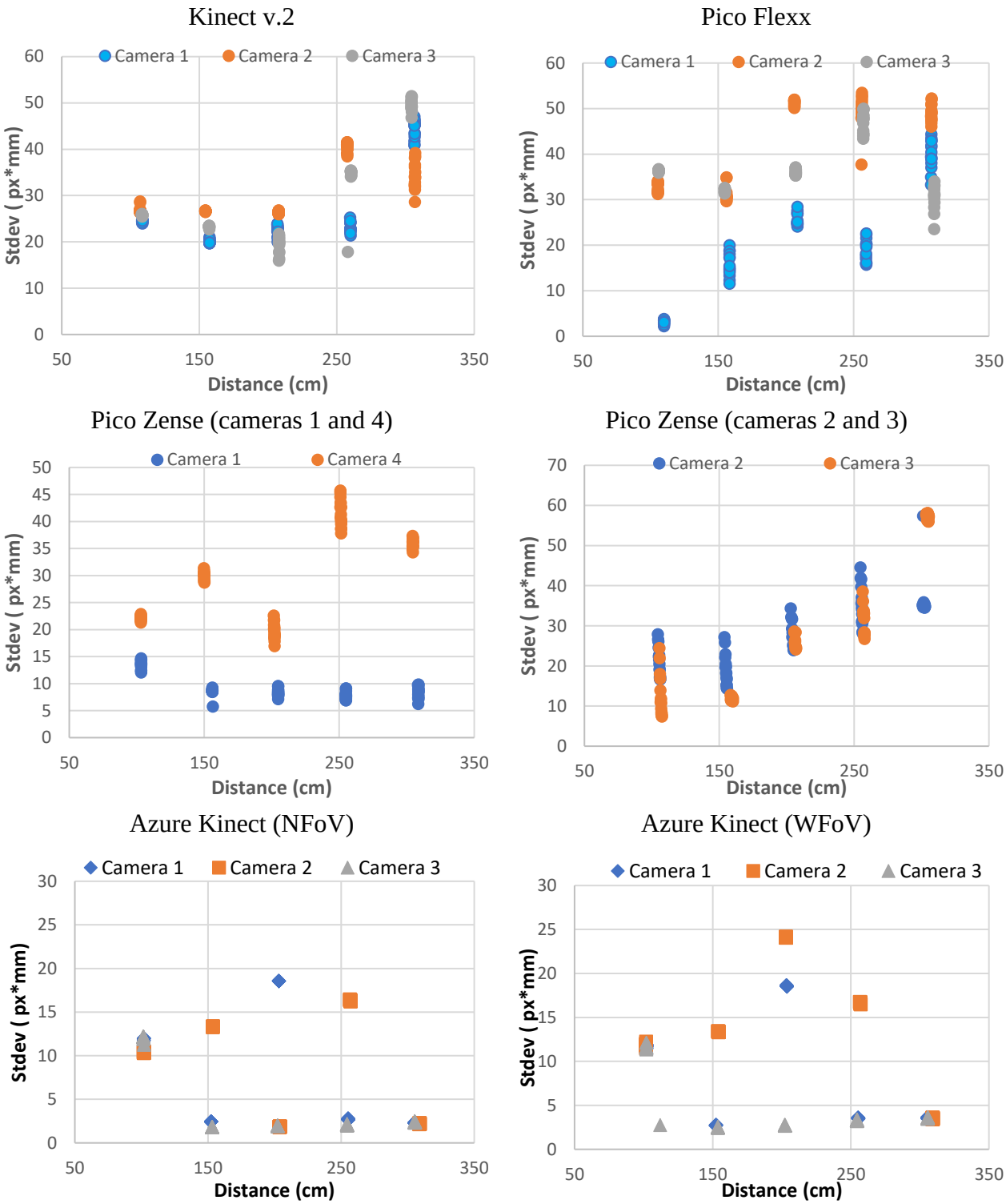

Figure 15. Standard deviation (std) of the depth values registered in the images obtained with the five cameras of the experiment (Kinect v.2, Pico Flexx, Pico Zense (cameras 1 and 4), Pico Zense (cameras 2 and 3), and Azure Kinect.

6.3.2 Board dimensions

For better organization of results, this topic has been divided for each camera. For each one, the area and volume calculations for the different dimensions of panels (10 x 10, 20 x 20, and 30 x 30 cm) are presented.

Summary of the average distance results registered for each camera

Figures 16-a and 16-b show the distance values and standard deviation of the distance values registered for each of the cameras. The recording of average distance values by the cameras were close to the positions defined for data collection (100, 150, 200, 250 and 300 cm), which demonstrates that the positioning of the cameras suffered little variation. The standard deviation of the recorded distance values varied quadratically as the distance between the cameras and the panels increased. The standard deviation values were below 1 cm for most cameras at all distances, except for Pico Flexx at 250 and 300 cm, with values of 1.1 and 1.3 cm, respectively and for Azure Kinect at 300 cm with a standard deviation of 2.9 cm.

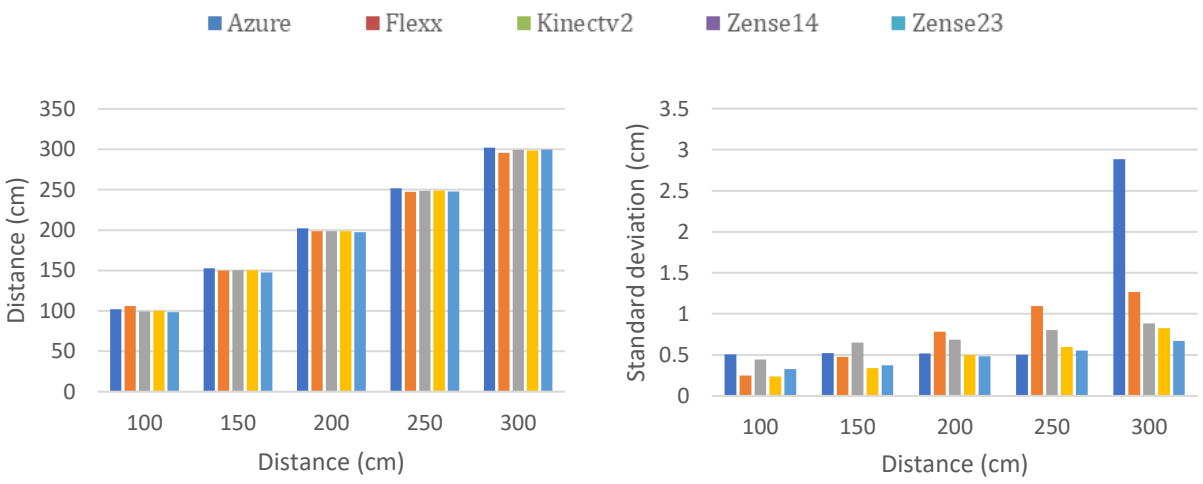

(a) (b)

Figure 16. Mean and standard deviation of the distance values registered from the boards with each of the cameras.

Kinect v.2

Figure 17 a, b, and c show the graphs of the area results (px*cm^{-2}) obtained for the square boards of 10, 20 and 30 cm, respectively. The results obtained by the images were close to the results calculated through the parameters of the cameras. The regression curves obtained for each of the boards showed a coefficient of determination close to 1 (Table 12), demonstrating that the equations were well fitted to the data, which were poorly dispersed.

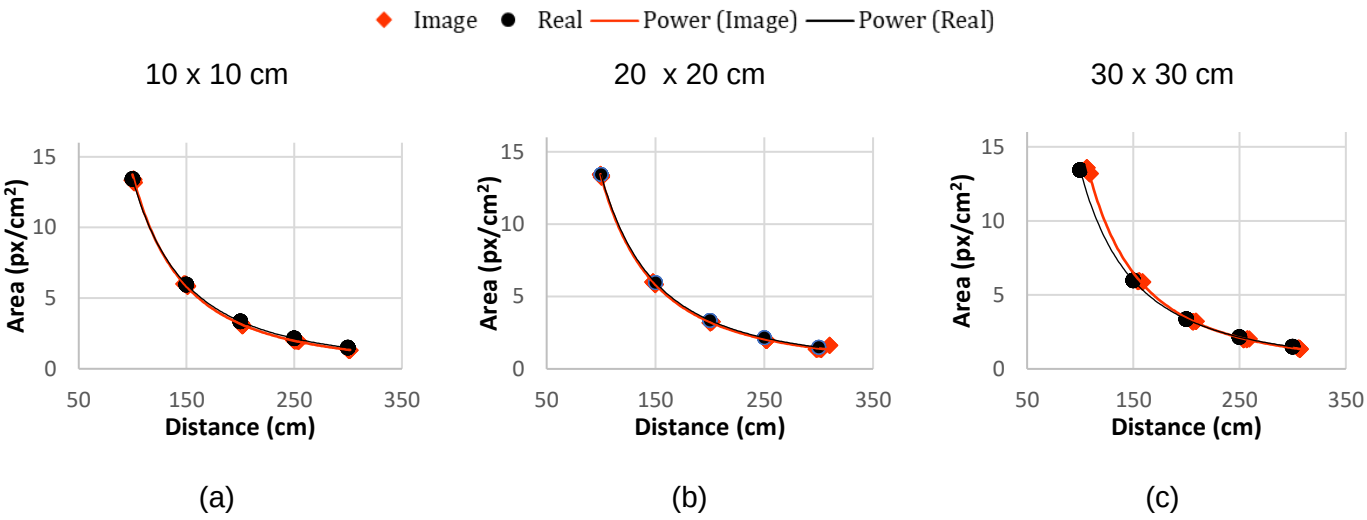

Figure 17. Area ratio (px*cm^{-2}) as a function of the distance (m) for each board ((a) 10 x 10 cm, (b) 20 x 20 cm, and (c) 30 x 30 cm) analyzed in the images obtained with the Microsoft Kinectv.2 camera.

Table 12. Coefficients of area equations (in px*cm^{-2}) obtained from the depth images of the three boards sizes (10 x 10 cm, 20 x 20 cm, and 30 x 30 cm) and the real equation obtained with the Kinect v.2 camera parameters

	Area Coefficients[1]		
Board (cm x cm)	**a**	**b**	**R^2**
10 x 10	225579	-2.108	0.9996
20 x 20	160049	-2.04	0.9997
30 x 30	380464	-2.192	0.9994
Real	134249	-2.000	1.0000

The comparison of the estimated and real volumes results is presented in Table 3. The mean distance values obtained from the images were close to the specified distances, with a mean standard deviation value of 0.69 cm. The highest standard deviation of the distances was recorded for the 10 x 10 cm board, and it decreased as the board size increased to 20 x 20 cm, and 30 x 30

cm at all distances. The error increased as the distance between the camera and the boards increased, and this was observed for all board sizes. The estimated volumes were underestimated compared to the actual values for all boards and distances, except for the 20 x 20 cm board at a 15 cm distance. The proportional error (estimated volume over actual volume) was below 11% for all cases and the average error was 6.58%. The smallest error was recorded at a 150 cm distance for the 20 cm2 board (-0.41%) and the largest at 300 cm for the 30 cm x 30 cm board (10.73%).

Table 13. Distance (mean and standard deviation (std) and theoretical volume (cm^3) recorded with Kinect v.2 camera.

Distance (cm)	**Board (cm^2)**	**Distance (mean ± std (cm))**	**Volume**		
			Estimated (cm^3)	**Real (cm^3)**	**Error (%)**
100	10	99.08 ± 0.66	964.63	1000	3.54%
	20	99.93 ± 0.36	7934.07	8000	0.82%
	30	99.07 ± 0.31	26261.13	27000	2.74%
150	10	150.52 ± 1.01	979.29	1000	2.07%
	20	151.17 ± 0.50	8032.92	8000	-0.41%
	30	149.69 ± 0.45	26562.02	27000	1.62%
200	10	198.34 ± 1.01	896.59	1000	10.34%
	20	199.05 ± 0.56	7516.41	8000	6.04%
	30	198.03 ± 0.48	25116.73	27000	6.98%
250	10	248.77 ± 1.19	892.73	1000	10.73%
	20	248.02 ± 0.70	7202.45	8000	9.97%
	30	248.47 ± 0.51	24717.51	27000	8.45%
300	10	299.37 ± 1.17	847.86	1000	15.21%
	20	300.08 ± 0.82	7192.06	8000	10.10%
	30	298.64 ± 0.67	24370.89	27000	9.74%

Pico Flexx

The results for the area of the images obtained with Pico Flexx ($px*cm^{-2}$) were also close to those calculated with the camera parameters, with coefficients of determination close to 1 for all board sizes (Figure 18 a, b, and c). The regression curves obtained for each of the boards showed a coefficient of determination close to 1 (Table 14), demonstrating that the equations were well fitted to the data, which were poorly dispersed.

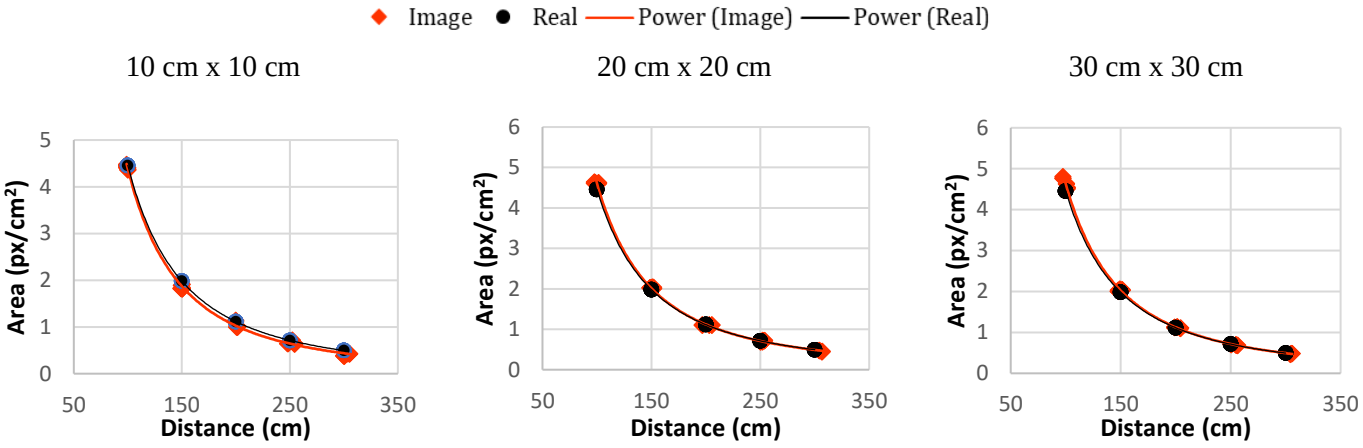

Figure 18. Coefficients of area equations (in px cm^{-2}) obtained from the depth images of the three boards sizes ((a) 10 x 10 cm , (b) 20 x 20 cm, and (c) 30 x 30 cm) and the real equation obtained with the Pico Flexx camera parameters.

Table 14. Coefficients of area equations (in px cm^{-2}) obtained from the depth images of the three boards sizes (10 x 10 cm, 20 x 20 cm, and 30 x 30 cm) and the real equation obtained with the Pico Flexx camera parameters.

	Area Coefficients[1]		
Board (cm x cm)	**a**	**b**	**R^2**
10 x 10	68106	-2.096	0.9991
20 x 20	55522	-2.041	0.9997
30 x 30	55356	-2.039	0.9993
Real	44576	-2.000	1.0000

The comparison of the estimated and actual volume results obtained with the Pico Flexx camera is presented in Table 5. The average distance values obtained in the images were close to the specified distance, with an average standard deviation of 1.52 cm. The largest standard deviation of distance was recorded at 250 cm for the 20 x 20 board (10.02 cm). The estimated volumes were either under or overestimated relative to the actual values. The minimum error between the actual and estimated volume was -0.2% cm^3 at a 100 cm distance for the 10 x 10 cm board, and the maximum was 18.70% cm^3 at a 300 cm distance for the 10 x 10 cm board. The average error for the estimated volumes was 5.79%.

Table 15. Distance (mean (m) and standard deviation (std)), and theoretical volume (cm^3) recorded with Pico Flexx camera.

Distance (cm)	Board (cm^2)	Distance (mean ± std (cm))	Volume		
			Estimated (cm^3)	Real (cm^3)	Error (%)
100	10	100.60 ± 0.27	1002	1000	-0.20%
	20	100.61 ± 0.22	8388.67	8000	-4.86%
	30	100.46 ± 0.22	28452.67	27000	-5.38%
150	10	149.89 ± 0.56	926.85	1000	7.32%
	20	149.33 ± 0.48	8099.15	8000	-1.24%
	30	150.42 ± 0.39	27786.90	27000	-2.91%
200	10	199.00 ± 1.09	929.16	1000	7.08%
	20	198.06 ± 0.54	7764.18	8000	2.95%
	30	198.25 ±0.72	26627.27	27000	1.38%
250	10	248.26 ± 1.45	912.46	1000	8.75%
	20	247.27 ± 10.08	7740.37	8000	3.25%
	30	246.16 ± 0.76	25382.49	27000	5.99%
300	10	297.02 ± 1.60	813.04	1000	18.70%
	20	294.70 ± 1.16	7216.33	8000	9.80%
	30	295.17 ± 0.94	25105.53	27000	7.02%

Pico Zense (cameras 1 and 4)

Regardless of the range parameter chosen for recording the images, the results obtained with the Pico Zense 1 and 4 cameras were well fitted to the regression curves plotted for the area results where the coefficients of determination where above 0.98 for all types of board sizes. In addition, they were close to the results calculated with the camera parameters (Figure 19; Table 16).

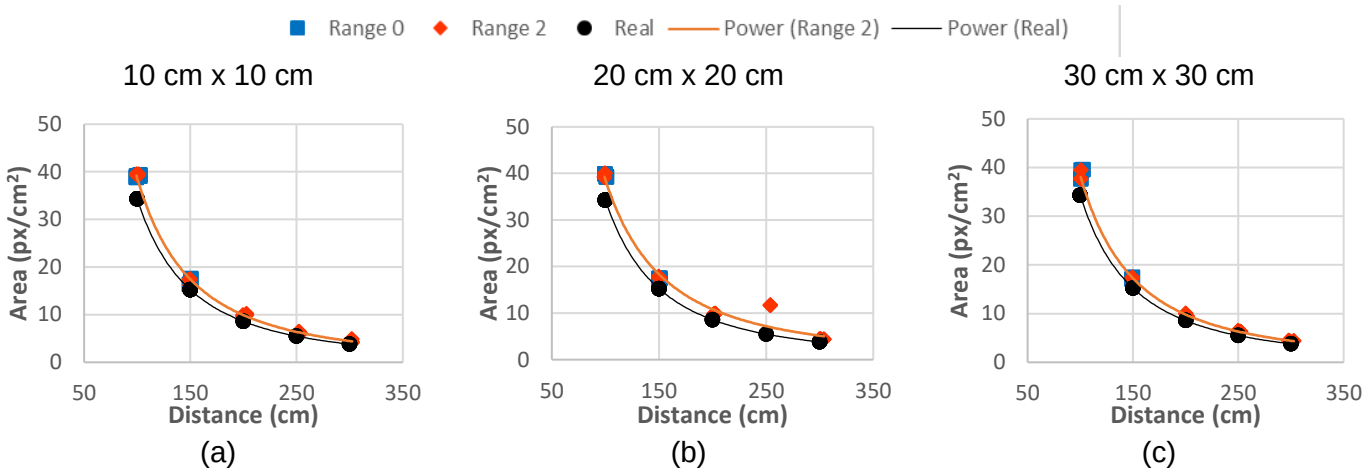

Figure 19. Area ratio (px*cm^{-2}) as a function of the distance (m) for each board ((a) 10 x 10 cm, (b) 20 x 20 cm, and (c) 30 x 30 cm) analyzed in the images obtained with Pico Zense (cameras 1 and 4).

Table 16. Coefficients of area equations (in px cm^{-2}) obtained from the depth images of the three boards sizes (10 x 10 cm, 20 x 20 cm, and 30 x 30 cm) and the real equation obtained with the Pico Zense camera (1 and 4) parameters.

	Area Coefficients[1]		
Board (cm x cm)	**a**	**b**	**R^2**
10 x 10	328135	-1.964	0.9976
20 x 20	180796	-1.835	0.9823
30 x 30	328041	-1.966	0.9987
Real	342925	-2.000	1.0000

The average distance values obtained between the cameras and the boards, as obtained from the images, were close to the actual distance for the Pico Zense 1 and 4 cameras (Table 7). The standard deviation values of the distance increased as the distance between the camera and the boards also increased. The error between the actual and estimated volumes was higher compared to the other cameras, averaging 13.63%. The minimum error was recorded at 150 cm distance for the 10 x 10 cm board (-10.50%), and the maximum error was recorded at 250 cm for the 20 x 20 cm board, representing 15.06% of the total volume.

Table 17. Distance (mean (m) and standard deviation (std)), and theoretical volume (cm^3) recorded with Pico Zense camera (1 and 4).

Distance	**Board**	**Distance (mean ± std (cm))**	**Volume**		
			Estimated (cm^3)	**Real (cm^3)**	**Error (%)**

100	10	99.69 ± 0.22	1140.79	1000	-14.08%
	20	100.66 ± 0.24	9352.93	8000	-16.91%
	30	99.36 ± 0.26	29845.84	27000	-10.54%
150	10	150.25 ± 0.37	1105.02	1000	-10.50%
	20	149.93 ± 0.32	9251.47	8000	-15.64%
	30	150.48 ± 0.30	31081.19	27000	-15.12%
200	10	198.74 ± 0.51	1139.03	1000	-13.90%
	20	198.03 ± 0.50	8984.40	8000	-12.31%
	30	199.13 ± 0.57	30089.74	27000	-11.44%
250	10	247.82 ± 0.70	1134.05	1000	-13.41%
	20	250.53 ± 0.52	9204.80	8000	-15.06%
	30	248.83 ± 0.57	30947.21	27000	-14.62%
300	10	298.03 ± 0.98	1145.04	1000	-14.50%
	20	297.83 ± 0.81	9009.49	8000	-12.62%
	30	300.29 ± 0.65	30709.80	27000	-13.74%

Pico Zense (cameras 2 and 3)

The different ranges also did not impact the area ratio results for the Pico Zense (cameras 2 and 3) (Figure 20), which were well fitted to the regression curves plotted for the results and close to the values calculated with the camera parameters (Table 18). The determination coefficients were close to 1 for all board sizes evaluated.

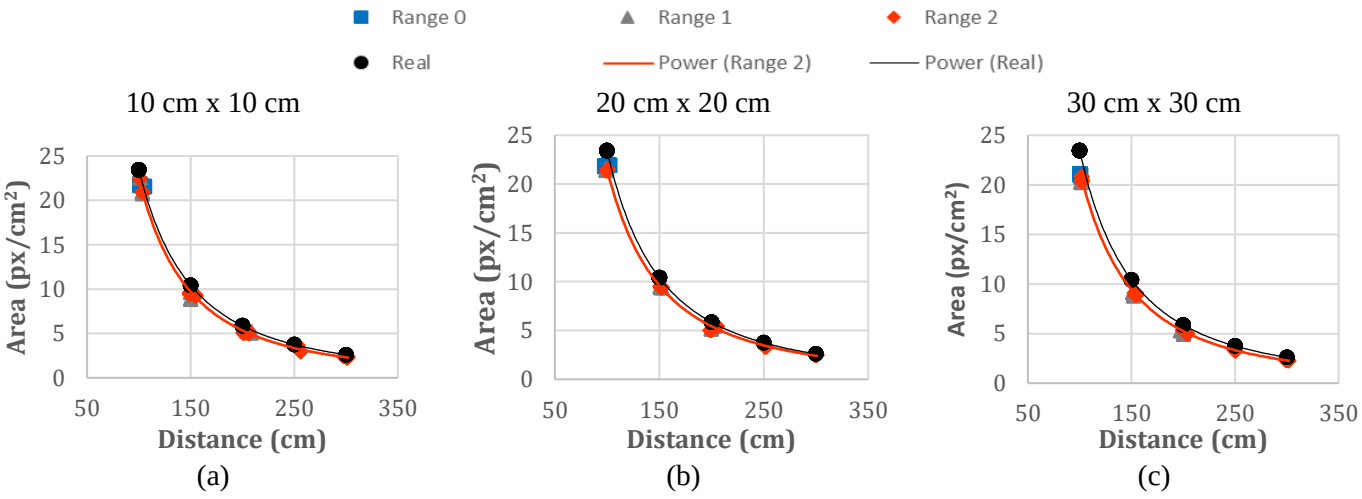

Figure 20. Area ratio (px cm^{-2}) as a function of the distance(m) from camera to the board (10 x 10 cm, 20 x 20 cm, and 30 x 30 cm) for Pico Zense cameras 2 and 3.

Table 18. Coefficients of area equations (in px cm^{-2}) obtained from the depth images of the three boards sizes (10 x 10, 20 x 20, and 30 x 30 cm) and the real equation obtained with the Pico Zense camera (2 and 3) parameters.

	Area Coefficients[1]		
Board (cm x cm)	**a**	**b**	**R^2**
10 x 10	313177	-2.072	0.999
20 x 20	204805	-1.989	0.999
30 x 30	257343	-2.039	0.9995
Real	234278	-2.000	1.0000

The mean distance values obtained from the images taken using the Pico Zense 2 and 3 cameras were close to the specified distance (Table 19) with a mean standard deviation of 0.49 cm. When comparing the estimated to the actual values, the average error in volume was 12.83%. The minimum error was recorded at 300 cm for the 20 x 20 cm panel (5.65%) and the maximum was recorded at 100 cm for the 30 x 30 cm panel (15.88%).

Table 19. Distance (mean (m) and standard deviation (std)), and theoretical volume (cm^3) recorded with Zense camera (2 and 3).

Distance (cm)	**Board (cm^2)**	**Distance (mean ± std (cm))**	**Volume**		
			Estimated (cm^3)	**Real (cm^3)**	**Error (%)**
100	10	97.75 ± 0.31	884.87	1000	11.51%
	20	99.46 ± 0.24	7239.33	8000	9.51%
	30	97.84 ± 0.43	22711.43	27000	15.88%
150	10	148.14 ± 0.35	877.43	1000	12.26%
	20	148.30 ± 0.34	7080.70	8000	11.49%
	30	145.82 ± 0.42	21976.38	27000	18.61%
200	10	196.38 ± 0.42	842.70	1000	15.73%
	20	197.67 ± 0.43	6952.55	8000	13.09%
	30	197.84 ± 0.61	23199.64	27000	14.08%
250	10	245.00 ± 0.61	822.97	1000	17.70%
	20	248.53 ± 0.50	7162.58	8000	10.47%
	30	250.04 ± 0.55	23715.52	27000	12.16%
300	10	299.20 ± 0.89	878.44	1000	12.16%
	20	299.58 ± 0.62	7548.07	8000	5.65%
	30	299.71 ± 0.59	23715.52	27000	12.16%

Azure Kinect (NFoV and WFoV)

Figure 21 and shows the area ratio results (px*cm^{-2}) of the different sizes of panels when using two viewing angles (NFoV and WFoV) from the Azure Kinect camera. The area results obtained from the images with the two fields of view were very close and were not close to the results calculated by the camera parameters. Regarding the regression curves, the lowest

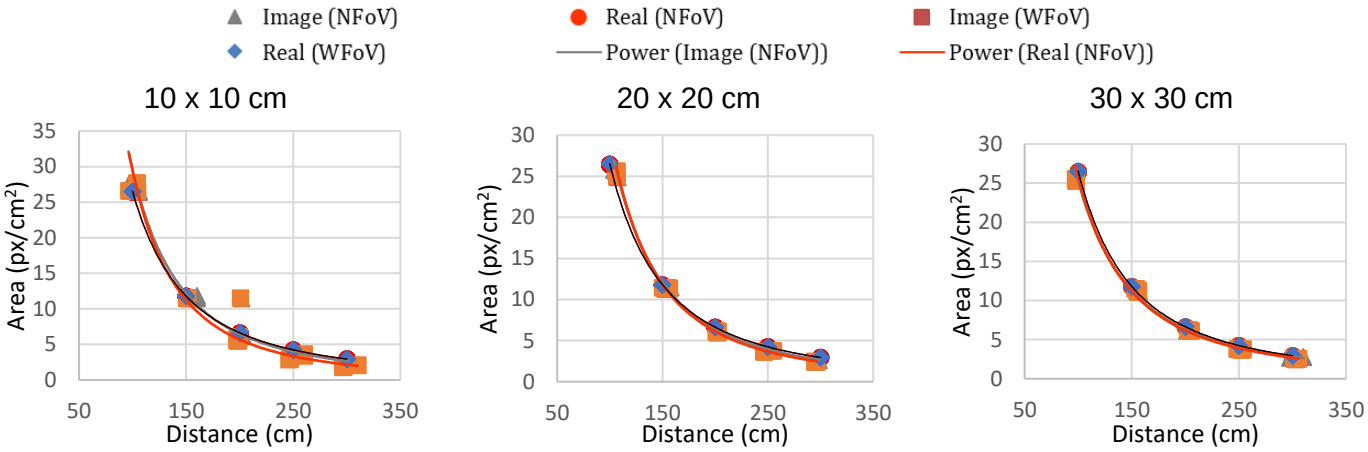

coefficients of determination were above 0.97 (Table 20).

Figure 21. Area ratio (px cm^{-2}) as a function of the distance(m) from camera to the board (10 x 10, 20 x 20, and 30 x 30 cm) for Azure Kinect camera (WFoV and NFoV).

Table 20. Coefficients of area equations (in px*cm^{-2}) obtained from the depth images of the three boards sizes (10 x 10, 20 x 20, and 30 x 30 cm) and the real equation obtained with the Azure Kinect camera parameters.

	NFoV - Area Coefficients[1]		
Board (cm x cm)	**a**	**b**	**R^2**
10 x 10	693192	-2.186	0.9773
20 x 20	706515	-2.191	0.9985
30 x 30	242806	-1.991	0.9967
Real	264382	-2.000	1
	WFoV - Area Coefficients[1]		
Board (cm x cm)	**a**	**b**	**R^2**
10 x 10	2000000	-2.372	0.9731
20 x 20	1000000	-2.293	0.9998
30 x 30	334669	-2.057	0.9957
Real	265421	-2.000	1.0000

The distance and volume results obtained with the Azure Kinect camera are presented in Table 21. The average distance values obtained from the images were close to the specified distances, with an average standard deviation of 0.99 cm. The highest standard deviations of distance were recorded when the camera was positioned at 300 cm, and these were the only values above 1 cm. The estimated volumes were either over or underestimated, with an average error of 4.36%. The smallest error in volume estimation was recorded at 100 cm for the 30 x 30 cm board, while the maximum error was for the 10 x 10 cm board.

The Azure Kinect camera was the camera that presented the smallest error when estimating the volume of the boards, followed by Pico Flexx, Kinect v.2, Pico Zense 2 and 3 and Pico Zense 1 and 4.

Table 21. Distance (mean (m) and standard deviation (std)), and theoretical volume (cm^3) recorded with Azure Kinect camera.

Distance (cm)	**Board (cm^2)**	**Distance (mean ± std (cm))**	**Volume**		
			Estimated (cm^3)	**Real (cm^3)**	**Error (%)**
100	10	102.92 ± 0.68	1069.34	1000	-6.93%
	20	100.74 ± 0.45	7793.79	8000	2.58%
	30	102.50 ± 0.38	27284.43	27000	-1.05%
150	10	152.57 ± 0.63	1010.98	1000	-1.10%
	20	152.07 ± 0.45	7996.95	8000	0.04%
	30	153.26 ± 0.49	27213.19	27000	-0.79%
200	10	201.26 ± 0.52	958.88	1000	4.11%
	20	201.80 ± 0.54	7707.16	8000	3.66%
	30	203.31 ± 0.49	26315.14	27000	2.54%
250	10	250.65 ± 0.42	986.24	1000	1.38%
	20	251.51 ± 0.58	7446.61	8000	6.92%
	30	253.56 ± 0.53	25846.31	27000	4.27%
300	10	300.49 ± 1.72	870.17	1000	12.98%
	20	302.36 ± 3.44	7258.02	8000	9.27%
	30	302.70 ± 3.50	24903.32	27000	7.77%

6.3.3 Radial Distortion

Figure 22 (a, b, and c) shows a general summary of the results on radial distortion for each camera in terms of coefficient of variation in all analyzed distances. In the diagonal position, the results had the greatest variation, mainly in the Kinect v.2 and Pico Zense cameras (cameras 2 and

3). When radial distortion was observed in the vertical position, Pico Zense (cameras 2 and 3) showed the greatest variation. For the cameras mentioned, these variations were greater when they were positioned at a 200 cm distance or more. Regarding the horizontal direction, were under 20% for most of the cameras. Regarding the horizontal direction, coefficients of variation were below 20% for most cameras, except for Kinect v.2, which at distances of 150, 200 and 250 cm exceeded 30%.

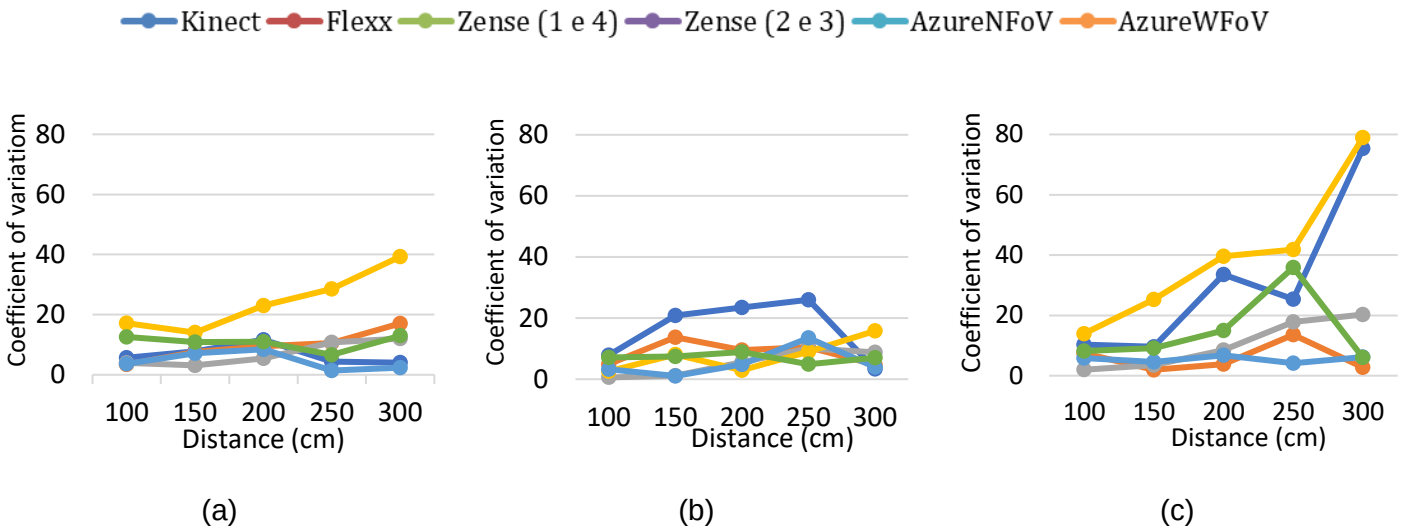

Figure 22. Coefficient of variation of the radial distortion data obtained for all cameras in the vertical (a), horizontal (b), and diagonal (b) directions.

Table 22 also shows all the results on radial distortion for each analyzed camera and board direction in terms of mean, standard deviation, and coefficient of variation. In general, in the vertical position, Pico Zense (cameras 2 and 3) was the camera that presented the highest CV result (22.42), followed by Azure Kinect - WFoV (10.80), Pico Flexx (9.64), Pico Zense (cameras 1 and 4) (7.45), Kinect v.2 (6.70) and Azure Kinect - NFoV (4.60).

Regarding the horizontal direction, the order of CV results (from highest to lowest) was Kinect v. 2 (16.30), Pico Flexx (8.69), Pico Zense (cameras 2 and 3) (7.60), Azure Kinect - WFoV (7.08), Azure Kinect - NFoV (5.35), and Pico Zense (cameras 1 and 4) (5.31). On the diagonal, the order of the results was Pico Zense (cameras 2 and 3) (32.40), Kinect v. 2 (30.83), Azure Kinect - WFoV (14.85), Pico Zense (cameras 1 and 4) (10.56), Pico Flexx (5.93), and Azure Kinect – NFoV (5.49).

Table 22. Mean, standard deviation (Std), and coefficient of variation (CV) of radial distortion values for each camera represented at five different distances (100, 150, 200, 250, and 300 cm).

Kinect V.2									
Direction	**Vertical**			**Horizontal**			**Diagonal**		
Distance (cm)	**Mean**	**Std**	**CV**	**Mean**	**Std**	**CV**	**Mean**	**Std**	**CV**
100	115.19	6.49	5.63	116.41	9.16	7.87	123.31	12.76	10.35
150	123.55	9.59	7.76	115.79	24.14	20.85	145.26	13.95	9.61
200	110.90	12.92	11.65	110.15	25.81	23.43	162.24	54.35	33.50
250	103.27	4.56	4.41	116.02	30.17	26.00	113.29	28.78	25.40
300	113.33	4.56	4.02	140.58	4.73	3.37	116.04	87.38	75.30
General	113.25	7.62	6.70	119.79	18.80	16.30	132.03	39.44	30.83
Pico Flexx									
Direction	**Vertical**			**Horizontal**			**Diagonal**		
Distance (cm)	**Mean**	**Std**	**CV**	**Mean**	**Std**	**CV**	**Mean**	**Std**	**CV**
100	133.61	4.58	3.43	132.12	6.56	4.97	138.69	10.38	7.48
150	129.08	9.80	7.59	130.57	17.92	13.73	98.43	1.93	1.96
200	122.52	11.64	9.50	121.29	11.55	9.52	129.32	4.94	3.82
250	120.16	12.74	10.60	123.59	12.94	10.47	115.58	15.69	13.57
300	120.46	20.57	17.08	112.44	5.36	4.76	108.52	3.05	2.81
General	125.17	11.87	9.64	124.00	10.87	8.69	118.11	7.19	5.93
Pico Zense - Cameras 1 and 4									
Direction	**Vertical**			**Horizonal**			**Diagonal**		
Distance (cm)/range	**Mean**	**Std**	**CV**	**Mean**	**Std**	**CV**	**Mean**	**Std**	**CV**
100/range0	121.93	8.35	6.85	131.54	6.29	4.78	128.34	5.12	3.99
100/range2	136.43	5.35	3.92	140.38	0.82	0.58	142.87	2.83	1.98
150/range0	119.57	12.00	10.04	107.21	6.63	6.18	123.60	21.95	17.76
150/range2	125.19	3.92	3.13	125.27	1.49	1.19	120.52	4.25	3.53
200/range2	106.75	5.80	5.43	118.91	6.66	5.60	113.02	9.63	8.52
250/range2	99.95	10.72	10.73	101.09	10.17	10.06	109.00	19.47	17.86
300/range2	103.74	12.47	12.02	102.78	9.02	8.78	111.53	22.60	20.27
General	116.22	8.37	7.45	118.17	5.87	5.31	121.27	12.26	10.56

continua

conclusão

Table 22. Mean, standard deviation (Std), and coefficient of variation (CV) of radial distortion values for each camera represented at five different distances.

Pico Zense - Cameras 2 and 3									
Direction	**Vertical**			**Horizonal**			**Diagonal**		
Distance (cm)/range	**Mean**	**Std**	**CV**	**Mean**	**Std**	**CV**	**Mean**	**Std**	**CV**
100/range0	84.93	18.64	21.94	102.84	9.06	8.81	94.53	14.96	15.82
100/range1	90.48	18.29	20.21	106.29	6.54	6.16	111.39	16.93	15.20
100/range2	101.95	17.49	17.16	112.48	2.91	2.59	118.43	16.52	13.95
150/range1	127.96	18.82	14.71	119.19	13.93	11.69	116.23	24.48	21.06
150/range2	114.29	16.03	14.03	111.99	9.03	8.06	115.07	29.03	25.23
200/range1	128.86	29.37	22.79	110.62	3.69	3.34	145.73	58.45	40.11
200/range2	101.78	23.43	23.02	99.96	2.92	2.92	133.90	53.01	39.59
250/range2	122.74	35.08	28.58	118.93	10.78	9.06	158.30	66.15	41.79
300/range2	153.79	60.44	39.30	121.33	19.16	15.79	163.75	129.20	78.90
General	114.09	26.40	22.42	111.52	8.67	7.60	128.59	45.41	32.40
Azure NFoV									
Direction	**Vertical**			**Horizontal**			**Diagonal**		
Distance (cm)	**Mean**	**Std**	**CV**	**Mean**	**Std**	**CV**	**Mean**	**Std**	**CV**
100	129.59	4.74	3.65	146.24	4.82	3.30	143.66	8.40	5.85
150	126.64	8.99	7.10	151.38	1.62	1.07	138.59	6.33	4.56
200	133.97	11.36	8.48	152.83	7.41	4.85	152.03	10.28	6.76
250	127.12	1.79	1.41	141.20	19.07	13.50	140.56	5.82	4.14
300	119.11	2.78	2.34	151.52	6.11	4.03	128.01	7.83	6.12
General	127.29	5.93	4.60	148.63	7.81	5.35	140.57	7.73	5.49
Azure WFoV									
Direction	**Vertical**			**Horizontal**			**Diagonal**		
Distance (cm)	**Mean**	**Std**	**CV**	**Mean**	**Std**	**CV**	**Mean**	**Std**	**CV**
100	111.07	13.93	12.54	140.37	9.97	7.10	129.29	10.61	8.20
150	108.34	11.80	10.89	144.21	10.75	7.45	126.82	11.61	9.15
200	115.75	12.70	10.97	137.03	12.21	8.91	109.15	16.35	14.98
250	108.14	7.15	6.62	138.75	6.78	4.89	130.14	46.69	35.88
300	92.50	12.00	12.97	111.58	7.86	7.04	125.02	7.55	6.04
General	107.16	11.51	10.80	134.39	9.51	7.08	124.08	18.56	14.85

6.3.3.1 Radial distortion per segment

Vertical direction

When the boards were positioned vertically in the FoV cameras (Figure 23), Pico Zense (cameras 2 and 3 was the one that presented the greatest coefficient of variation, and also, at 200 and 300 cm away, it was the one that presented the greatest difference in At 300 cm distance, the Pico Flexx also showed a greater variation compared to other cameras and also to its own cv values observed at closer distances.

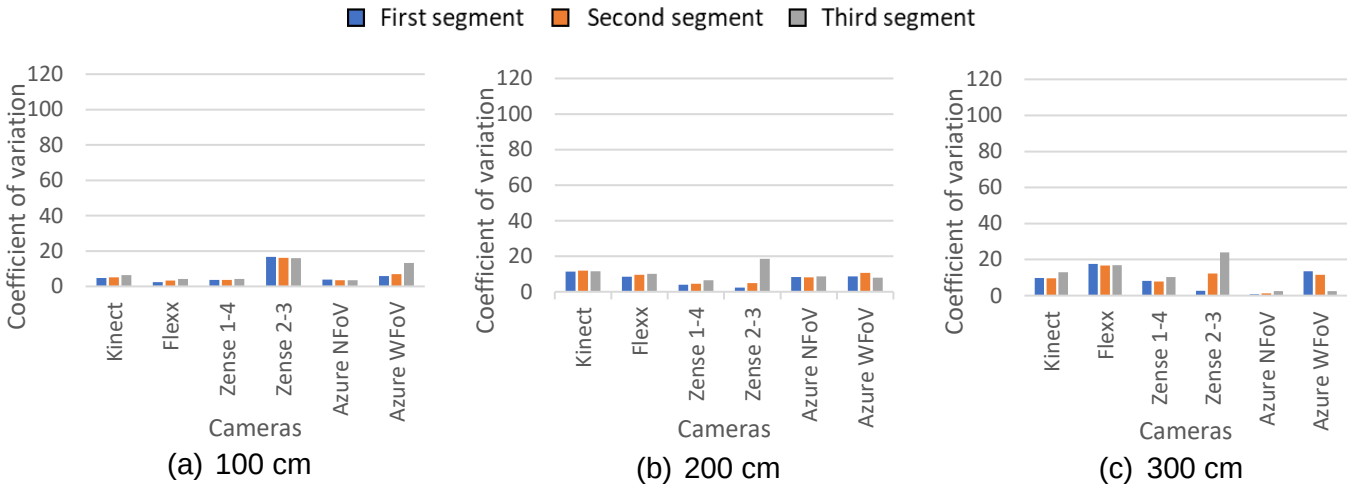

Figure 23. Comparison of the values of the coefficients of variation of the three segments analyzed in the images obtained from the board in the vertical direction of the cameras field of view at three collection distances (100 cm, 200 cm, and 300 cm).

Horizontal direction

With the boards in the horizontal position of the field of view (Figure 24), Pico Zense (cameras 2 and 3) and Kinect v.2 showed the highest coefficients of variation at 100 and 200 cm away, respectively. The greatest differences between the segments were presented by Pico Zense (cameras 2 and 3) at 200 cm and 300 cm distance. Most cv values for all cameras and distances were below 20%. Exceptions were found for Kinect v.2 at 200 cm and Pico Zense (cameras 2 and 3), where the third segment presented a variation of 24.03%.

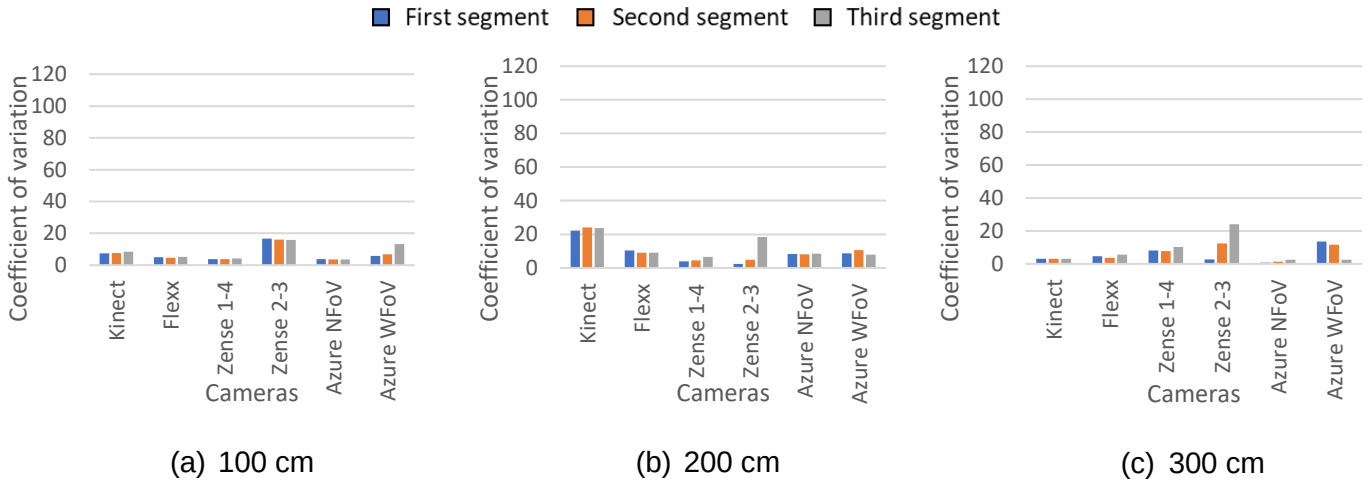

(a) 100 cm (b) 200 cm (c) 300 cm

Figure 24. Comparison of the values of the coefficients of variation of the three segments analyzed in the images obtained from the board in the horizontal direction of the cameras field of view at three collection distances (100 cm, 200 cm, and 300 cm).

Diagonal direction

Cameras in general showed greater distortion when the boards were positioned diagonally compared to the other positions (vertical and horizontal). At a 100 cm distance, despite all CV values being below 20%, a greater difference between the third and other segments can be observed for Kinect v.2 and Pico Zense cameras (cameras 2 and 3). These differences between segments were accentuated at 200 and 300 cm distances for all cameras. At 200 cm the cv values of Kinect v.2 and the third Pico Zense segment (cameras 2 and 3) exceeded 20%. At 300 cm, these same cameras showed very high coefficients of variation for the third segment, which exceeded 120% for Kinect v.2 and 60% for Pico Zense (cameras 2 and 3).

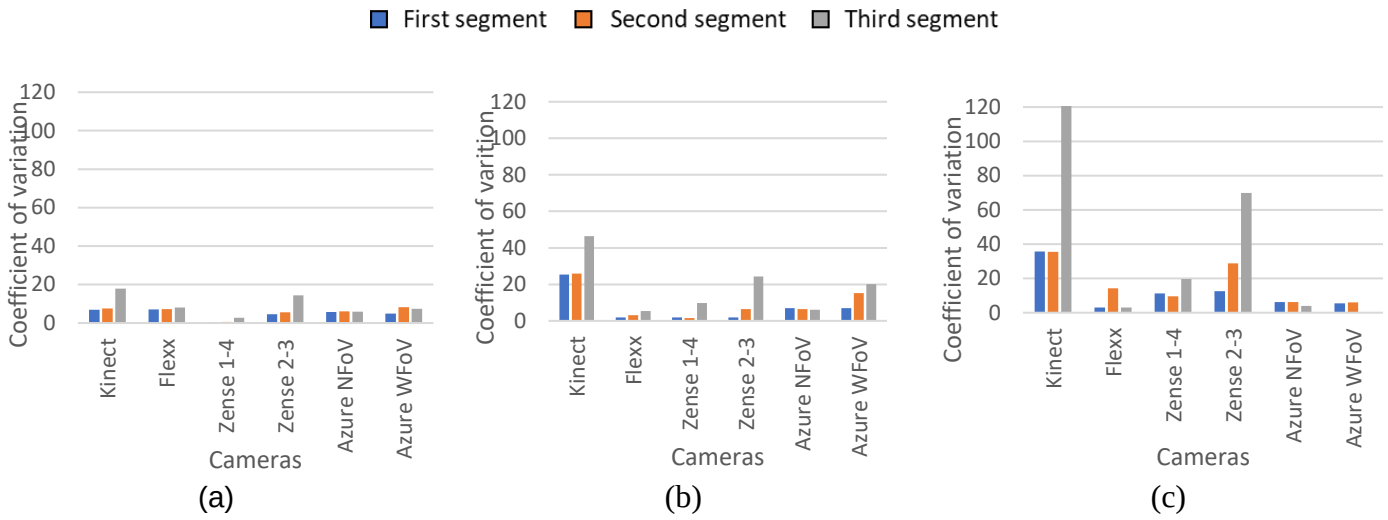

Figure 25. Comparison of the values of the coefficients of variation of the three segments analyzed in the images obtained from the board in the diagonal direction of the cameras field of view at three collection distances (100 cm, 200 cm, and 300 cm).

6.4 Discussion

This study explored several systematic errors in signals obtained from time-of-flight depth cameras, as these errors can affect the accuracy of the results and can vary between cameras. The first analysis aimed to examine repeatability in recording depth data by cameras in a sequence of images of the same object. In the second analysis, a study was conducted on the variation of pixel dimensions in images captured of different board sizes by different cameras. To do this, the area ratio and the volume of the pixels representing the panels in the images were calculated. The final topic addressed radial distortion by comparing distance measurements in three segments of the cameras' field of view, from the center to the edge of the images.

Regarding the repeatability analysis, it was expected that the standard deviation of the depth values would increase as the cameras moved away from the boards since more objects enter the scene with distance, and the reflections of infrared rays from these objects could interfere in the calculation of the depth values. Contrary to expectations, this increase in standard deviation with the distance was not observed. What was observed was a variation in standard deviation values between cameras of the same brand, and that the Azure Kinect camera was the one that presented the greatest consistency in the recorded values, with the lowest standard deviation recorded. Tölgyessy et al. (2021) compared, through repeatability analysis, the three generations of Microsoft

depth cameras (Kinect, Kinect v.2 and Azure Kinect). The authors found that the latest generation (Azure Kinect) has evolved compared to previous versions and the repeatability data found showed a standard deviation below 17 mm, as presented in the Microsoft official documentation. In this study, using three different cameras, the standard deviation values averaged 6.81 mm (min = 1.79 mm; max = 18.55 mm) for NFoV mode and 8.89 mm (min = 2.45 mm; max = 24.09 mm). One difference found between this study and the one conducted by Tölgyessy et al. (2021) was the object of evaluation of the repeatability values, while Tölgyessy et al. (2021) investigated a flat wall, in this study a board away from the wall was used. This may have been a noise source, as differences between planes can cause errors in distance calculations at the edges due to the inconsistency of light reflected from the two planes (Haider & Hel-Or, 2022).

When observing pixel dimensions, all cameras presented similar curves between the experimental and theoretical data (Figures 17-21) with the ratio values for area ($px*cm^{-2}$) decreasing as the distance between the cameras and the boards increased. This behavior was expected, since FoV encompasses more objects on the scene as the distance increases, but the pixels quantity remains the same. Therefore, the number of pixels per centimeter decreases. The determination coefficients for the four cameras were above 0.97 for the area-to-distance ratio equations, demonstrating that the data were well-fitted to the regression curves. The similar behavior of the area ratio curves shows that the camera measurements are consistent with the actual measurements.

Area data remained stable in the central regions of the boards and showed more variation at the edges (Figure 26 a and b). As mentioned before these noises reflect an inconsistency in reflected light for depth calculation at edges. Fursattel et al. (2016) suggested that these errors can be intensified when the distance between foreground and background is large, and if the foreground has a higher reflectivity than the background. In this study, the foam boards were covered with blue tape and were positioned in front of a white wall, so the foreground had a lower reflectivity than the background, which may have contributed to the errors on the edge of the images.

Other studies have reported variations in planar surfaces with images obtained from ToF sensors. Khoshelham & Elberink (2012) evaluated the relationship between random error and sensor distance by measuring a flat surface at various distances from 0.5 m to 5.0 m. The authors observed that the errors increase quadratically from a few millimeters at 0.5 m distance to about 4 cm at the maximum collection distance. The authors observed that the errors increase quadratically

from a few millimeters at 0.5 m distance to about 4 cm at the maximum collection distance. The same happened with the distance values observed for the boards, where the standard deviation values increased quadratically from the smallest distance (100 cm) to the largest (300 cm). Pico Zense cameras had the lowest standard deviation values at all distances. The highest standard deviation value recorded was for the Azure Kinect camera at 300 cm. This was the only data that exceeded 1.5 cm at all data collection distances.

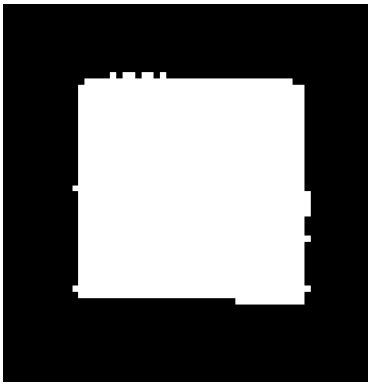

a

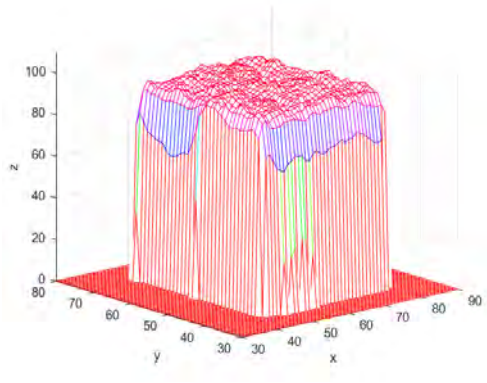

b

Figure 26. (a) Area and (b) projected volume of a foam board captured by a depth camera.

Volume data had more variation than area results for all cameras. It is worth mentioning that the positioning of the cameras at the time of collection was a source of error added to the distance values recorded by the sensors. Although the collection distances have been pre-established, the positioning may vary by a few centimeters when positioning the tripod for image collection. The result of the volume projection is a calculation that depends on the number of pixels (resolution) and distance values recorded by each camera, therefore cameras with higher resolutions and with less variation in the distance values recorded tend to present more consistent volume results. In this study, Azure Kinect was the camera that presented the best results in terms of volume.

The radial distortion was expected to show a growth from the center to the edges of the image. In the case of the experiment, the depth difference between the edges of the bar and the background was an important source of noise in all observed segments of the images (Figure 16). It is known that there is a lens-related radial distortion, which increases proportionally with the distance between the camera and the target. In addition, the ToF light emission technology itself is

responsible for these noises since the illumination power generally decreased from the center relative to the edges and there can be interference from different reflected light paths. Despite these interferences, the Pico Zense (1 and 4) and Azure Kinect cameras had the lowest coefficient of variation values in the radial distortion data and the smallest difference between the analyzed segments.

6.5 Summary of the results

Table 23 shows the summary of the main results obtained with the four ToF cameras tested in this work. In terms of repeatability, Azure Kinect was the camera that presented the best results in this paper. Based on the standard deviation results, Pico Zense showed the best distance results. For the area data, the Kinect v.2, Pico Flex, and Pico Zense cameras (2 and 3) presented the closest equations to the equations obtained through the camera parameters. Nevertheless, all cameras showed similar curves between the experimental and theoretical data. Regarding radial distortion, Pico Zense (1 and 4) and Azure Kinect cameras were the ones that presented the lowest values of coefficient of variation in the recorded data and the ones that presented the smallest difference between the analyzed segments. Azure Kinect camera was the best camera in terms of measure range, FoV and depth resolution. The cost of Kinect v.2 is the lowest, on the other hand it is the only one that is not being manufactured, as it has been replaced by Azure Kinect.

Table 23. Summary of the main results obtained with the four different cameras.

Parameter		***Cameras***				
		Kinect v.2	***Flexx***	***Zense*** (1,4)	***Zense (2.3)***	***Azure***
Repeatability						✓
Accuracy	*Distance*			✓	✓	
	Area	✓	✓		✓	
	Volume					✓
Radial distortion				✓		✓
Measure range						✓
Field of view						✓
Depth resolution						✓
Cost		✓				
Availability			✓	✓	✓	✓

6.6 Conclusion

In this study, Azure Kinect camera presented the best results in terms of repeatability and volume estimation. Pico Zense (cameras 2 and 3) presented the smaller standard deviation values for distance measurements. Kinect v.2 camera presented the best results for area measurements.

Acknowledgement

This work was supported by the Coordenação de Aperfeiçoamento Pessoal (CAPES) [001, 2019], Pirassununga, Brazil.

6.7 References

Chen, C., Zhu, W., Steibel, J., Siegford, J., Wurtz, K., Han, J., & Norton, T. (2020). Recognition of aggressive episodes of pigs based on convolutional neural network and long short-term memory. Computers and Electronics in Agriculture, 169(October 2019), 105166. https://doi.org/10.1016/j.compag.2019.105166

Condotta, I. C. F. S., Brown-Brandl, T. M., Pitla, S. K., Stinn, J. P., & Silva-Miranda, K. O. (2020). Evaluation of low-cost depth cameras for agricultural applications. Computers and Electronics in Agriculture, 173(April), 105394. https://doi.org/10.1016/j.compag.2020.105394

Condotta, I. C. F. S., Brown-Brandl, T. M., Silva-Miranda, K. O., & Stinn, J. P. (2018). Evaluation of a depth sensor for mass estimation of growing and finishing pigs. Biosystems Engineering, 173, 11–18. https://doi.org/10.1016/j.biosystemseng.2018.03.002

Fursattel, P., Placht, S., Balda, M., Schaller, C., Hofmann, H., Maier, A., & Riess, C. (2016). A comparative error analysis of current time-of-flight sensors. IEEE Transactions on Computational Imaging, 2(1), 27–41. https://doi.org/10.1109/TCI.2015.2510506

Haider, A., & Hel-Or, H. (2022). What Can We Learn from Depth Camera Sensor Noise? Sensors, 22(14). https://doi.org/10.3390/s22145448

Horaud, R., Hansard, M., Evangelidis, G., Clément, M., Horaud, R., Hansard, M., Evangelidis, G., Clément, M., Overview, A., Horaud, R., Hansard, M., & Evangelidis, G. (2016). An Overview of Depth Cameras and Range Scanners Based on Time-of-Flight Technologies To cite this version : HAL Id : hal-01325045 An Overview of Depth Cameras and Range Scanners Based on Time-of-Flight Technologies.

Khoshelham, K., & Elberink, S. O. (2012). Accuracy and resolution of kinect depth data for indoor mapping applications. Sensors, 12(2), 1437–1454. https://doi.org/10.3390/s120201437

Lachat, E., Macher, H., Landes, T., & Grussenmeyer, P. (2015). Assessment and calibration of a RGB-D camera (Kinect v2 Sensor) towards a potential use for close-range 3D modeling. Remote Sensing, 7(10), 13070–13097. https://doi.org/10.3390/rs71013070

Microsoft. Azure Kinect Depth Camera. Available online: https://learn.microsoft.com/en-us/azure/kinect-dk/depth-camera#camera-performance (accessed on 9 June 2023).

Tölgyessy, M., Dekan, M., & Chovanec, L. (2021). Skeleton tracking accuracy and precision

evaluation of Kinect V1, Kinect V2, and the azure kinect. Applied Sciences (Switzerland), 11(12), 1–23. https://doi.org/10.3390/app11125756

Van Hertem, T., Schlageter Tello, A., Viazzi, S., Steensels, M., Bahr, C., Romanini, C. E. B., Lokhorst, K., Maltz, E., Halachmi, I., & Berckmans, D. (2018). Implementation of an automatic 3D vision monitor for dairy cow locomotion in a commercial farm. Biosystems Engineering, 173, 166–175. https://doi.org/10.1016/j.biosystemseng.2017.08.011

Zhu, X., Chen, C., Zheng, B., Yang, X., Gan, H., Zheng, C., Yang, A., Mao, L., & Xue, Y. (2020). Automatic recognition of lactating sow postures by refined two-stream RGB-D faster R-CNN. Biosystems Engineering, 189, 116–132. https://doi.org/10.1016/j.biosystemseng.2019.11.013

7 CONSIDERAÇÔES FINAIS

O desenvolvimento deste trabalho se deu em três capítulos principais. O primeiro estudo investigou a performance de leitões em baias com configurações alternativas às gaiolas de parto tradicionais, nas quais se diferiam pelo posicionamento da gaiola da matriz dentro da baia. Os resultados indicaram que a porcentagem de sobreposições foi influenciada pelas diferentes configurações de gaiolas de parto estudadas (padrão, offset e diagonal) quando as matrizes com mortalidade superior a dois leitões foram selecionadas. Os leitões no tratamento offset apresentaram uma porcentagem menor de sobreposições do que os mantidos no tratamento padrão, com uma diferença de aproximadamente 0,6%. Nesse estudo, que avaliou 651 porcas com um número médio de leitões nascidos vivos igual a 12,86, esse valor representaria a sobrevivência de 50 leitões.

O estudo também demonstrou a influência da parição e da estação do ano nas características de desempenho dos leitões. A porcentagem de sobreposições foi maior no outono e no verão do que nas outras estações. Com relação ao ganho de peso médio diário, o valor foi menor no verão. Essas diferenças devem ser destacadas, considerando que os animais foram alojados em ambientes climatizados, com um certo nível de automação. Uma explicação para essas diferenças pode ter sido em função do aumento da umidade relativa dentro da instalação no verão e no outono, quando as almofadas de resfriamento evaporativo eram ativadas para atenuar a alta temperatura do ar. O aumento da umidade relativa pode ter causado desconforto térmico nas matrizes e alterado seu comportamento, o que, consequentemente, afetou o desempenho dos leitões. As matrizes em desconforto térmico tendem a reduzir a ingestão de alimentos e água e a frequência das mudanças posturais. Essas mudanças podem afetar a qualidade e a quantidade de leite, bem como sua

disponibilidade para amamentação e a porcentagem de sobreposições. Outras explicações podem estar relacionadas às temperaturas mais altas encontradas no verão e no outono, o que faz com que os leitões tenham menos probabilidade de procurar uma fonte de aquecimento e se tornem mais vulneráveis ao esmagamento.

As matrizes de paridade 1 apresentaram leitões com menor ganho de peso diário do que as mais velhas (paridades 2, 3 e 4). A melhor habilidade materna das matrizes multíparas pode ser uma explicação para a diferença encontrada. As matrizes primíparas tendem a ser mais reativas aos leitões e, quando jovens, estão lidando com seu próprio desenvolvimento. Assim, pode ser que as matrizes estivessem menos disponíveis para amamentar e, além disso, parte da energia que poderia ser usada para a produção de leite deveria estar sendo usada para seu próprio desenvolvimento.

Estudos futuros podem ser desenvolvidos avaliando o comportamento de matrizes e leitões nas diferentes configurações de gaiolas de parto estudadas e essa análise pode ser associada com as características de desempenho dos leitões. Além disso, as variações nos dados de desempenho dos leitões encontrados entre as estações e as diferentes paridades das matrizes podem ser explicadas pelo padrão comportamental dos animais.

O segundo capítulo tratou do desenvolvimento de um modelo classificador de posturas de matrizes, baseado em Redes Neurais Convolucionais (CNN). Entender os padrões comportamentais das matrizes durante o período de lactação pode trazer informações importantes sobre a saúde e o bem-estar dos animais e auxiliar os produtores na detecção de problemas e melhorar o manejo do seu rebanho. A intenção do desenvolvimento de um modelo classificador de posturas é substituir a investigação comportamental manual, que necessita de tempo e observadores treinados, por um método automático de avaliação de imagens. Neste estudo diferentes tipos de imagens foram utilizadas no desenvolvimento de modelos computacionais para a classificação de cinco posturas de matrizes (ajoelhada, em pé, sentada, decúbito lateral e decúbito ventral). Foram desenvolvidos modelos de classificação com imagens coloridas (RGB: *red*, *green*, *blue* - vermelho, verde, azul), imagens de profundidade transformadas em escala de cinza (grayscale) e as imagens RGB e grayscale combinadas (mixed). O modelo que utilizou somente imagens de profundidade apresentou os melhores resultados de classificação, seguido pelo modelo mixed e o RGB com acurácias de 92.36%, 91.44% e 85.14%, respectivamente. O melhor modelo modelo (grayscale) demonstrou potencial para classificação das posturas das matrizes, com destaque para as posturas de trasição (ajoelhada e sentada), difíceis de serem detectadas em

imagens RGB com vista superior dos animais. Além disso, as imagens de profundidade possuem a vantagem de utilização em ambientes com baixa luminosidade, já que a tecnologia trabalha emissão da luz infravermelha para a obtenção da informação de profundidade e não dependem da luz visível para a formação das imagens, como é o caso das imagens coloridas tradicionais.

Outros estudos podem contribuir para o desenvolvimento de modelos cada vez mais precisos, utilizando um banco de dados maior, avaliando diferentes combinações de imagens, modelos computacionais, tipos de alojamentos, raças de animais e analisando diferentes comportamentos.

No último capítulo deste estudo, foram comparadas diferentes câmeras de profundidade baseadas na tecnologia de tempo-de-vôo (time-of-flight) já que estes tipos de sensores estão sujeitos a erros que afetam o registro dos dados de profundidade. Apesar das medições serem afetadas por diferentes fatores, as propriedades intrínsecas de cada câmera (especificações e algoritmos de processamento) também podem contribuir influenciar a precisão dos resultados. Dessa forma este útlimo estudo comparou quatro câmeras ToF (Kinect v.2, Pico Zense, Pico Flexx e Azure Kinect) em termos de repetibilidade na captura de imagens de cenas estáticas, do cálculo de dimensões de painéis a partir de imagens e da distorção radial entre o centro e as bordas das imagens. As câmeras com tecnologias mais recentes (Pico Zense e Azure Kinect) apresentaram os melhores resultados nos testes elaborados em relação às demais.

Na área animal estes testes são importantes pois refletem a capacidade destas câmeras de detectar objetos ou animais nos sistemas produtivos por meio de imagens. Além disso, estas câmeras são podem contribuir no desenvolvimento de diferentes sistemas de monitoramento automático baseados em visão computacional. Como mencionado anteriormente, outra vantagem de utilização destas câmeras, é a capacidade de monitoramento de ambientes com baixa luminosidade, permitindo o monitoramento dos animais 24 horas por dia.

Os processos de validação são importantes para garantir que os sensores coletem informações precisas e para a escolha do sensor que melhor atenda às necessidades do usuário. Outros estudos podem ser desenvolvidos para avaliar as diferentes câmeras e tecnologias que estão constantemente sendo lançadas. Além disso, as informações coletadas pelas câmeras de profundidade podem ser aprimoradas com a utilização de diferentes algoritmos de processamento de imagem, como técnicas de filtragem e correção de ruídos.